BRUNEL UNIVERSITY LONDON

Fault Detection in Rotating Machinery Using Acoustic Emission

By

Juan Luis Ferrando Chacon

A thesis submitted for the degree of Doctor of Philosophy

In the

School of Engineering and Design

October 2015

BRUNEL UNIVERSITY LONDON

Abstract

School of Engineering and Design

Engineering Doctorate

by Juan Luis Ferrando Chacon

Rotating machinery is a critical asset of industrial plants worldwide. Bearings and gearboxes are two of the most common components found in rotating machinery of industrial plants. The malfunction of bearings and gearboxes lead the machine to fail and often these failures occur catastrophically leading to personnel injuries. Therefore it is of high importance to identify the deterioration at an early stage. Among the techniques applied to detect damage in rotating machinery, acoustic emission has been a prevalent field of research for its potential to detect defects at an earlier stage than other more established techniques such as vibration analysis and oil analysis. However, to reliably detect the fault at an early stage de-noising techniques often must be applied to reduce the AE noise generated by neighbouring components and normal component operation. For this purpose a novel signal processing algorithm has been developed combining Wavelet Packets as a pre-processor, Hilbert Transform, Autocorrelation function and Fast Fourier transform. The combination of these techniques allows identification of g repetitive patterns in the AE signal that are attributable to bearing and gear damage. The enhancement for early stage defect detection in bearings and gears provided by this method is beneficial in planning maintenance in advance, reducing machinery down-time and consequently reducing the costs associated with bearing breakdown. The effectiveness of the proposed method has been investigated experimentally using seeded and naturally developed defects in gears and bearings. In addition, research into the optimal Wavelet Packet node that offers the best de-noising results has been performed showing that the 250-750 kHz band gives the best SNR results.

The detection of shaft angular misalignment using Acoustic Emission has been investigated and compared with acceleration spectra. The results obtained show enhancements of AE in detection

shaft angular misalignment over vibration analysis in SNR and stability with varying operational conditions.

Keywords: acoustic emission, condition monitoring, bearing, gearbox, misalignment, de-noising, fault detection, wavelet transform.

Acknowledgements

I am very grateful to my supervisors Professor Wamadeva Balachandran and Tat-Hean Gan for their support and encouragement during my PhD. I would also like express my gratitude to Vassilios Kappatos for his help and advice. Heartfelt thanks goes to Alicia for standing by me every day both in good times and bad times. I want to extend my thanks to Ignacio Garcia de Carellan, Bhavin Engineer, Borja Hernandez, Shehan Lowe, Sina Fateri and all the other colleagues with whom I enjoyed sharing this great experience. Last (but not least) thanks to Estefania Artigao for helping me to have the opportunity to carry out this PhD.

Contents

List of figures

List of abbreviations

NWCC	National Wind Coordinating Committee
CM	Condition Monitoring
AE	Acoustic Emission
SNR	Signal-to-noise Ratio
WP	Wavelet Packet
HT	Hilbert Transform
ACF	Autocorrelation function
FFT	Fast Fourier Transform
SAM	Shaft Angular Misalignment
NDT	Non-destructive Testing
GRP	Glass Reinforced Plastic
PZT	Lead Zirconate Titanate
WT	Wavelet Transform
RMS	Root Mean Square
CF	Crest Factor
IE	Information Entropy
CWT	Continuous Wavelet Transform
STFT	Short Time Fourier Transform
WVD	Wigner Ville Distribution
CWD	Choi Williams Distribution
CSD	Cone Shape Distribution
ANN	Artificial Neural Network
HFRT	High Frequency Resonance Technique
ALE	Adaptive Line Enhancer
MCSA	Motor Current Signature Analysis
DWT	Discrete Wavelet Transform
DFT	Discrete Wavelet Transform
BPFO	Ball Passing Frequency Outer
GMF	Gear Mesh Frequency

Chapter 1

Introduction

1.1. Motivation

Rotating machinery is extensively used in a range of mechanical transmission systems and plays an important role in industrial applications. The severe working environment in industrial plants frequently causes rotating machinery to fail unexpectedly reducing machinery reliability. Unexpected machinery failure dramatically affects the cost of the final product and decreases the

safety in industrial plants because machines often fail catastrophically causing injury to personnel. Usually, to avoid this problem, preventive maintenance is performed in industrial plants to increase the machinery reliability and increase safety. Preventive maintenance is maintenance that is periodically carried out on the machinery to diminish the likelihood of failure. However, preventive maintenance is inefficient and expensive because it does not take into account the condition of the machine. According to the report issued by the National Wind Coordinating Committee (NWCC), in the wind turbine industry, maintenance costs accounts for 21% of the total power per annum costs. 75% of these costs are due to unscheduled maintenance [1].

A solution implemented to reduce the maintenance costs and increase safety in industrial plants is to apply condition monitoring (CM). CM is the process of monitoring parameters with the purpose of identifying a changing trend, which is generally produced by developing faults. CM allows predictive maintenance solution to be carried out. Predictive maintenance is a solution in which the condition of in-service equipment is known based on CM in order to predict when maintenance should be performed. Predictive maintenance allows scheduling the maintenance at a time when it is most cost-effective. Predictive maintenance is less expensive and time consuming than the traditional preventive maintenance, in which the machinery parts are replaced using the theoretical expected life, replacing parts which could be fit for purpose.

Bearings are vital components found in the vast majority of rotating machines. Bearings have received considerable attention as the majority of the rotating machinery problems are caused by faulty bearings [2]. While the price of a single bearing is minimal, there are greater costs associated with bearing failures that may cause a forced shut-down [3].

The gearbox is another key component in rotating machines and the costs associated with gearbox maintenance are high. As an illustrative example, the failure of the gearbox contributes 21% to the total downtime of wind turbines [4]. Gearbox failure not only increases the costs associated with machinery down-time but also causes fatalities. A helicopter crashed in the North Sea in 2007 due to a catastrophic failure in the gearbox, resulting in the death of 16 passengers

on board [5]. Thus, if faults in gearboxes go undetected, they can incur high costs and a reduction in safety.

In addition, generally throughout industry, there is a direction towards increased speed of rotating machinery [6]. This trend brings machine operation close to critical speeds and for this reason misalignment is becoming an increasingly important consideration in rotating machines. Misalignment occurs when two or more shafts in a rotating machine are not on the same centreline. Misalignment problems may cause up to 70% of the vibration problems observed in rotating machines [7].

There are numerous CM techniques being used to assess the integrity of rotating machinery including vibration analysis, oil analysis, motor current signature analysis and thermography. However, in recent years, acoustic emission (AE) has become a prevalent field for research as CM technique. AE technique provides two advantages to CM of rotating machinery, (i) fault detection at an early stage and (ii) the application for low speed rotating machine diagnosis, which is not achievable with the most established technique, vibration analysis [8]. AE has been applied as a non-destructive technique for fault detection for the last 50 years in several applications including monitoring the integrity of structures, pressure vessels, pipelines and rotating machinery. However, only a limited number of AE products for monitoring rotating machinery in comparison with vibration analysis are currently in the market [9, 10].

The main limitations of AE applied to rotating machinery fault detection are due to (i) the difficulty in processing, interpreting and classifying the information extracted from the signals, (ii) high levels of noise and (iii) the attenuation of the AE signals, particularly through joints [11][12]. Particularly, AE measurements are generally of low magnitude due to the high attenuation in the transmission of AE signals from the source to the sensor, which is normally installed in the component housing. This reduces the effectiveness of the AE for fault detection at an early stage. Thus, further investigation has to be carried out to apply AE for machinery early stage fault diagnosis as a reliable solution.

Hence, the ultimate aim of this research is concerned with the development of advance signal processing techniques to detect defects at an early stage in roller bearings and straight bevel gears. This is achieved by increasing the Signal-to-Noise Ratio (SNR) of the AE signals generated by the friction between the defects and other components, reducing the AE noise from other sources. Thus, the combination of Wavelet Packets (WP), Hilbert Transform (HT), Autocorrelation Function (ACF) and Fast Fourier Transform (FFT) analysis was investigated for this purpose.

In addition, the detection of shaft angular misalignment using AE technique is investigated in this thesis. This is a new application of AE which increases the fault detection capabilities of this technique. This investigation seeks to allow the use of AE technique not only as a complementary technique, as it is described in the literature [13], but as a technique that can detect a broad range of faults in rotating machinery.

1.2. Aims of the research

In the recent years CM systems are being adopted more and more in industrial plants as they provide resource savings and increase safety. As explained in the previous section, AE provides numerous advantages to CM of rotating machinery. However, to become a widely implemented technique some drawbacks of CM, highlighted in the previous section, have to be overcome. This research attempts to overcome some of these drawbacks. Thus, the specific objectives of this research are:

- To review the state of the art of fault detection in rotating machinery using AE.
- To develop novel algorithms using advanced signal processing techniques for bearings and gears in early stage defect detection.
- To validate the effectiveness of the novel algorithms in tapered bearings, spherical bearings and straight bevel gears with both seeded and naturally developed defects.

- To investigate the potential detection of shaft angular misalignment (SAM) using AE by studying the impact of operational conditions.

1.3. Methodology

Noise reduction in the AE signal is the main challenge to detect defects at an early stage. The selection of suitable signal processing techniques for this purpose was the initial task. A preliminary experiment was carried out capturing AE signals from defected and non-defected bearings in order to find the similarities and differences between the signals and determine the most appropriate signal processing techniques. The signals obtained were decomposed in the time-frequency domain (to determine the frequency components present in the signals). It was observed that most of the AE noise was produced by normal bearing operation while the AE generated by neighbouring components were present in the 100-250 kHz band. As a result, frequency based technique for de-noising, was expected to provide an increased SNR in the AE signals. Thus, WP was selected to enhance the performance of envelope analysis due to its optimum resolution at high frequencies [14]. Furthermore, the ACF was investigated as a post-processor in combination with WP to increase the SNR of the AE signals.

Once the method was formulated, it was validated in different conditions. Firstly, an experiment investigating the effect of different SNR conditions was conducted. Noise baseline addition up to 21 dB was accomplished to increase the noise in the AE signal generated in a defected bearing to simulate extremely low SNR conditions. In addition, experiments were conducted to analyse the performance of the proposed method to assess the algorithm detecting tapered roller bearings outer race defects and straight bevel gear defects. Furthermore, to validate the algorithm in industrial conditions, a spherical roller bearing with fatigue developed spall in the outer race was employed.

The potential use of AE to detect shaft misalignment was also investigated. Misalignment is a major source of vibrations in rotating machinery [15]. Thus, the early detection of this fault is crucial to avoid machinery failures. In order to investigate the impact of operational conditions

on SAM detection using AE, 9 different conditions of load and speed were examined in a test rig. The results obtained with AE were also compared with the well-known acceleration spectrum.

1.4. Organisation of the thesis

Chapter 2 provides a broad overview to the research background including basic principles of AE, AE applied to rotating machinery fault diagnosis, AE sensors and basic principles of bearings and gearboxes. Chapter 3 presents a review of published literature of AE applied to rotating machinery fault detection including time-domain methods, wavelet transform, envelope analysis, classification methods and cyclostationarity analysis. In addition, a comparison between different CM techniques is also presented in chapter 3. Chapter 4 presents a novel method for bearing localised defect detection at an early stage using AE. Chapter 5 presents further validation of the previous method in gears and a spherical roller bearing. These include naturally developed defects in the bearing outer race and gear fault detection. Chapter 6 presents a novel application of AE. This is SAM detection. The results of AE are compared with acceleration spectrum analysis. The conclusions of the research are further discussed in chapter 7, where the contributions to the knowledge are also reviewed. In addition, further proposed work is presented in chapter 7.

1.5. Contribution to new knowledge

- **Combination of Wavelet Packets, Hilbert Transform and Autocorrelation function for AE signal de-noising applied to localised defect detection for bearings and gears.** This is the first time that these techniques have been combined for defect detection in rotating machinery using AE signals. The combination of these techniques significantly improves the SNR in comparison with the traditional envelope analysis by 35 dB. The method has been applied on defect detection in spherical and tapered roller

bearings and bevel gears. **This is the first know attempt to detect defects using AE on bevel gears.**

- **In general, the WP nodes corresponding to frequency bands between 250 and 750 kHz offer the optimal de-noising capabilities**. **However, the optimal frequency band varies for different conditions and is affected by the distance from the defect to the AE sensor**. The higher the distance from the AE sensor to the defect, the optimal WP node shifts to lower frequencies.
- **AE signals processed with envelope analysis show advantages in the detection of SAM over acceleration spectrum in SNR and stability for varying operational conditions.**

1.6. Publications arising from the PhD

- Juan Luis Ferrando Chacon, Estefania Artigao Andicoberry, Vassilios Kappatos, Georgios Asfis, Tat-Hean Gan and Wamadeva Balachandran "Shaft angular misalignment detection using acoustic emission" Applied Acoustics, Vol. 85, pp. 12-22, 2014.
- Juan Luis Ferrando Chacon, Vassilios Kappatos, Wamadeva Balachandran and Tat-Hean Gan "A novel approach for incipient defect detection in rolling bearings using acoustic emission technique", Applied Acoustics,Vol. 89, pp. 88–100, 2014.
- Juan Luis Ferrando Chacon, Estefania Artigao Andicoberry, Vassilios Kappatos, Mayorkinos Papaelias, Cem Selcuk and Tat-Hean Gan "An Experimental Study on the Applicability of Acoustic Emission for Wind Turbine gearbox Health Diagnosis" Low Frequency Noise, Vibration and Active Control, submitted.
- Juan Luis Ferrando Chacon, Estefania Artigao Andicoberry, Tat-Hean Gan, Georgios Asfis and Wamadeva Balachandran "A comparative study on the use

of acoustic emission and vibration analysis for angular misalignment detection using envelope analysis", The 10th International Conference on Condition Monitoring and Machinery Failure Prevention Technologies, Krakow, June 2013.

- Juan Luis Ferrando Chacon, Wamadeva Balachandran and Tat-Hean Gan "Acoustic Emission Technique Applied for Angular Misalignment Fault Detection Using Envelope Analysis"Brunel University School of Engineering and Design Research Student Conference - ResCon13, June 2013
- Juan Luis Ferrando Chacon, Wamadeva Balachandran and Tat-Hean Gan "A novel algorithm for bearing fault detection using acoustic emission"Brunel University School of Engineering and Design Research Student Conference – ResCon14, June 2014.
- Victor Kalinin, Alexander Stopps, Juan Luis Ferrando Chacon, Estefania Artigao, Vassilious Kappatos, Cem Selcuk and Tat-Hean Gan, Denja Lekou, and Ravin Ginige "The Application of Acoustic Emission and a Novel Torque sensor Design for Condition Monitoring of Wind Turbine Drivetrain", The 53rd Annual Conference of The British Institute of Non-Destructive Testing,2014.
- Victor Kalinin, Alexander Stopps, Juan Luis Ferrando Chacon, Estefania Artigao, Vassilious Kappatos, Cem Selcuk and Tat-Hean Gan, Denja Lekou, and Alvaro Garcia Ruiz, "Novel torque sensor design and enhanced envelope method of acoustic emission signals in condition monitoring of the nacelle in wind turbines" The 11th International Conference on Condition Monitoring and Machinery Failure Prevention Technologies, Manchester, 2014.

Chapter 2

Introduction to acoustic emissions and rotating machinery

2.1. Introduction

AE is a relatively new technique in CM and is not as widely applied as other techniques such as vibration and oil analysis. AE applied in rotating machinery fault diagnosis uses many terms and concepts that will be constantly used in this thesis. Therefore, a general description of the AE technique is provided. The application of AE to rotating machinery CM differs from other more

common applications such as structural or tank monitoring which will be also detailed in this chapter. In addition a brief introduction to AE sensor types and a description and the sensor calibration techniques are presented.

2.2. Basic principles of AE

AE is defined as transient elastic waves generated from a rapid release of strain energy caused by a deformation or damage within or on the surface of a material [16]. This mechanical process is attributed to various phenomena such as crack initiation and growth, deformation, rubbing, leakage, etc. The most detectible AE signals occur when a loaded material experiences plastic deformation or when a material is loaded at or near its yield stress [17]. When plastic deformation takes place, atomic planes slip past each other through the movement of dislocations. These phenomena produce elastic waves that travel in the material. Since the origin of AE activity is microscopic, the AE signal is broadband making it an efficient approach for early stage damage detection [18]. A graphical explanation is shown in Figure 2-1. It shows the AE generated by crack initiation within the material and the transmission of the AE wave to the sensor attached to the surface of the object. The AE sensor, which is usually made of piezoelectric material, transforms the elastic waves into electrical signals to be processed and analysed.

AE technique is considered a unique Non-destructive testing (NDT) technique, since in order to generate AE signals the material has to be loaded and cracks must occur. Thus, AE must be applied during loading, while other NDT techniques are applied before or after loading the specimen.

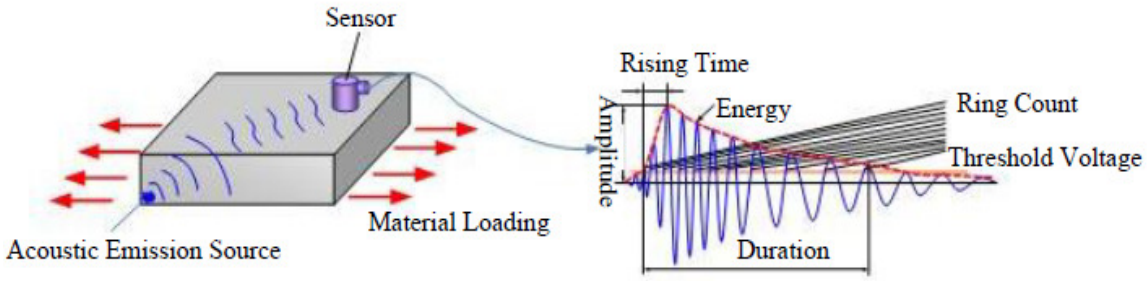

Figure 2-1: The principle of AE testing.

AE waves cover a broad frequency range between 100 kHz and 1 MHz [19]. Because of the high frequency content of the AE signals, attenuation is a major obstacle for this technique. In general, the attenuation is linearly dependent on frequency [20] and occurs due to several factors. The most important ones are geometric spreading, scattering and absorption. When the source is close to the sensing element, the most influential factor is geometric spreading. However, at longer distances the scattering and energy absorption dominate [21]. Furthermore, a considerable attenuation is also produced when the AE signal crosses joints.

In general, overall ultrasound attenuation is characterized by the following exponential decrease of the pressure amplitude p and of the amplitude of the acoustic intensity I with the traveling distance z [22]:

$$p = p_0 e^{-\alpha z} \tag{2.1}$$

$$I = I_0 e^{-2\alpha z} \tag{2.2}$$

where p_0 and I_0 are the pressure and intensity at z = 0, respectively. The coefficient $\alpha$is the pressure frequency-dependent attenuation coefficient expressed as:

$$\alpha[dB \cdot cm^{-1}] = \frac{1}{z} \cdot 10ln\frac{I_0}{I} = 8.68\alpha[cm^{-1}] \tag{2.3}$$

In order to artificially simulate AE events to evaluate the attenuation of the waves in certain material, or to test the coupling between the sensor and the surface, typically the Hsu-Nielsen source is used [23]. This test consists of breaking a 0.5 mm diameter pencil lead tip

approximately 3 mm by pressing it against the surface of the material. This source generates a burst similar to a natural AE event. In addition, the amplitude of the burst generated by the Hsu-Nielsen source is within the range of the common crack sources. The Hsu-Nielsen source has become accepted as a simulation for AE sources. The signals recorded by the measuring system are a function of source effects, wave propagation effects, sensor transfer functions and instrumentation effects. An example of the effect of the transfer function of the AE sensor to the step response produced by a capillary break is show in Figure 2-2 [24]. These five graphs show the theoretical displacement produced by a capillary break in a 50mm thick steel block, the measured displacement using a capacitive sensor and the responses of 3 different AE sensors (PAC R15, PAC NANO30 AND DW B1025). While the real displacement produced by pencil lead break is impulse-like function, the responses of the different sensors to this input are attributed to the transfer function of the sensor which depends on the incident wave types as different vibration modes of a sensing element are excited non-uniquely [25].

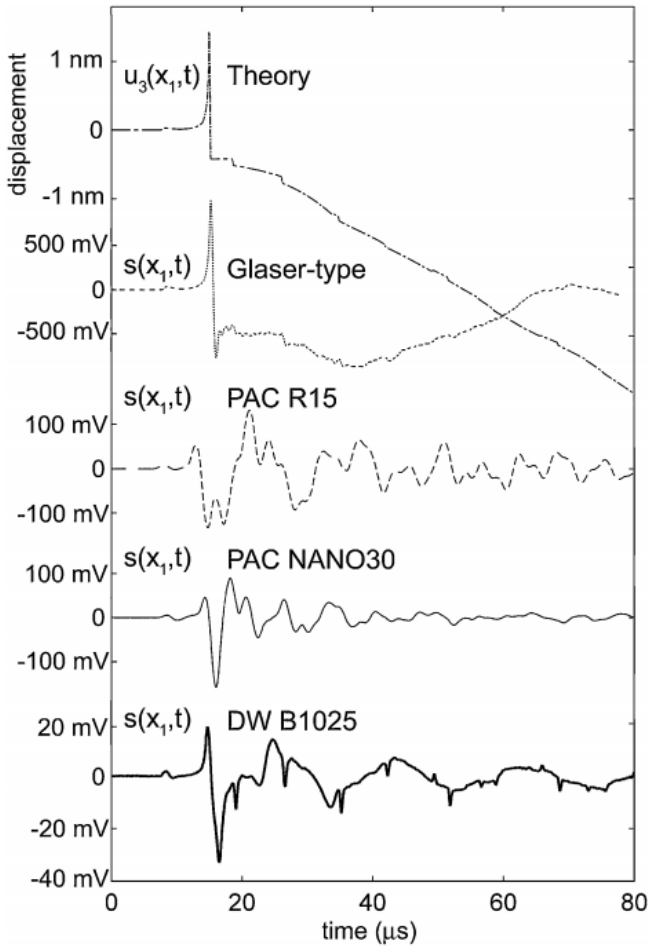

Figure 2-2: Theoretical displacement of the surface produce by capillary break and response of different type of AE sensors [24].

The usual procedure to generate an attenuation graph is to break a lead several times at different distances from the sensor and record the maximum amplitude of the signal measured. Averaging the values at each distance generates a graph recording the attenuation of the AE signal with the distance in the object under investigation. As example, Figure 2-3 shows the attenuation curve generated by performing pencil lead breaks in a steel bar. This graph is particularly important to determine the distance between sensors in a particular application.

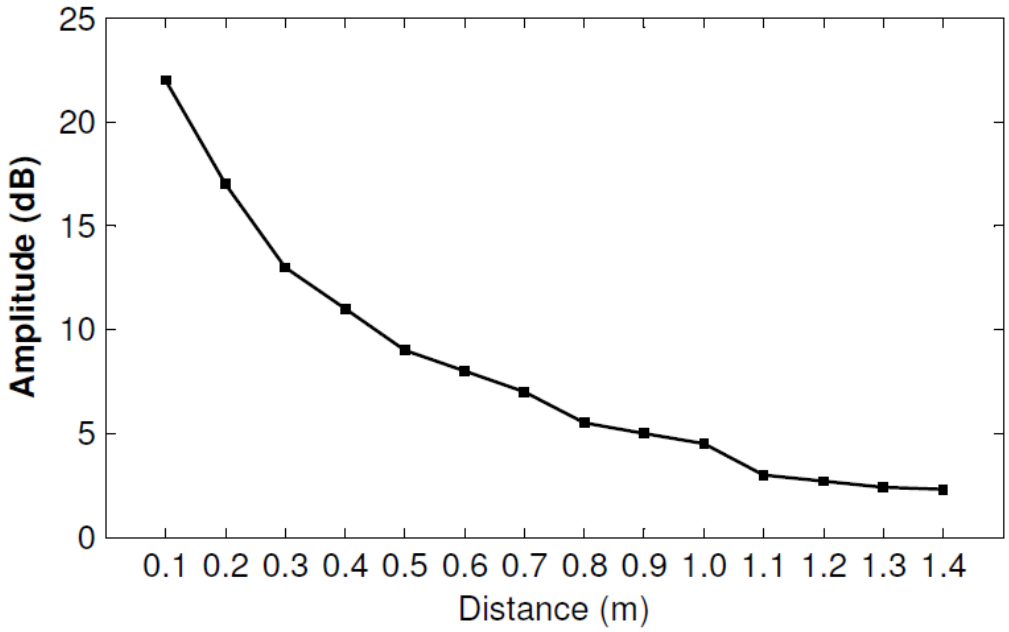

Figure 2-3: Example of the graph produced in the attenuation test.

According to the monitoring strategy, two different approaches are applied to analyse the AE signals. These are shown in Figure 2-4:

- Burst type emission: Burst type emission is expected when the monitored sources of emission are non-repeatable and occur discretely; independent in the time-domain, such as local catastrophic yielding, crack growth, cavitation, corrosion, etc.[26].
- Continuous type: Refers to a waveform where transient bursts are not discriminated. AE is produced by the overlapping of numerous individual AE

events such as those occurring in friction processes or produced by leakages in storage tanks.

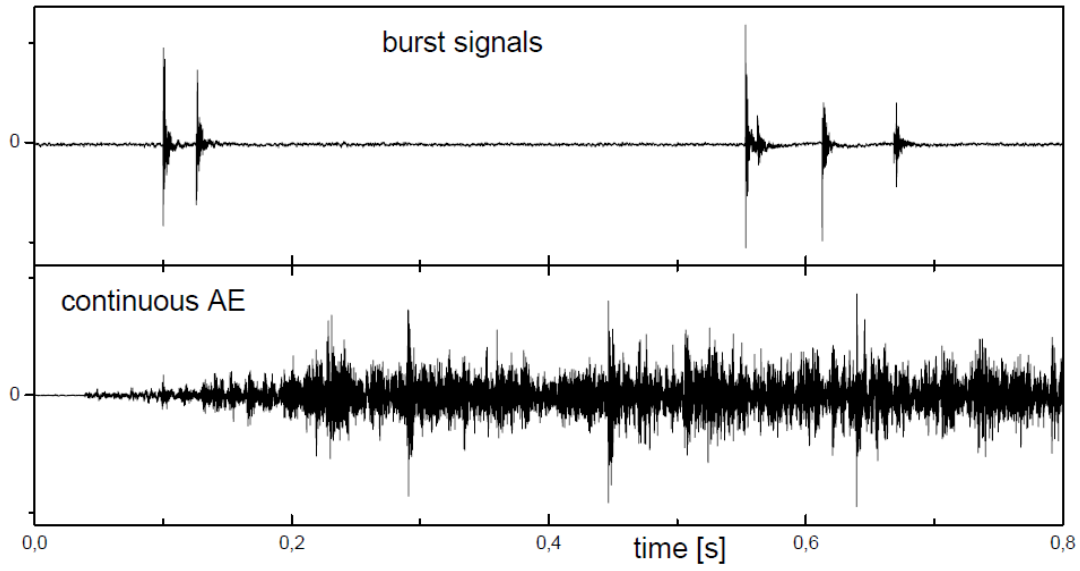

Figure 2-4: Example of burst signals compared to a continuous emission of acoustic waves [27].

2.3. Applications of AE

The different materials in which AE has been applied include the following [28]:

- Composite materials and polymers: sandwich composite, glass-reinforced plastic (GRP) and carbon fibre.
- Metals: steel, carbon steel, alloy, aluminium, aluminium alloys, magnesium alloys, and others (e.g., copper and its alloys, uranium alloys, titanium, and zirconium alloys).
- Concrete, reinforced concrete.
- Rocks.
- Wood.

AE has been applied in numerous applications to date. These applications include the following [29]:

- Behaviour of materials in metals, ceramics, composites and rocks including crack propagation, yielding, fatigue, corrosion, stress corrosion, creep, fibre fracture and delamination.
- Non-destructive testing during manufacturing processes: material processing, phase transformation in metals and alloys (martensitic transformation), detects defects, fabrication, deforming processes, welding and brazing and weld monitoring for process control.
- Continuous monitoring and periodic testing (pressure vessels, pipelines, bridges, cables), loose part detection, leak detection and rotating machinery fault detection
- Special applications: petrochemical and chemical (storage tanks, reactor vessels, offshore platforms, drill pipe, pipelines, valves), electric utilities (nuclear reactor vessels, piping, steam generators, ceramic insulators, transformers, aerial devices), aircraft and aerospace (fatigue cracks, corrosion, composite structures) and electronics (loose particles in electronic components, bonding, substrate cracking).

2.4. AE in rotating machinery

AE accompanies most of the known processes occurring in solids [30]. In rotating machinery, AE is defined as transient elastic waves generated by the interaction of two surfaces in relative motion [31]. Sources of AE in rotating machinery include impacting, cyclic fatigue, leakage, friction, material loss, etc. [12]. In rotating machinery, friction-related processes are the main source of AE. Several physical and chemical processes occur simultaneously in friction. The principal are mechanical and chemical interaction of surfaces in contact, structural and chemical changes and damage of surfaces. The main sources of AE in friction are the following [30]:

- Elastic interaction, impacts
- Changes in stress-strain state of a local volume of solid surface layer

- Plastic deformation, damage
- Generation, motion and interaction of dislocations
- Energy liberation at repeated deformation or phase hardening-weakening and damage of surface layer
- Changes in friction surface structure
- Formation of microcracks, micropores and new surfaces because of wear
- Appearance of wear debris
- Surface spalling and formation of fatigue pit

The key advantage AE in monitoring rotating machinery is that it offers earlier defect detection than other techniques [32]. In addition, it also offers other benefits such as subsurface crack detection and the fact that the high frequency content of AE signals makes it immune to machinery noise (usually <50 kHz) which can be eliminated using a simple high pass filter [33] .

2.5. AE sensors

AE sensors are usually made of piezoelectric materials. These materials have the characteristic of generating electric fields when they undergo deformation. The Output signal is a function of the displacement of the measured surface in contact with the sensor. The function is not only dependent on time but also on the position within the measurement area of the transducer. AE sensors are sensitive to displacement normal to the surface in which they are installed [34]. The type of sensor selected strongly influence the shape of the electrical signal measured due to the different sensitivity, frequency response, temperature impact, resonant frequency and directionality.

The most widely used material of this type is lead zirconate titanate (PZT) because it offers the highest sensitivity among the piezoelectric sensors. Also, there are other type of AE sensors in the market including interferometers and capacitance sensors. Interferometers are utilised when sensitivity at higher frequencies, up to several MHz, are required. The sensitivity and bandwidth of the different sensors are shown in Table 2-1.

Table 2-1: Sensitivity of different types of transducers [34].

TYPE OF TRANSDUCER	SENSITIVITY (m)	BANDWIDTH (MHz)
Piezoelectric resonant	10^{-13}	0.1 to 0.3
Piezoelectric wideband	10^{-12}	0.1 to 2
Capacitance	10^{-11}	DC to 50
Laser interferometer	10^{-10}	0.05 to 100

The piezoelectric element is enclosed in the sensor case as illustrated in Figure 2-5. It is a passive sensor and the electrical response of the sensor to the AE signals is the proportional to the weighted average of the displacement and it can be described as follows:

$$U(t) = \frac{1}{A}\iint_S u(x,y,t)r(x,y)dxdy \qquad (2.4)$$

Where $R(x,y)$ is the local sensitivity of the transducer face, S is the surface of contact, A the area of the surface S and $u(x,\mathrm{y},\mathrm{t})$ is the displacement on the surface.

Voltage generated by AE sensors are usually of very low amplitude (μV or few mV). For this reason an amplification stage is usually necessary. The most common gains used for amplifying AE signals are 20dB, 40dB and 60dB depending on the amplitude of the source.

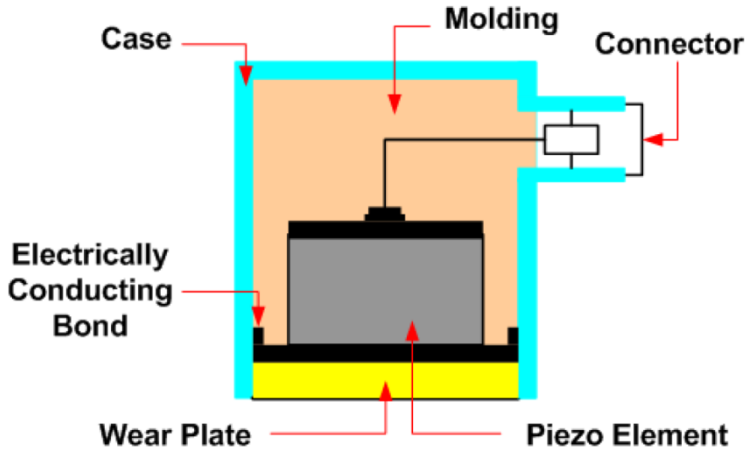

Figure 2-5: AE sensor schematic [35].

AE sensors are commonly classified into different groups:

- Wideband: The frequency response of these sensors is wide, sometimes up to 2 MHz and considerably flat. The drawback is the low sensitivity which produces lower voltage for the same displacement than resonant sensors. These sensors are used when frequency analysis is required in signal post-processing.
- Resonant: These sensors have a narrow frequency response but the peak sensitivity is higher than wideband sensors. The size of the piezoelectric element affects the resonant frequency of the AE-sensor. In general the resonant frequency is higher for smaller piezo-elements [36]. The most common resonant frequencies of these sensors are in the range between 150 and 300 kHz.

In rotating machines, the AE sensors should be placed close to potentially faulty components and in the same location from one test to the next. Locating sensors onto rotating parts would also improve fault detection significantly [37].

2.5.1. AE sensor calibration

The objective of the sensor calibration is to find the response of the sensor to an input signal at different frequencies. A typical calibration graph of a sensor can be found in Figure 2-6.

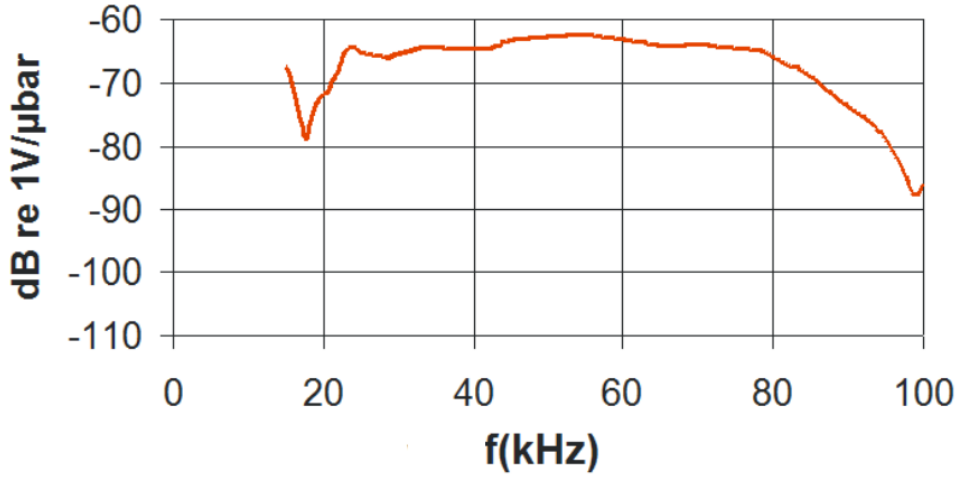

Figure 2-6: Example of a typical AE sensor calibration graph [38].

Sensor calibration is carried out using the following approaches [34]:

- Primary calibration: For this type of calibration the absolute value of the input signal and waveform are needed. A source with known characteristics must be provided. In [39] and [40] two different primary method of calibration are described (step function and reciprocity). In step function calibration a standard reference capacitance transducer is used and the step-force is generated by the fracture of a glass capillary. The response of the sensor being calibrated to the step-force source is compared with the reference transducer, which measures the surface displacement due to the elastic surface waves. In reciprocity calibrations two different sensors are used, the emitter and the receiver. The current absorbed by the emitter and voltage across the receiving sensor are captured. This process is repeated for three AE sensor pairs. Then the voltages and currents acquired from these sensors are processed to obtain the frequency response[41].

- Secondary calibration: In this case a reference sensor with known characteristics is required. The calibration process is carried out comparing the outputs of that sensor and the one that has to be calibrated. The information given by the second calibration is more limited than the primary in terms of frequency and error of calibration [42].

2.5.2. Couplants for AE sensors

The use of a couplant is of high importance when the sensor is attached to the surface to obtain measurements with high SNR. The couplant works matching acoustic impedance between the AE sensor and the surface in which it is attached, impeding the air to be in the contact area between the sensor and the surface. The acoustic impedance (Z) of material is defined as:

$$Z = \rho V \tag{2.5}$$

where ρ is the density and V the velocity of the acoustic waves in the material.

Due to the low acoustic impedance of air in comparison with contact surfaces, it allows very little transmission of acoustic energy at the typical frequencies of AE. Thus, the use of a couplant can greatly improve this transmission by around 2 times at 100 kHz and more than 10 times at 500 kHz [43]. Figure 2-7 shows the difference in transmission among different common AE couplants for different frequencies. A description of the application procedure and further details can be found in the "ATSME Standard Guide for Mounting Piezoelectric Acoustic Emission Sensors" [44].

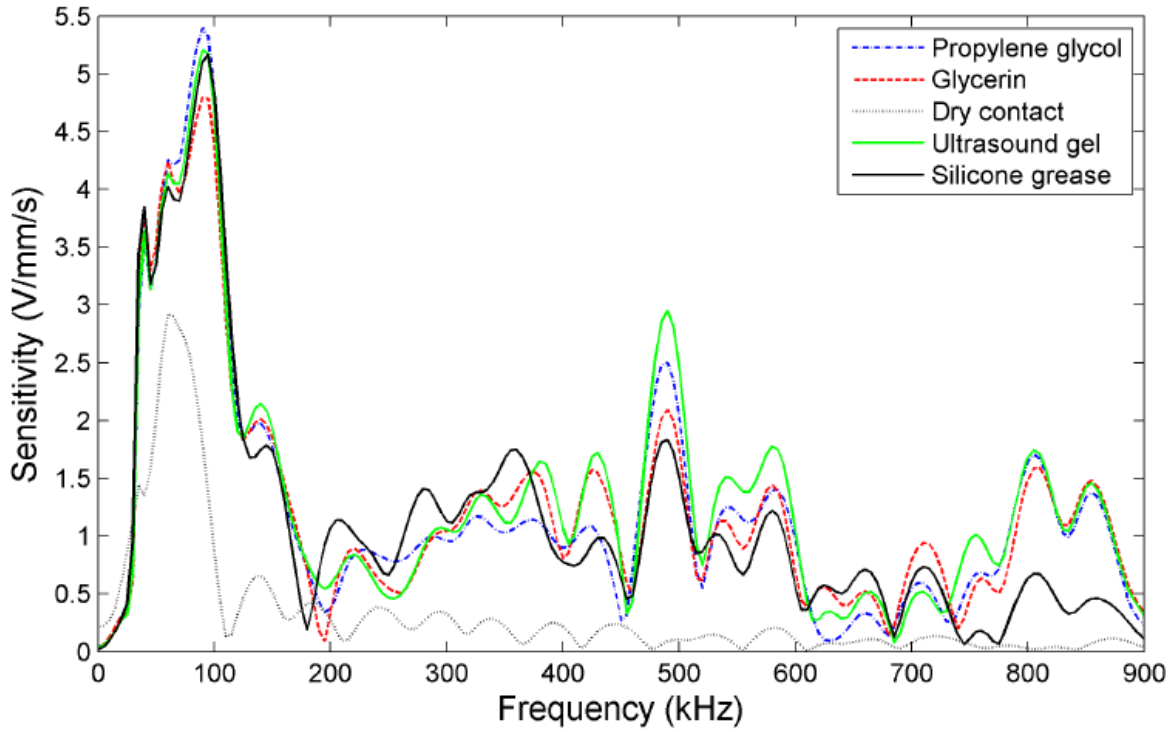

Figure 2-7: Sensitivity of AE sensor using different couplants [43].

2.6. Bearings

Bearings are mechanical devices that allow relative motion between two surfaces with restricted friction. Bearings are found widespread in domestic and industrial applications and are critical components of rotating machinery. Bearing monitoring has received considerable attention as the majority of the problems with rotating machinery are caused by faulty bearings [2]. Hence, the detection of faults in bearing using CM systems is of high importance to avoid these problems. The roller bearings consist of an inner race, outer race, rolling elements and cage (Figure 2-8).

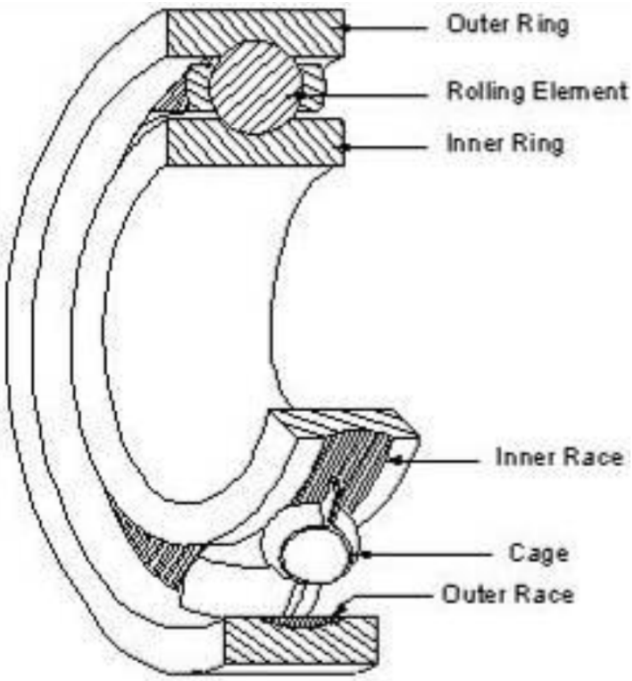

Figure 2-8: Bearing components [45].

There are numerous types of bearings in the market. The type of bearing is selected mainly according to the type of operation and the load and speed of the application. The most widely used types of bearings are the following:

- Plain bearing: It consists just in two surfaces in relative motion with lubrication and no rolling elements are used.
- Magnetic bearing: The load is supported by a magnetic field. This is applied to very high rotating speed machines. The main inconvenience of this is that it requires power to generate the magnetic field.
- Fluid bearing: This type of bearing supports the load using a thin layer of gas or fluid. The main disadvantage is that the power consumption is higher than roller bearings.
- Rolling-element bearing such as ball bearings and roller bearings. In this group the most common types are the followings:
    - Ball Bearing: This type of bearings is very common in rotating machines acting as support by reducing the friction and providing a

smoother operation for the machine. It consists of a large outer ring, a small inner ring, balls between the rings and a cage to prevent the balls collision.

- Cylindrical Roller Bearings: In this type of bearing, the rolling is done by the cylinders leading to better distributing of loads across the broader surface by having a greater contact area with linear contact area with outer ring. As a result, they are suitable for high speed applications as they support a relatively high radial capacity of load.
- Tapered Roller Bearing: They are made of a tapered inner and outer ring which results in enduring high combined load, such as continuously acting radial and axial loads. To provide true rolling and low friction, the projection of the raceway lines meet on a common point on the axis.
- Needle Roller Bearing: The advantages of this type of bearings are (i) smaller cross-section, (ii) higher load-carrying capacity, (iii) greater rigidity and (iv) lower inertia forces. They are suitable for use under severe condition.
- Spherical Bearing: As the spherical bearing allows angular rotation, they are good at accommodating misalignment as they are suitable for movement oscillation.

The failure of bearings consists of the following stages[46]:

- Pre-failure: This is the first stage of bearing failure. In this stage micro-cracks and microscopic spalls are developed. An important advantage of AE is that it is sensitive to micro-crack initiation and growth in metals [47] and consequently is capable of detecting defects at this stage.

- Failure: In this stage the cracks and spalls grow and are visible to the human eye. Several localised defects can appear in the surface of the bearing components.
- Catastrophic failure: This stage leads to a rapid failure of the bearing. Significant increases in temperature are caused as result.

The expected life of a bearing for a particular operational condition of load and speed can be easily calculated. The logarithm of the reciprocal of the probability of survival S can be expressed as a power function of the orthogonal shear stress τ_0 life N, depth to the maximum orthogonal shear stress Z_0 and stressed volume V, i.e. [48],

$$ln\frac{1}{S} = \frac{\tau_o^{C_1} N^e}{Z_0^{C_2}} V \tag{2.6}$$

Where e is the Wiebul factor, $C_{1,2}$ are material dependent coefficients with values functions of elasticity, fracture and fatigue limit, and,

$$V = alZ_0 \tag{2.7}$$

where a is the semi major axis of the Hertzian contact ellipse, and l the length of the running track of the race. Then,

$$ln\frac{1}{S} = \frac{\tau_o^{C_1} N^e al}{Z_0^{C_2-1}} \tag{2.8}$$

The rating life of a group of identical bearings is generally defined as the number of revolutions (or operating time at a stated speed) which will be attained by 90% of the group before replacement is necessary[49]. The normal failure mode of a bearing is flaking or spalling. These phenomena are caused by rapid metal fatigue in cyclically stressed surfaces. However, in most cases the failure occurs previous to the expected life. There are many causes for this including overload, inadequate or unsuitable lubrication, careless handling, ineffective sealing, or fits that are too tight, with resultant insufficient internal bearing clearance [50]. The most common bearing failure modes are the following:

- Flaking or spalling
- True brinelling
- False brinelling
- Overheating
- Overload
- Oil contamination
- Lubricant failure
- Corrosion
- Misalignment

2.7. Gearboxes

A Gearbox consists of gears and gear trains to generate speed and torque conversions from a rotating source to another device. Gearboxes are widespread in industrial and domestic applications for automobiles and wind turbines. The main components that are included in any gearbox are bearings, gears and shafts (Figure 2-9). There is a variety of gear types for transmission; however, spur and helical gears are the most common. Spur gears are the simplest type of gear, consisting of a cylinder or disk with teeth along the edge and each tooth being straight and parallel to the axis of rotation. This type of gear is used for low operational speeds. On the other hand, with helical gears the edges of the teeth are not parallel to the axis of rotation but at an angle. This angle provides a smoother operation than spur gears which makes it an efficient solution in high torque and high speed applications. Bevel gears are used when the axes of the two shafts intersect; the surfaces of the gears have a conical shape. Other types of gears also found in different applications are hypoid, worm, double helical, etc.

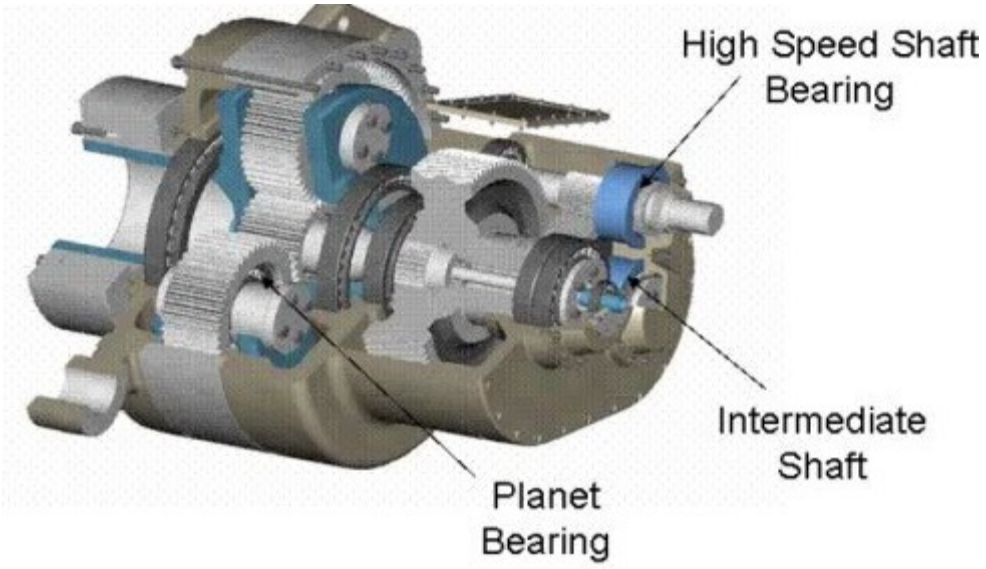

Figure 2-9: Gearbox schematic [51].

Although kinematic the motion of a pair of gears is analogous to that of a pair of two pitch cylinders which roll without slip, the action on the meshing teeth consists of a combination of both rolling and sliding. Gear tooth sliding velocity is defined as the difference between rolling velocities between during the mesh. The equation to calculate the sliding velocity is as follows:

$$V_s = V_{RPA} - V_{RGA} \tag{2.9}$$

Where Vs is the sliding velocity, V_{rpa} is the rolling velocity at a point A, pinion and V_{rga} is the rolling velocity.

Chapter 3

Literature review

3.1. Introduction

This state of the art commences with an overview of the signal processing techniques using for fault detection in rotating machinery using AE. Next, a detailed literature review is given regarding the rotor dynamic faults, emphasizing the misalignments. Furthermore, a description of bearing and gear fault detection using AE is presented. This literature review concludes with a

discussion of other techniques applied in CM including vibration analysis, oil analysis, thermography and torque and a comparison between them.

3.2. Signal processing techniques applied for AE for rotating machinery fault diagnosis

In this section the signal processing techniques for AE monitoring in rotating machinery are explained. The traditional method and most commonly applied due to the simplicity, is to extract features from the time-domain signal and assess these parameters to detect increasing trends which are associated to bearing deterioration. However, more advanced signal processing techniques including wavelet transform (WT), classification methods, cyclostationarity theory and envelope analysis are also explained. Numerous techniques applied to AE have been extracted from vibration literature. However, because the characteristics of AE signals are quite different from those of the vibration signals acquired by accelerometers, this signal processing methods have to be reconsidered to be applied to AE signals [52]. Thus, techniques that have been successfully applied in vibration signals may not be able to be applied directly to AE signals.

3.2.1. Time-domain methods

In order to characterise the AE signals acquired the most applied and simple approach is to extract the features from the time-domain signal and trend them finding increasing patterns that are related with particular faults. Rotating machinery failure modes such as spalling, pitting, flaking, oil contaminants, oil starvation, etc. produce an increase in AE features that can lead to diagnosis of the fault.

One of the most common features extracted from AE signals is the root mean square (RMS). This is a statistical measure of the magnitude of a varying quantity. An increase in the global signal produced by a distributed defect or oil starvation is expected to show an increase in this feature. Mathematically the RMS of a signal $x(t)$between the instants T1 and T2 it is defined as:

$$RMS = \sqrt{\frac{1}{T_2 - T_1}\int_{T_1}^{T_2}[x(t)]^2 dt} \quad (3.1)$$

where x(t) is the signal in the time domain.

Several studies were published investigating the influence on this feature produced by the introduction of defect in bearings. Al-Ghamda and Mba [53] studied the effect on AE RMS and vibration RMS produced by a radially loaded bearing, increasing defect size. The defects were artificially seeded in the outer race. They concluded that AE RMS increased with increasing defect severity. The authors also highlighted the high impact of load and speed on the AE RMS.

The energy is a measure of the true energy and is derived from the integral of the squared voltage. It calculates the area defined by the signal curve. The energy E_s of a signal $x(t)$ is defined as:

$$E_s = \int_{-\infty}^{\infty} |x(t)|^2 \, dt \quad (3.2)$$

The peak amplitude is the maximum voltage value in the signal. Tandon and Nakra [54] evaluated the peak amplitude value as parameter for defect detection in roller bearings. They concluded that AE peak amplitude provided an indication of defects irrespective of the defect size.

The crest factor (CF) is calculated from the peak amplitude of the waveform divided by the RMS value of the waveform. The CF of an AE signal provides an estimate of the amount of impact wear in a bearing. However, the CF is a reliable indicator only in the presence of incipient defects while it does not respond enough to significantly increasing damage in the bearing; as the damage increased CF values reduced to the undamaged levels [55].

$$CF = \frac{|x|_{peak}}{x_{rms}} \quad (3.3)$$

Information entropy (IE) is usually defined as a measure of uncertainty of a process. As the working condition of a machine system deteriorates due to the initiation and/or progression of structural defects, the number of frequency components contained in the AE signal increase,

resulting in a decrease in its regularity and an increase in its corresponding information entropy value. Elforjani et al. [55] showed that, by employing information entropy, the presence of a crack onset and its propagation in bearings can be detected by the AE technique. The IE of a discrete random variable x is defined as:

$$IE = -\sum_{i=1}^{N} P_i \cdot \log(P_i) \tag{3.4}$$

Where P is the probability mass function.

Counts is possibly the most employed feature for defect detection in roller bearings. Counts is defined as the number of times that a predefined threshold is crossed by the AE signal. Choudhary et al. [56] applied AE for different size defect identification at changing the rotating speed of the rig. It was observed that AE counts were low for defect-free bearings. They also observed that speed had a direct impact in the counts parameter. The threshold selection is one of the conventional questions to extract this feature. Changing the threshold level will have a significant impact in the count number. However, as discussed in [57], the relationship between bearing mechanical integrity and AE counts is independent of the chosen threshold level, although a threshold of at least 30% of the lowest speed and load operating condition is recommended.

3.2.2. Wavelet transform

The WT is a mathematical tool which transforms sequential data in time axis to the spectral data in both time and frequency [58]. In contrast with sinusoids, wavelets are localised in both the time and frequency domains, so wavelet signal processing is suitable for non-stationary signals, whose spectral content changes over time. Thus, due to the AE signals generated by a defected bearing are intrinsically non-stationary and the outstanding ability WT to analyse these non-stationary signals, the WT provide an improvement in the diagnosis of the bearing integrity.

A comparison of the performances of different time-frequency analysis methods is shown in Table 3-1.

Table 3-1: Comparison of different time-frequency analysis methods [59].

Method	Resolution	Interference term	Speed
Continuous Wavelet Transform (CWT)	Good frequency resolution and low time resolution for low-frequency components; low frequency resolution and good time resolution for high-frequency components	No	Fast
Short Time Fourier transform (STFT)	Dependent on window function, good time or frequency resolution	No	Slower than CWT
Wigner–Ville distribution (WVD)	Good time and frequency resolution	Severe interference terms	Slower than STFT
Choi–Willams distribution (CWD)	Good time and frequency resolution	Less interference terms than WVD	Very slow
Cone-shaped distribution (CSD)	Good time and frequency resolution	Less interference terms then CWD	Very slow

The application of WT to rotating machinery fault diagnosis is quite extensive, particularly in vibration analysis. Yan et al. reviewed the application of wavelets for fault diagnosis in rotating machinery [60]. One of the most effective applications of wavelets is noise reduction. The wavelet transform-based method can produce considerable higher de-noising quality than conventional methods [61][62]. It has been applied in two different approaches, single-scale, in which a certain wavelet node is chosen as the most efficient de-noising the AE signal from an unwanted noise source and multi-scale, in which different scales are used to characterise or de-noise the AE signal. The main application of the first is to select the most efficient bandwidth of the vibrations signals as pre-processor in the envelope analysis when the resonance frequency of the bearing is unknown. Traditionally, DWT decomposition tree has been applied to AE and

vibration signals to for signal de-noising. However, this decomposition filter may not be precise enough to obtain necessary information from the signal. A more detailed frequency resolution can be obtained by implementing WP transform to the signal. The WP is a generalization of the Wavelet decomposition that offers further decomposition. In the DWT, each decomposition level is calculated by passing the wavelet approximation coefficients through low and high pass quadrature mirror filters (Figure 3-1). The n-level decomposition generates n+1 wavelet nodes.

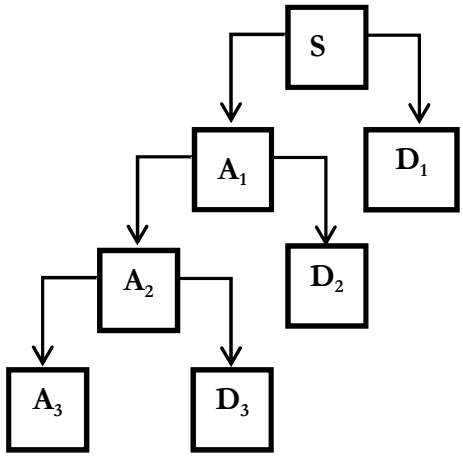

Figure 3-1: 3-level DWT decomposition tree.

However in the WP, both the detail and approximation coefficients are decomposed. This generates more than 2n-1 different decompositions. This is known as a WP decomposition tree (Figure 3-2). It should be noted that the DWT decomposition tree is part of the WP decomposition tree.

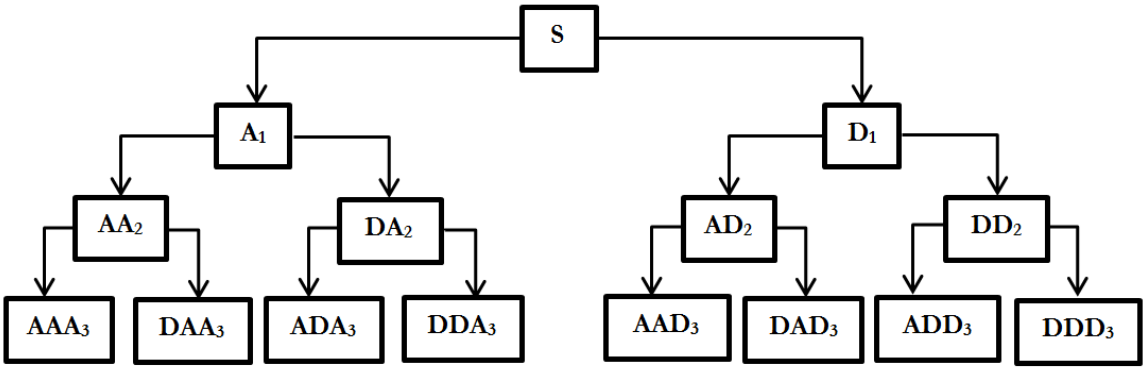

Figure 3-2: 3-Level WP decomposition tree.

One of the few investigations about the application of WP to AE signals was carried out by Feng and Schlindwein [63] who developed a new technique using the normalised wavelet packets quantifiers as a new tool for CM using AE. However, the bandwidth in which the WP analysis was performed was limited. The authors used a sampling rate of 200 kHz and they downsampled the signals to 80 kHz. Therefore, the effective bandwidth of the analysis was reduced to 40 kHz. They investigated the detection of two different faults, localised defect and oil contamination. The authors concluded that applying this novel signal processing technique, both localised defects and advanced contamination faults can be detected and the WP relative energy of band B (20, 30kHz) was the optimal quantifier. Wang et al. [65] investigated the propagation of the AE signal across turbine runners using WP. The authors indicated that WP is an effective tool in extracting the attenuation characteristics of the AE signal.

Bo and Yu [66] studied the application of the Db6 Wavelet for bearing defect detection. Two different cases were studied, roller defected bearings and grease contamination. The type of defect created was not detailed. The authors concluded that the bands of 125-250 kHz and 250-500 kHz contained most of the information regarding the defect and grease contamination respectively. Feng et al. [61]studied de-noising problem of AE signal by using DWT thresholding methods. The Donoho-Johnstone threshold method [67] and parameter method were studied and compared in order to reduce the noise in the AE. Law et al. [68] presented an approach based on WP decomposition and Hilbert-Huang transform (WPD-HHT) for spindle bearings CM. The authors remarked that the simulated results showed that the method was effective for detecting all instantaneous frequencies. Loutas et al. [69] performed a study in a single-stage gearbox with artificially induced gear cracks using AE and vibration analysis. They extracted conventional parameters from both AE and vibration signals as well as some novel parameters such as energy and entropy extracted from the WT nodes.

3.2.3. Classification methods

Different classification methods have been applied to categorise the data obtained from AE sensors. Among them, artificial neural networks (ANN) have been possibly the most investigated

classification method. This approach has been applied to rotating machinery fault detection to solve the problem of the complex classification process. ANN can model complex relationships between inputs and outputs to find patterns in data. It is an imitation of the human brain, where information processing is performed. An ANN is composed of units call neurons. Every neuron receives an input through connexions and generates an output. The output is composed through three functions:

1 The propagation function. It is generally the sum of each input multiplied by the weight of the interconnection.

2 An activation function that modifies the previous one. It can be removed and the propagation function is used as output.

3 A transfer function that is applied to the output value of the activation function. It is used to limit the output of the neuron. The most common are the sigmoid function with output values between 0 and 1, and the hyperbolic function with output values between -1 and 1.

The ANN is trained to recognise signals from a healthy component and then indicates when the AE deviates from this normal condition. In general, the ANN does not process the raw AE signal. Contrary, it uses as input the results of various processing techniques, such as features extracted from the time domain signal or wavelet analysis, learning how these techniques perform with of healthy and faulty data. Taha and Widiyati[70] applied two different learning tasks for ANN, function approximation and pattern recognition, for detection and monitoring of defects in ball bearing. They concluded that function approximation learning tasks are more accurate than pattern recognition learning tasks for ball bearing defect monitoring. In [71] the authors investigated a combination of continuous WT to extract several features from a sound signal, acquired using a microphone, and ANN for classification for gearbox fault detection. The authors pointed out that the sound emission can be used to monitor the condition of the gear-set platform and the proposed system achieved a fault recognition rate of 98% in the experimental

gear-set platform. Al-Raheem et al. [72] applied the Laplace-Wavelet to identify bearing fault characteristic frequencies classifying the data using three types of ANN, namely, Multilayer Perceptron with BP algorithm, Radial Basis Function network, and Probabilistic Neural Network. The results showed the relative effectiveness of the three classifiers in detection of the bearing condition with different learning speeds and success rates.

Support vector machine is also a classification technique that has been applied with AE signals for fault detection in rotating machinery. Support vector machines are supervised learning models with associated learning algorithms that analyse data and recognise patterns, used for classification and regression analysis. It was first introduced by Vladimir Vapnik for the problem of pattern recognition. Samanta et al. [73] compared the performance of bearing fault detection using two different classifiers, namely, ANN and support vector machines. They used six features from the signals and gave 100% classification for both ANNs and SVMs. The authors concluded the potential application of genetic algorithms for the selection of features and the classification of the parameters in machine condition detection. Widodo et al. [74] applied multi-class relevance vector machine for defect detection in low speed bearings. This study was aimed at finding a reliable method for low speed machines fault diagnosis based on AE signal. The result showed that multi-class relevance vector machine offers a promising approach for fault diagnosis of low speed machines.

3.2.4. Envelope analysis

Envelope analysis is a well-known technique used to detect periodic variations in the amplitude of the signal. It is widely used in vibration analysis to detect localised defects. It is usually accomplished using the following procedure: (i) band pass filter (ii) signal rectification (iii) Hilbert transform and (iv) spectral analysis. In the first step, the signal is filtered around the resonance frequency of the bearing. However, in AE, as the resonant frequency is not a matter of study since this frequency is considered as noise (vibrations) by the band pass filtered and is generally excluded from the process. When the envelope is extracted, the time-domain signal is

transformed into the frequency domain using a FFT to study the frequency content of the demodulated signal. The frequencies presented in this spectrum are related to the defected bearing component. They can be calculated as follows:

$$\mathrm{BPFI} = \frac{\mathrm{Nb}}{2} \cdot \mathrm{S}\left(1 + \frac{\mathrm{Bd}}{\mathrm{Pd}}\cos\emptyset\right) \tag{3.5}$$

$$\mathrm{BPFO} = \frac{\mathrm{Nb}}{2} \cdot \mathrm{S}\left(1 - \frac{\mathrm{Bd}}{\mathrm{Pd}}\cos\emptyset\right) \tag{3.6}$$

$$\mathrm{BSF} = \frac{\mathrm{Pd}}{2\mathrm{Bd}} \cdot \mathrm{S}\left(1 - \left(\frac{\mathrm{Bd}}{\mathrm{Pd}}\right)^2 (\cos\emptyset)^2\right) \tag{3.7}$$

$$\mathrm{FTF} = \frac{\mathrm{S}}{2}\left[1 - \left(\frac{\mathrm{Bd}}{\mathrm{Pd}}\cos\emptyset\right)\right] \tag{3.8}$$

RPM – Revolutions per minute

S- Revolutions per second or relative speed difference between inner and outer race

BPFI – Ball pass frequency of inner race

BPFO – Ball pass frequency of outer race

BFS – Ball spin frequency

FTF – Fundamental train frequency

Bd – Ball or roller diameter

Nb – Number of balls or rollers

Pd – Pitch diameter

ϕ- Contact angle

The most common technique to extract the envelope to the AE signals is the HT. Applying HT to the signal provides some additional information about the amplitude, instantaneous phase and frequency of vibrations [75]. The Hilbert Transform $h(t)$ of a function $x(t)$ is defined as:

$$h(t) = H\{x(t)\} = \frac{1}{\pi}\int_{-\infty}^{\infty} \frac{x(\tau)}{t-\tau} d\tau \quad (3.9)$$

The HT of $x(t)$ ($H\{x(t)\}$) is the convolution of $x(t)$with the signal $1/\pi t$. Hence, it can be interpreted as the output of a system linear time-invariant system with input $h(t)$ and impulse response $1/\pi t$. The envelope analysis technique was successfully applied using AE signals for bearing localised defect detection by Elforjani and Mba [55]. Further explanation of envelope extraction is presented in section 4.2.

Several enhancements to the traditional envelope analysis have been studied in the recent years. Most of the studies were performed for vibration analysis. On the other hand, studies to enhance the envelope analysis for AE signals have been limited. Kim et al. [76] proposed the DWT as pre-processor to de-noise the AE signal for gearbox defect detection. Because of the complex process to determine the optimum frequency band to extract the envelope, WT was used as a pre-processor, decomposing the signal in different frequency bands. The authors achieved improved results determining the characteristic fault frequencies in gear fault detection using the DWT as pre-processor for the envelope analysis.

3.2.5. Cyclostationarity theory

Increasing interest is growing in the recent years around Cyclostationarity analysis in machinery fault detection. This technique has been applied previously in several applications such as telecommunications, telemetry, radar and sonar applications. Wide-sense cyclostationary stochastic processes have autocorrelation functions that vary periodically with time [77]. A random signal $x(t)$ is considered cyclostationary if it satisfies the following:

- It is cyclostationary with respect to the mean, namely, the mean of the signal is a periodic function:

$$E[x(t+T_o)] = E[x(t)] \tag{3.10}$$

- It is cyclostationary in the autocorrelation domain with period T_0 as follows:

$$R_x(t, t+\tau) = R_x(t+T_o, t+T_o+\tau) \tag{3.11}$$

The earliest studies regarding the application of cyclostationarity theory in machinery fault detection were performed by Randal and Antoni using vibration signals [78]. The application of this technique to vibration analysis is quite extensive. However, only a small number of studies have been published for AE. Kilundu et al. [79] presented a study that characterises the cyclostationary aspect of AE signals acquired from a defective bearing. The authors compared the cyclic spectral correlation, a tool dedicated to evidence the presence of cyclostationarity, with the traditional envelope analysis. This comparison revealed that the cyclic spectral correlation was more efficient than the traditional envelope analysis to identify the defect present in the bearing outer race. However, this success was not found with inner race defects. Molina Vicuña[80] introduced the cyclostationary character of AE signals acquired from a planetary gearbox. The authors indicated the need for higher cyclic frequency resolution. However, this was not done due to the high computational demands needed. Thus, this investigation emphasises the main drawback of the cyclostationarity analysis, which is the inapplicability for real-time diagnosis due to the high computational complexity [81].

3.2.6. Other methods

Lin et al. [82] accomplished an investigation into the application of Hilbert-Huang transform to bearing fault detection in winds turbine using AE. The results obtained showed that AE in the wind turbine bearing can be described in terms of features like frequency and energy, and inferences can be made about the kinds of damage processes taking place in the bearing. Thus, the Hilbert-Huang transform analysis method has a good potential for the AE signal processing in wind turbines. Lin et al. [83] presented a practical approach for CM of low speed machinery using Peak-Hold-Down algorithm. The purpose of this method was to reduce the amount of data in order to enable rapid data transfer in remote CM application, particularly for low speed

rotating machinery in which the amount of data is large. He et al. [84] combined short-time RMS and autocorrelation function for bearing defect diagnosis. The results showed that the proposed method is effective to extract the characteristic frequency of the bearing using the AE signals. Shiroishi et al. [85] combined the high frequency resonance technique (HFRT) and adaptive line enhancer (ALE) to detect localised defects using AE and vibration measurements. They concluded that the proposed method applied to AE signals were better than vibration in detecting outer race defects but the AE sensor was not sensitive to the inner race defects tested. In [86] the authors applied morphological filtering to eliminate colour noise in frequency domain to de-noise the AE signal acquired from a defected bearing. The simulation results showed that that the proposed methodology can achieve significant noise reduction, and is beneficial to the subsequent processing and analysis of signals.

3.3. AE for the detection of rotor-dynamic faults

Common rotor-dynamic faults include self-excited vibration, generated due to system instability, and, vibration produced by externally applied load, such as cracked rotors or bent shafts, misalignment and unbalance [87].The diagnostics of rotor faults has been gaining importance in recent years [88]. These types of faults generate frictional rubbing between the rotor and the static components such as bearings. The rotor-dynamic faults generate partial or continuous interactions. The first type produces brief intermittent contacts and the second describes more constant contact between rotor and stator. Several authors have investigated the AE generated birotor-stator interaction. Zhansheng Liu et. Al [89] compared vibration analysis and AE for the detection of the seal rubbing on a rotor rig. The authors conclude that AE offered earlier fault detection than vibration analysis, allowing the user to detect the rubbing-impact of the rotor system, unachievable with vibration analysis. Hall and Mba [90] proved the use of Kolmogorov-Smirnov statistics for discriminating different classes of shaft-seal rubbing. Again, Hall and Mba [91] presented a case study to investigate the rotor-stator rubbing in an operational 500 MEW turbine using AE. The authors were able to locate the position of the rubbing using phase delay between adjacent AE modulations.

Although several studies have been conducted to detect rotor-stator interaction using AE, no detailed investigation regarding the rotor-stator AE signals produced by misalignment has been investigated. As one of the topics of this thesis is misalignment fault detection using AE, the state of the art of misalignment fault is presented. Traditionally, vibration analysis has been applied to detect this type of faults in rotating machinery. However, it presents some drawbacks that are discussed in the next section.

3.3.1. Misalignment

Shaft misalignment occurs when the shafts are not on the same centreline. Misalignment is one of the most common faults and yet it is still not fully understood [92]. There are two different types of shaft misalignment: (i) shaft angular misalignment in which shaft centrelines intersect, and (ii) shaft parallel misalignment in which shaft centrelines are parallel (Figure 3-3). In fact, in most cases the misalignment is caused by a combination of both.

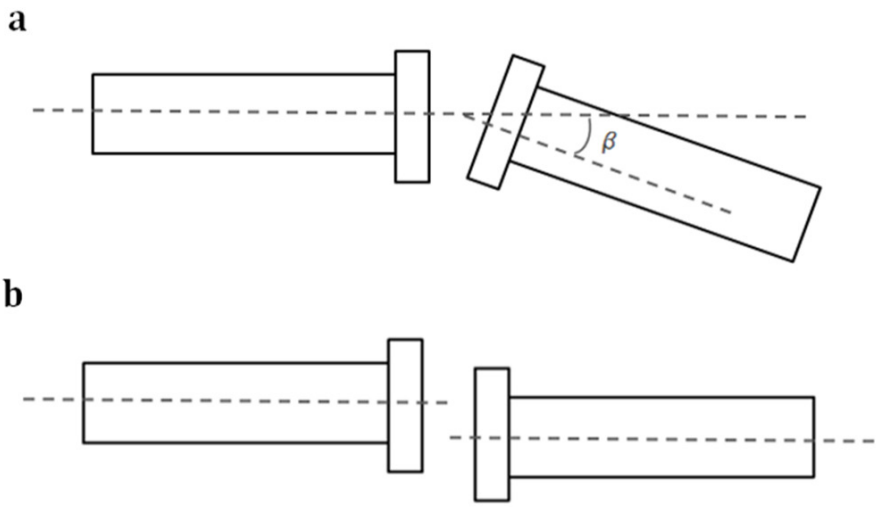

Figure 3-3: Graphical explanation of (a) SAM and (b) parallel misalignment.

Several studies have been accomplished on misaligned shaft dynamics, including modelling its effects. Most of these studies show the main peak at the shaft rotation frequency (1X) and smaller peaks at the harmonic frequencies (2X, 3X and 4X) in the vibration spectrum. Pennacchi et al. [93] presented a study in order to model this fault accurately. The ratios of 1X/2X, 1X/3X and 1X/4X harmonics of vibration signals in bearings were investigated, showing changes

according to the severity of parallel and angular misalignment. They concluded that (i) nonlinear effects are evident in both types of misalignment and (ii) the ratio between the higher harmonic components and the 1X component in angular misalignment is greater than parallel misalignment. Hili et al. [94] carried out a study of angular misalignment characterization and developed a theoretical model. They found three characteristic peak frequencies in the shaft behaviour: (i) the most prominent being at 1X; (ii) a smaller peak at 2X; and (iii) the last peak corresponding to the natural frequency of the system. Sidebands of the rotation frequency around it were also visible. Al-Hussain [95] presented a study of the effect of angular misalignment of two rigid rotors connected through a flexible mechanical coupling. The results showed that an increase in angular misalignment, or mechanical coupling stiffness terms, leads to an increase of the model stability region. However, the variability of the signature, produced by misalignment at different operational conditions of load and speed in the vibration spectrum, is one of the main drawbacks of vibration analysis [96]. Toth and Ganeriwala [97] studied the vibration signature for misalignment under a varying operating and design conditions such as speed, type and level of misalignment, coupling types and machinery dynamic stiffness. The aim was to develop a misalignment model and diagnostics procedure. Measurements were performed at three different shaft speeds, using three types of couplings, rigid, spiral and rubber, three shaft diameters and multiple misalignment configurations which include parallel and angular types with three different severity levels. The results indicated that the rotor speed, the coupling and shaft stiffness, have high impact on the vibration signature. The authors concluded that the signature of misalignment produced in vibration spectrum was unsteady for different operational conditions.

Although several AE studies have been conducted to detect crack onset and propagation, spalls and wear using AE technique, the detection of rotor-dynamic faults such as misalignment using AE technique has not been fully investigated. One of the studies regarding this problem was carried out by Gu et al. [98]. The combination of WT and envelope analysis was applied to the AE signals captured from a misaligned and defected gearbox. Misalignment was created by a

twisted case caused by arc-welding to fix the base. They found a peak at 1X in the spectrum of the envelope AE signal that was attributed to gear misalignment. Toutountzakis and Mba [99] presented an experimental investigation on the application of AE for gear defect diagnosis. They observed that the AE RMS and energy were greater with misalignment than was observed for background noise under defect free conditions. Sikorska and Mba [37] indicated that misalignment generates low frequency modulation of the background continuous AE level also common in reciprocating machinery signals. However, in this study, they refer to this modulation produced in the AE signals as noise that can limits the detection of other faults. However, in this thesis, that modulation is investigated in detail to detect misalignment at different load and speed conditions.

3.4. Sources of noise in AE

AE has shown to be more reliable in early stage defect detection than vibration analysis in numerous investigations [100]. However, AE signals produced by early stage defect are usually of low amplitude. Thus, since AE signals generally contain high levels of noise, this must be reduced in order to detect faults at an early stage.

In AE, what is considered as noise varies from one application to the next. The noise in the AE signal may come from the following sources [37]:

i. Distorted signal components due to beyond the limits of mechanisms in the signal acquisition process including periodic transient events, such as valve activity, electro-magnetic interference and radio frequency interference.
ii. Residual, periodic electronic noise generated or captured in the electronic components (amplifier, power supply, filter, data acquisition card).
iii. Quasi-periodic transient impulses such as wear of seals or bearing localised defects (when not looking for incipient seal or bearing faults).

iv. Modulation produced at low frequency in the AE signal due to shaft or gear misalignment or reciprocating machines.

v. AE noise from mechanisms of no interest to the analysis being performed. These include AE activity generated by the operation of healthy machines.

Due to the diversity of sources and the high level of the noise in AE signals, one of the most investigated topics in the application of AE to rotating machinery is the AE signal de-noising. Thus, numerous de-noising techniques have been applied for noise suppression in the AE signal such as empirical mode decomposition, spectral kurtosis, morphological filters and Wavelet transform [19][101][86].

3.5. Influence of operational conditions on AE

3.5.1. Influence of load

Increasing the load results in an increase of the real contact area between bearing components. This is due to the increase of the contact spot number while the spot dimensions grow insignificantly [30]. The pressure undertaken by each junction is constant and thus the real contact area is proportional to the load [102]. Parameters such as RMS and counts have been demonstrated to correlate directly with increasing load [54][57].

3.5.2. Influence of speed

Increasing the rotating speed of a rotating machine has a direct impact in AE generation. Morhain and Mba [57] studied the effect of speed in the AE produced by a spherical roller bearing. They obtained a direct correlation between RMS value and rotating speed.

3.5.3. Influence of lubrication condition

Most of bearings fail because rolling elements and raceways are not properly separated by a protective lubricant film [103]. Contaminants and lubricant starvation lead to an increase in wear rate produced by an increase in asperity contact between bearing surfaces. Miettinen and

Andersson [104] accomplished an investigation to clarify how the contaminants in the grease influence the AE of the rolling bearing. They observed changes in the time-domain AE signal even with the lowest concentration of contaminants tested (0.02 weight% of quartz dust or 0.075 weight% of steel M2 powder). Furthermore, they observed that small size contaminant particles generated a higher AE pulse count level than large size particles.

3.5.4. Influence of Temperature

Tan and Mba [105] studied the effect of temperature on the AE generation in spur gears. They attributed the increase of AE RMS with load and speed indirectly due to an increase of oil temperature. Load and speed caused an increase in lubricant temperature. The increase of lubricant temperature leads to a reduction in lubricant film thickness and as a result the asperity contact between surfaces increases. The authors observed that the lubricant temperature is the dominant factor in the AE generation and the load or speed is a secondary factor of the oil temperature.

3.6. Fault detection in bearings using AE

Bearing failure modes include friction processes producing, seizure, flaking, fluting, spalling, pitting, etc. [12] . All these modes are known sources of AE. Several studies have been carried out to detect this type of bearing faults using AE. Tandon and Choudhury [33] reviewed vibration and AE methods to defect detection in rolling element bearings stating that AE had a promising future for bearing early defect diagnosis.

Several studies have been carried out regarding defect size identification of bearings extracting the AE features from the time-domain signal. Tandon and Nakra [54] carried out an experimental investigation regarding defect detection in the inner race, outer race and balls. The results showed that AE performed better in detecting defects in a deep grove ball bearing at lower speeds than vibration parameters such as acceleration, envelope detected acceleration, overall sound intensity and sound pressure and shock pulse. However, no information about

sensor mounting and placing was provided. The authors concluded that, in general, AE and envelope detected acceleration offered the best results in detecting defects. Mba [106] studied the changes produced in AE signals by changing the speed, load and defect size in the outer and inner race. The authors observed that increases in rotational speed and load produced an increment in RMS value. Small and large defects introduced in the outer race resulted in an increase in RMS value. In the case of defects in the inner race, the same tendency was not observed with line defects. The author concluded that RMS values and counts were validated as a robust technique for detecting bearing damage using AE. Al-Ghamda and D. Mba[53] investigated the relationship between AE RMS value, amplitude and kurtosis for different defect sizes. In addition, the authors also studied the dominant source of AE generated by seeded defects. The authors concluded that the primary source of AE was the material protrusions above the mean surface roughness and the burst duration was directly correlated to the seeded defect length along the race in the direction of the rolling action. Tandon and Nakra [107] performed a comparative study between AE and vibration analysis for bearing defect detection. The vibration and acoustic measurements performed were: overall vibration acceleration, envelope detected acceleration, overall sound intensity and sound pressure, shock pulse, and AE ringdown counts and peak amplitude. They concluded that in general, the detectability of defects at lower speeds is highest by acoustic emission and lowest by the shock pulse method. Saad Al-Dossary et al [108] investigated the application AE for characterising the defect sizes on a radially loaded bearing. They observed that the energy values correlated with increase defect severity for inner and outer race. Furthermore, burst duration was shown to be as a good parameter to find geometric size of outer race. However, this does not apply to the inner race. Tandon et al. [109] investigated the detection of inner and outer race bearing faults of different sizes at different loads. They observed that AE peak amplitude and shock pulse maximum normalised value level increase as defect size increases. They concluded that AE performed better identifying the defects than vibration analysis and motor current signature analysis.

Al-Balushi et al. [110] proposed an Energy Index technique for detecting masked AE signatures associated with the loss of mechanical integrity in bearings. Energy Index tested under both simulated and real AE signals. The Energy Index is defined as the square of the ratio of RMS of a part of a signal to the RMS. of the entire signal. The equation to calculate the Energy Index is as follows:

$$Energy\ Index = \left(\frac{RMS_{segment}}{RMS_{total}}\right)^{N} \tag{3.12}$$

By increasing the power (N) of the Energy Index, the values that are above the average RMS are amplified and those that are below the average RMS are highly attenuated. The main advantage of this technique is the suitability for detecting short duration AE burst even where SNR is low. The authors concluded that Energy Index technique was effective in detecting AE burst buried in random noise offering an improvement in the diagnosis. However, no information about sensors, mounting, amplification or filtering was provided.

In the recent past there have been investigations regarding AE in low speed rotating machinery. The importance of these studies lies with the limitations of vibration analysis to be applied for fault detection in low speed rotating machinery [111]. Thus, complementary CM techniques such as AE are applied in this case.

To date, most of the investigations regarding defect detection in bearings were accomplished in artificially defected bearings. A small number of publications have addressed the detection of naturally developed defects. One of them was accomplished by Elforjani and Mba [55], who presented a study about the detection of degradation in bearings at low speeds. To accelerate the bearing degradation, one race of the thrust ball bearing was replaced with the flat race of the thrust roller bearing. A housing was constructed to allow placement of sensors directly into the race. The authors introduced information entropy as a new method to detect degradation in bearings and applied three non-linear power spectral estimation methods (Prony's Energy Method, Eigen-Analysis and Auto-regressive). Prony's Energy method showed an advantage over the other techniques in that it could produce relatively large frequency components. They

also correlated AE burst duration with defect size obtaining positive results. Nohál et al [100] investigated the detection and monitoring of the onset and propagation of natural defects of steel specimens using AE technique. To assess the deterioration of the bearing the authors extracted RMS and counts using different threshold levels from the time-domain AE signal. They also compared the performance of AE with vibration analysis. In the test performed, the authors observed that AE was able to identify the micropitting in the bearing race, while the changes in the vibration signal only started in the latest stage of deterioration, when a large spall in the race arouse.

3.7. Fault detection in gears using AE

The AE technique applied to gearbox fault detection is still in its infancy. Only a few publications have assessed the possibility to apply AE technique in gearboxes. One of the earliest investigations of AE in gearboxes was carried out by Miyachika et al [112]. The study consisted of bending fatigue testing using AE technique in spur gears. Three different gears were used; two of them were made of SC415 hardened steel and the other made of S45C steel without hardening. The parameters obtained from this investigation were frequency spectrum, cumulative event count, peak amplitude and event count rate. The authors concluded that the prediction of crack initiation was possible only for hardened gear but not for normalised gears.

Eftekharnejad and Mba [113] presented a study to detect different size seeded faults in steel helical gears. An AE sensor was attached to the gearbox pinion. The signals acquired were compared with vibration analysis. In order to control the temperature a thermocouple was installed in the oil bath. To produce the faults a drill was used. The authors extracted two conclusions. Firstly, the observation that seeded defects in helical gears was evident in AE waveform. This is not the case reported for spur gears by Toutountzakis et al [114]. Secondly, the direct relation between volume of defect and RMS of the AE signals.

Tan et al. [115] carried out a study with spur gears in which they stated that the protrusions produced around the edge of the seeded defect were the cause of AE activity.

Toutountzakis and Mba [99] investigated the relation between background AE noise and rotational speed in oil bath lubricated gearboxes with and without misalignment. The gear set employed was made of 045M15 steel with no heat treatment. A constant torque was applied in all tests. Two AE sensors were used, one attached to the driven gear wheel and the other on the ball bearing casing of the driven gear wheel shaft. Energy and RMS values were processed in real time. The background noise was evaluated at 600, 1300 and 1800 rpm, initially with misalignment and in a later stage, without misalignment. In the case with no defects the results were that increasing rotational speed resulted in an increment in AE RMS and energy in both AE sensors. The change in rotational speed resulted in a significant increment of RMS and energy values but a gradual decrease of these values to a base level was observed. In the investigation with misalignment at 1300 rpm the AE values showed indications of reaching a base level, as in the previous case, but the values began to rise and move upwards in both sensors. The method to produce the misalignment in the rig is not described in the paper as well as the grade of misalignment produced. The author highlighted the viability of AE for gear defect diagnosis and the possibility to detect the gear defect from the bearing casing. Loutas et al. [69] carried out a study on a single stage gearbox with artificial defects with emphasis on the signal processing. The aim of this investigation was to extract conventional parameters as well as novel parameters using also wavelet analysis to link them with fault progression. In addition, the authors compared them with the well-known vibration analysis. The defect consists of a transverse cut of 25% of root thickness of the tooth. In conclusion the author emphasised the superiority of AE technique over vibration regarding the detection of early crack propagation.

Raka Hamzah and Mba [116] presented an experimental study which correlated AE activity to different load and speed conditions during the operation of a set of helical and spur gears. The gearboxes used were lubricated by an oil bath. Test gears were made of 045M15 steel with no heat treatment. A thermocouple was employed to measure lubricant and gear metal temperature. They noticed that the specific film was related with AE RMS in both helical and spur gears. However, when AE levels were higher for helical gears, the relative changes in AE levels as a

function of changes in specific film thickness were higher for spur gears. As for the effect of speed it was noticed that an increase in speed resulted in an increase of AE RMS for all load conditions. The authors concluded that AE is more sensitive to changes in specific film thickness under combination of rolling and sliding (spur gear) than pure rolling (helical). Furthermore, the variations in AE levels in helical gearboxes are attributed not only to the influence of asperity levels but also to the variation in the contact length during meshing.

Eftekharnejad et al. [117] compared motor current signature analysis (MCSA), vibration and AE to identify the presence of a naturally fatigued pinion shaft in an operating gearbox. However, during the tests the transmission shaft fatigued unexpectedly. This naturally fatigued shaft offered an opportunity to assess the potential of the three different measuring technologies to identify this problem. The shaft was loaded until breaking andmonitored over 426 hours. Results showed that the surface damage was only detected by AE and vibration techniques while MCSA did not show any correlation. The rupture of shaft after 385 hours was detected using AE and vibration sensors but it was required to apply envelope analysis to detect it. The authors concluded that the presence of a cracked shaft was detected by all three technologies. Qu et al. [118] presented new approach combining a heterodyne based frequency reduction technique with time synchronous averaging and spectral kurtosis to process AE signals and extract features as condition indictors for gear fault detection. Partial tooth cut faults were seeded in a gearbox test rig and experimentally tested. Condition indicators, such as RMS, kurtosis, and crest factor, were computed from the raw signals applying time synchronous averaging. The authors concluded that among all indicators investigated, kurtosis related condition indicators showed the best performance of detecting the gear tooth crack in all the testing conditions.

3.8. Other condition monitoring techniques

3.8.1. Vibration analysis

The use of vibration analysis is one of the fundamental tools for CM. It has been developed extensively over a period of approximately 35 years [119]. This technology is currently the most

widespread method for CM in rotating machinery. It can be utilised in all rotating equipment on site. It is used to isolate the location of damage to rotating components, as well as to inform quantitatively about the amount of damage produced.

The type of sensors used depends on the frequency range. Position, velocity and acceleration are measured for low, medium and high frequency respectively. The change in the system vibrations can be produced by cracks, unbalance, misalignment, rubbing, wear, deterioration, etc.

In order to interpret the vibration signal it requires complex methods which need specialised operators. Currently there are numerous automated applications that generate data analysis automatically. The most popular method is to demodulate the vibration signal to find some frequencies on it. These frequencies correspond to certain mechanical defects in components (for example, spurious produced by bearing defect), unbalance or misalignment. By examining these frequencies the location of the problem can be identified.

The main limitation of this technique is the low sensitivity to faults at low speed [32]. Low speed rotating machinery generates relatively low energy loss rates from damage related processes and therefore vibration analysis is not as sensitive as AE [28].

3.8.2. Thermography

Slight temperature variations across a surface can be discovered with visual inspection and non-destructive testing with thermography. Inadequate lubricant, defective bearings, and misalignment can overheat couplings, shafts and gearboxes [41]. Modern infrared cameras and diagnostic software are suitable for on-line process monitoring. A typical image produced by IR camera is shown in Figure 3-4.

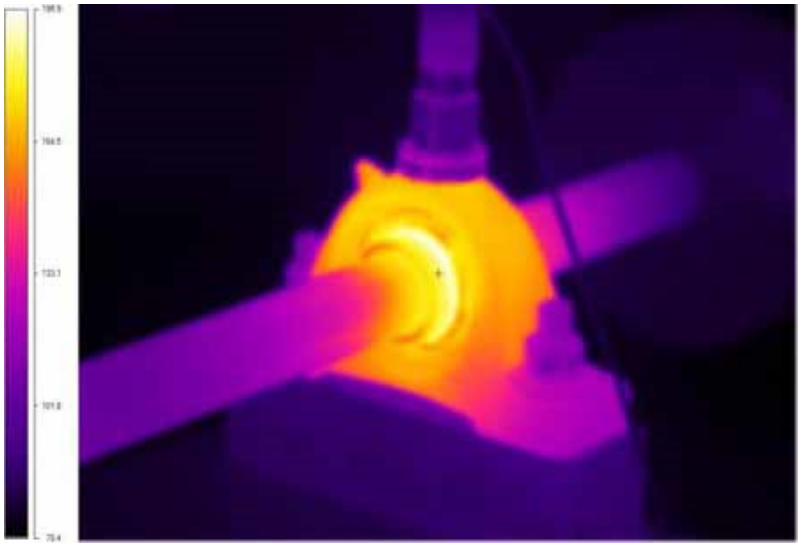

Figure 3-4: Image produced by an IR camera

In order to monitor the conditions as well as diagnose the machine faults, signal processing techniques are firstly required to process the data acquired from the machine. The most popular technique which frequently uses for processing IR signals is FFT.

3.8.3. Oil analysis

CM based on oil analysis can be used to predict failure. It is usually carried out due to two different purposes. Firstly, to find out wear debris produced by friction in machinery associated with degradation of the components. The second one is to identify the oil properties including the base oil, additives and contaminants which can produce problems in the machinery.

The main aspects that influence the condition of the lubricating oil are, elevated temperature, presence of air, water, fuel or other lubricants and solid matter including wear debris, dust and dirt[120]. Contaminants such as dust and wear debris alter the performance of lubricant. These changes always produce a change of dielectric constant in the lubricant. Therefore, any abnormal state such as contaminant ingression, wear debris or chemical products can be located by monitoring the dielectric constant of the lubricant [121].

3.8.4. Torque

Torque measurements have been utilised for rotating machinery fault detection. The rotor defects may cause either a torsional vibrations or a change in the torque-speed ratio. Such information can be used to detect rotor faults, e.g. mass imbalance [4]. The measurement of torque is of high importance for the precise machinery assembly, the improvement of machine performance and the control part about power transmission system [84].

Torque measurements are usually carried out using the next technologies:

- Strain gauges applied to a rotating shaft or axle.
- Surface acoustic wave devices attached to the shaft.
- Twist angle measurement or phase shift measurement.

3.8.5. Advantages and disadvantages of the condition monitoring methods

The Table 3-2 summarises the advantages and disadvantages of the previous explained techniques:

Table 3-2: Summary of the different condition monitoring techniques

Technique	**Advantages**	**Disadvantages**
AE	• Suitable for low speed • Early stage detection • Frequency range far from mechanical noise • Non-intrusive	• Expensive • High sampling rate which generates large amount of data • High attenuation of the AE signal, particularly in joints
Vibration analysis	• Standardised • Reliable	• Poor performance in low speed machinery • Not for early stage defect detection

Oil analysis	• Reliable	• Mostly off-line • Only applicable in lubricated parts
Thermography	• Standardised	• Expensive • Not for early stage detection • Mostly off-line
Torque	• Suitable for on-line monitoring	• Intrusive • Expensive

3.9. Summary

Although there are several techniques for monitoring rotating machinery, as discussed in section 3.8.5AE offers the advantage of earlier fault detection than other techniques. However, as presented in section 3.4, noise is a crucial problem in AE. This noise can come from several sources. One of the most important sources is genuine AE produced by neighbourhood components or AE generated within the same component under investigation that carries no information about the defect itself (i.e. noise produced by normal bearing operation when looking at localised defects). For this reason, the development of de-noising algorithms to deal with this noise is extremely important when the aim is to detect defects in early stage as the SNR is extremely low. Several de-noising techniques have been applied to date to AE. Among them, DWT has been applied to de-noise AE signals. However, as presented in section3.2.2, WP offers higher de-noising capabilities than the DWT, particularly in the high frequency range. Thus, Chapter 4 presents a study combining the use of WP as pre-processor and autocorrelation function as postprocessor for the envelope analysis for the detection of seeded localised defects in bearings using AE. Furthermore, the performance of the proposed method for detecting a naturally developed defect in the outer race of aspherical roller bearing and bevel gear defects is presented in Chapter 5.

Section 3.3.1reviewed the detection of misalignment using vibration analysis and its importance. However, it presents some drawbacks. One of them is the high impact of operational conditions in the vibration signature. For this reason, to overcome this problem, an experimental study regarding the application of AE and envelope analysis for the detection of SAM is presented in section chapter 6.

Chapter 4

Combination of Wavelet Packet and Autocorrelation function (WP-ACF) for incipient defect detection using AE

4.1. Introduction

This chapter investigates a novel technique for early stage defect detection in bearings using AE. The importance of this investigation falls on the importance of bearing monitoring as bearings are critical components in rotating machinery and the majority of machinery failures are caused by bearing malfunction [2]. In addition, in most cases the bearing failure occurs previous to the

expected life. For these reasons, this chapter describes a novel technique using AE that aims to detect bearing defects in early stage. To detect defects in early stage the reduction of the noise in the AE signals is extremely important. Numerous de-noising techniques have been developed for noise suppression in the AE signal. Possibly, the discrete wavelet transform (DWT) is the most established technique for AE signal de-noising. However, due to the fact that the decomposition treats only the approximation component at each level using the dyadic filter bank, the results of frequency resolution in higher-level DWT decompositions are less accurate [57]. It may cause problems while applying DWT in AE signals in which the important information is located in higher frequency components. Thus, the frequency resolution of the DWT may not be precise enough to extract necessary information from the decomposed component of the signal. For this reason, the Wavelet packet, which is a generalisation of WT, offers better de-noising ability for non-stationary signals such as the AE signals produced by a defected bearing.

In order to further enhance the detection of the transients produced in the early stage defect in the AE signals, the autocorrelation function is applied. The ACF is widely used to find patterns in a signal, particularly, to find periodicity in a noisy signal. This function has not been widely applied in AE bearing defect detection. The only study regarding this topic was carried out by He et al. [84] who combined short-time RMS and ACF to extract the bearing fault characteristic frequency from a defected specimen. The results showed that the proposed method was very effective in estimating the bearing fault characteristic frequency from the AE signal. However, in extremely low SNR conditions, such as those present when the defect is at an incipient state, the combination of these two techniques may not be able to extract the periodicities of the AE signal generated by the defected bearing.

In order to further de-noise the AE signal and the proposed method (WP-ACF) aims to reduce the AE generated from the normal bearing operation and to enhance the AE burst produced by localised defects. For this reason, an enhanced envelope analysis is proposed that combines WP as a pre-processor, HT for envelope extraction and ACF to find periodic patterns in the AE

envelope prior to applying the FFT to de-noise the AE signal and detect incipient defected bearings. Thus, a novel method is proposed that combines the advantages of these signal processing techniques to provide a robust and effective approach for bearing localised defect detection in low SNR conditions such as the conditions existing in the early stages of defected bearings. An experimental study using a tapered roller bearing is carried out to evaluate the reliability and effectiveness of the proposed method. Furthermore, the results obtained are compared with the traditional envelope analysis.

4.2. Problem definition and proposed method

Failure alarm for a rolling element bearing is often based on the detection of the onset of localised defects [122]. Once a localised defect emerges in the inner or outer race of the bearing, an impact occurs every time the rolling element crosses the defected area of the bearing race. As a result, a high frequency AE burst is generated periodically due to (i) elastic or plastic deformation of asperities, (ii) fracture of asperities or (iii) the adhesion between asperities [102][30]. Envelope analysis is a well-known technique for bearing fault detection and it is suitable for the detection of these types of defects. It has been applied to vibration and AE signals to detect periodic increases in the amplitude of the signal caused by defected components in bearings [55][83][123]. Typically, envelope analysis refers to the following procedures: (i) band-pass filtering (ii) signal rectification, (iii) HT and (iv) power spectrum extraction. Figure 4-1shows a visual explanation of the burst produced by the impact in the AE signal (blue) and the envelope of the AE signal is shown in red.

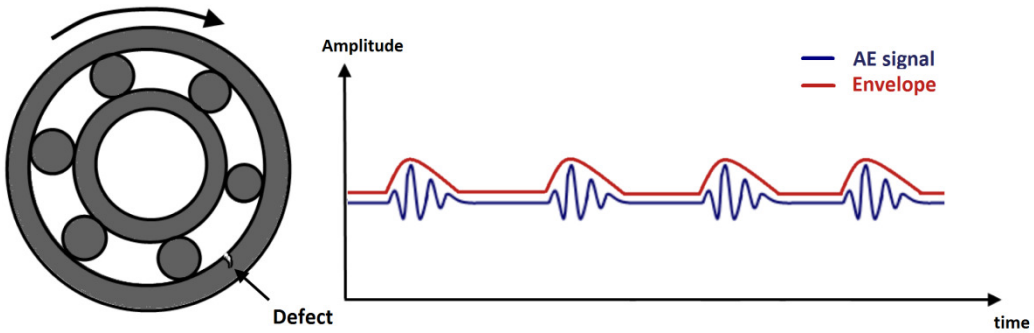

Figure 4-1: Graphical explanation of the modulation produced by a defected bearing and the envelope extraction.

However, when the defect is in an incipient state, the AE background noise caused by normal operation can be of higher amplitude than the AE burst produced by the interaction of asperities between the defected area and other components such as rolling elements. For this reason, the incipient defects are extremely difficult to detect. As a result, the envelope spectrum will not show the peak at the frequency in which the impact is produced. As an illustrative example, three different SNR scenarios simulating the AE signal produced by a defected bearing are shown in Figure 4-2. They represent the problem of the traditional envelope analysis under low SNR conditions. In high SNR condition the impacts are clearly shown in the time-domain signal and the envelope spectrum shows prominent peaks which inform about the existence of a defect in the bearing. However, in low SNR conditions the detection is not achievable using traditional envelope analysis.

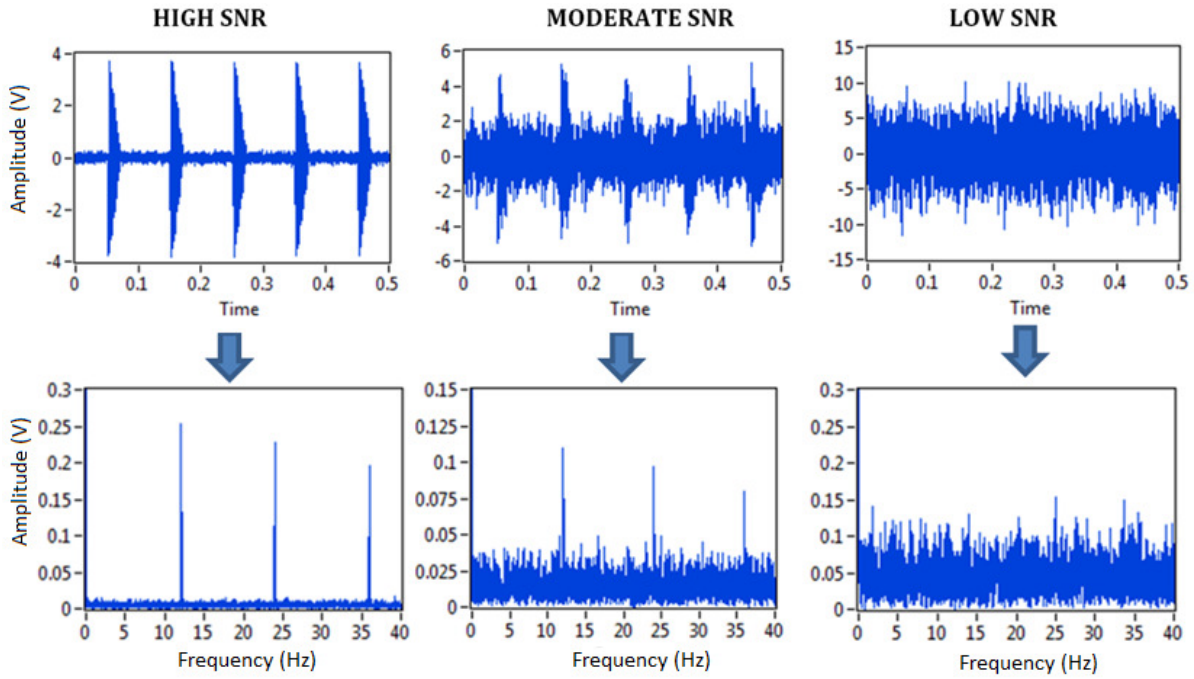

Figure 4-2: Simulated time-domain AE signal (top) and Envelope spectrum (bottom) under 3 different SNR conditions.

For this reason, the proposed method enhances the envelope analysis for low SNR conditions. It combines the HT envelope with the autocorrelation function and the WP to obtain a prominent peak in the AE envelope spectrum, even for an extremely noisy AE signal. A block diagram of the proposed method is shown in Figure 4-3. It consists of the following steps:

Step 1 ***AE signal acquisition***

Step 2 ***Signal de-noising*** using WP. The WP can be considered as a pre-processor of the proposed method. It divides the bandwidth of the signal into narrow frequency bands to select the most appropriate band with the highest SNR ratio.

Step 3 ***Envelope extraction*** applying the HT.

Step 4 ***Pattern recognition*** using the ACF. It is applied to the signal envelope to find cyclic patterns in the data produced by the impact between the rolling elements and the defect and, as a result, a cleaner envelope spectrum is obtained.

Step 5 ***Frequency domain conversion*** applying the FFT.

Step 6 ***Peak search*** to identify the peaks that indicate the existence of defects.

The output of the WP-ACF envelope is the frequency spectrum of the autocorrelation function. This spectrum shows peaks at different frequencies according to the defected component of the bearing. These are the inner race, outer race and rolling elements.

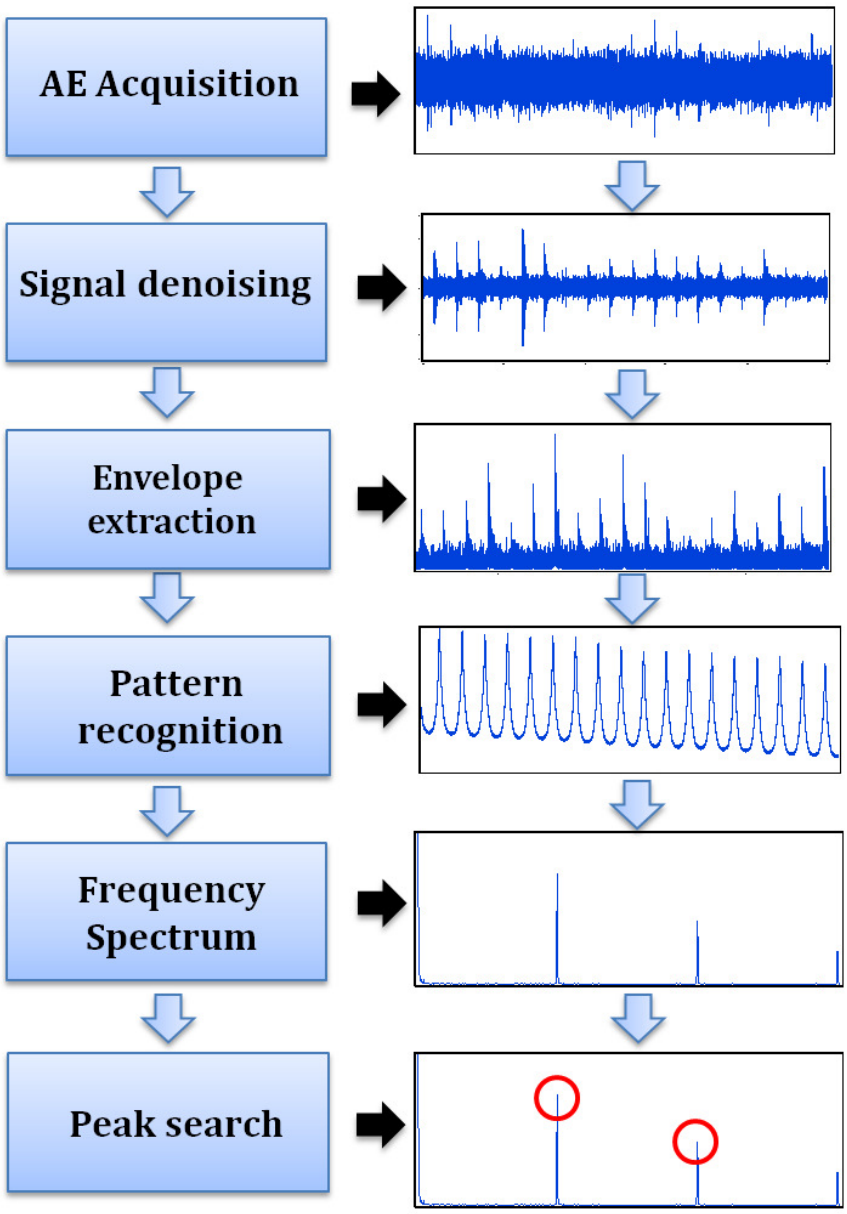

Figure 4-3: Flow chart of the proposed method.

The WP is used as pre-processor to de-noise the AE signals. WP is a generalization of wavelet decomposition. The CWT is a decomposition of an input function using scaled and translated versions of a Wavelet function known as mother Wavelet. Mathematically the Wavelet coefficients are extracted using the function below:

$$WT_{\psi}\{x\}(a,b) = \langle x, \psi_{a,b} \rangle = \int x(t)\psi_{a,b}(t)dt \tag{4.1}$$

where $\psi_{a,b}$ is the mother Wavelet which is defined as:

$$\psi_{a,b} = \frac{1}{\sqrt{a}}\psi\left(\frac{t-b}{a}\right)$$

where a and b are defined as scale and position respectively.

The DWT is the analogous mathematical tool of CWT for discrete functions. It is used for digital signal analysis. The DWT consists of identifying the parameters $c_k d_{j,k}, k \in \mathbb{N}, j \in \mathbb{N}$ of the equation:

$$f(t) = \sum_{k=-\infty}^{\infty} c_k \phi(t-k) + \sum_{k=-\infty}^{\infty} \sum_{j=0}^{\infty} d_{j,k} \psi(2^j t - k) \quad (4.2)$$

Where $\phi(t)$ and $\psi(t)$ are the function known respectively as father Wavelet and mother Wavelet. The father Wavelet is in fact a scaling function that depends on the mother Wavelet. The $\phi(t)$ and $\psi(t)$ can be calculated as sequences $h = \{h_n\} n \in \mathbb{Z}$ and $g = \{g_n\} n \in \mathbb{Z}$:

$$h_n = \langle \psi_{1,n}, \psi_{0,0} \rangle_e \psi(t) = \sqrt{2} \sum_{n\mathbb{Z}\in} h_n \, \phi(2t-n) \quad (4.3)$$

and

$$g_n = \langle \phi_{1,n}, \phi_{0,0} \rangle_e \phi(t) = \sqrt{2} \sum_{n\mathbb{Z}\in} g_n \, \phi(2t-n) \quad (4.4)$$

These two sequences are the basis of the DWT.

The common procedure of applying the DWT is through filter bank with a filter determined by the coefficients $h = \{h_n\} n \in \mathbb{Z},$ corresponding to a high-pass filter and $g = \{g_n\} n \in \mathbb{Z},$ corresponding to a low-pass filter.

The filters h and g are linear operators that can be applied to a digital input signal x as a convolution:

$$c(n) = \sum_k g(k) x(n-k) = g * x \quad (4.5)$$

and

$$d(n) = \sum_k h(k) x(n-k) = h * x \quad (4.6)$$

The signal $c(n)$ is known as approximation and $d(n)$ as detail.

It is possible to repeat the filters shown in equations 4.5 and 4.6 generating a cascade of high-pass and low-pass filters. Consequently, the results are the shown in Figure 4-4(a). This tree is known as a filter bank. However, this decomposition filter may not be precise enough to obtain necessary information from the signal. A more detailed frequency resolution can be obtained by implementing WP transform to the signal (Figure 4-4 (b)). The WP is a generalization of the Wavelet decomposition that offers further decomposition. Consequently, it provides better frequency resolution for the decomposition of the signal[124]. In a similar manner as the DWT, the WP decomposition tree is obtained by:

$$c_{j+1}^{2p}[m] = \sqrt{2}\sum_{n=-\infty}^{\infty} g[n-2m]c_j^p[n] \tag{4.7}$$

$$c_{j+1}^{2p+1}[m] = \sqrt{2}\sum_{n=-\infty}^{\infty} h[n-2m]c_j^p[n] \tag{4.8}$$

where j is the depth of the node and p indexes the nodes in the same depth, every c_j^p with p even is associated to approximations and every c_j^p with p odd is associated to details. Thus, this low pass and high pass filters are applied to the AE signal in order to select the node that offers higher de-noising capabilities.

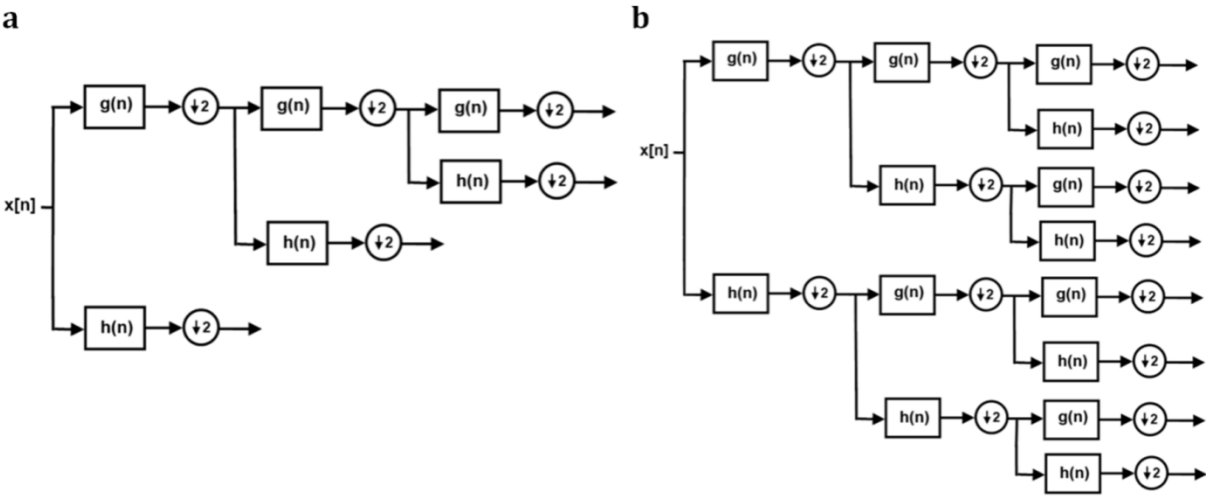

Figure 4-4: A comparison between the three-level (a) DWT and (b) WP decomposition.

Once the signal has been decomposed using in different frequency bands using the WP, the envelope of the different bands is extracted using the Hilbert transform. The HT of a discrete signal is given by the following equation:

$$H\{x[n]\} = \frac{1}{\pi}\sum_{i=-\infty}^{\infty}\frac{x[i]}{N-i} \tag{4.9}$$

Being N the number of samples and $x[i]$ the discrete samples of the signal.HT is often interpreted as a 90 degrees phase shifter. From the signal x(t), the complex analytic signal can be described as:

$$A\{x[n]\} = x[n] + jH\{x[n]\} = E[n]e^{j\varphi[n]} \quad , \tag{4.10}$$

being the modulus $E[n] = \sqrt{x[n]^2 + H\{x[n]\}^2}$ and phase $\varphi[n] = tan^{-1}(H\{x[n]\}/x[n])$ are known as the envelope and instantaneous frequency respectively.

Once the envelope has been extracted using the HT the ACF is applied to obtain the elements Y of the discrete input signal x using the following equation:

$$Y_j = \sum_{K=0}^{N-1}\overline{x_k}\cdot x_{j+k} \tag{4.11}$$

for j = –(N–1), –(N–2), …, –1, 0, 1, …, (N–2), (N–1)

where Y is the sequence whose indexing can be negative, N the number of elements in the input sequence x and $\bar{x}$is the complex conjugate of x.

The elements of the output sequence R_{xx} are related to the elements in the sequence Y by

$$R_{xx_i} = Y_{i-(N-1)} \tag{4.12}$$

for i = 0, 1, 2, … , 2N–2

The final step of the proposed method is to transform the values obtained using the ACF to the frequency domain using FFT. The FFT computes the discrete Fourier transform (DFT) of the input sequence with a fast Fourier transform algorithm. The DFT is defined as:

$$Y_k = \sum_{n=0}^{N-1} x_n e^{-j2\pi kn/N} \tag{4.13}$$

for $n = 0, 1, 2, \ldots, N-1$

where x is the input sequence, N is the number of elements of x, and Y is the transform result.

4.3. Experimental validation

In order to evaluate the performance of the WP-ACF method, an experimental investigation has been conducted using a tapered roller bearing with a seeded defect in the outer race. One AE sensor has been used to acquire the AE signals from the case of the bearing mode HR 30326J from NSK and identify the optimum wavelet parameters such as mother Wavelet, decomposition level and WP node. Noise baseline addition is applied to the signal reducing the SNR to validate the method under extremely low conditions (up to 21 dB added noise). In addition, a comparison between the proposed method and the traditional envelope analysis is also presented.

4.3.1. Experimental setup

The test rig (Figure 4-5) was designed to represent the shaft arrangement in a typical 2MW wind turbine. The shaft was supported by three test bearings; one spherical roller bearing and two tapered roller bearings. The load was generated by hydraulic actuators, applying axial and radial loads through the slave bearings. A thrust bearing was used as the axial slave bearing and a spherical bearing as the radial slave.

A 30kW motor was used to power the test rig with a nominal speed of 1650 rpm. It was controlled through a variable frequency drive that modified the rotational speed. The rated axial

and radial load of the rig was 40 kN and 140 kN, respectively. The test rig was capable of reproducing a wide range of dynamic loads typically experienced by wind turbine drive train.

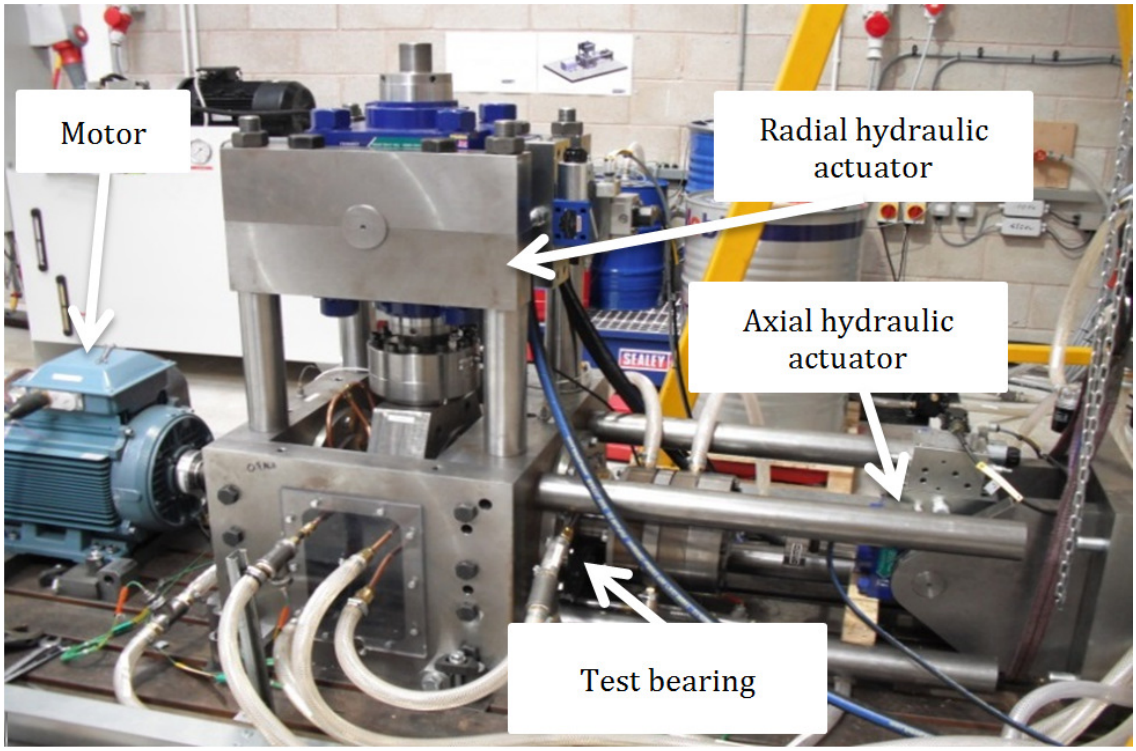

Figure 4-5: Test rig (Courtesy of Romax Technology Ltd.).

The bearing used in this investigation was NSK HR 30326J. This is a single row tapered roller bearings composed of an outer ring and an inner ring with a group of conical roller sustained by basket shape cage. The characteristics of the bearing are the following:

- Internal diameter: 130mm;
- External diameter: 280mm;
- Width: 72mm;
- Weight: 18 kg.

4.3.2. Instrumentation

One Vallen VS900RIC AE transducer was employed. This sensor was selected for this investigation due to the following reasons:

- Wideband and flat response operative from 100 kHz to 1 MHz
- High sensitivity
- It is operative in a wide range of temperatures (-40 to 85 °C).
- It includes an internal amplifier which makes the AE signals less affected by noise.

The frequency response of the sensor is displayed in Figure 4-6 showing peak sensitivity at 350 kHz.

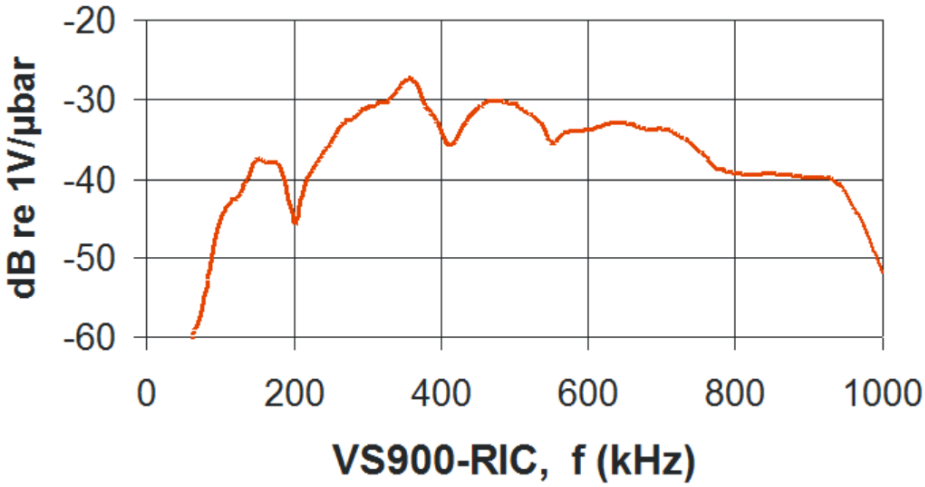

Figure 4-6: Frequency response of the VS-900RIC sensor

The signal was band-pass filtered from 70 kHz to 500 kHz. The sensor was attached to the test bearing using a magnetic holder as shown in Figure 4-7. Ultrasonic couplant was used to ensure good transmission from the bearing case to the AE sensor due to the good frequency performance (refer to section 2.5.2). Ultragel II® was selected for this task which is a water-based gel suitable for a broad range of temperatures (-25 °C to 100 °C). The sensor internal preamplifier was powered through a decoupling box connected to a linear power supply. The decoupling box was connected to a commercial data acquisition card through a coaxial cable. The data acquisition card used was NI 9223 with a maximum sampling rate of 1MSamples/sec, 16-bit resolution and ±10V input range. The sampling rate was set at the maximum for this card, 1MSsamples/sec. The data was acquired, processed and saved using LabView® Software.

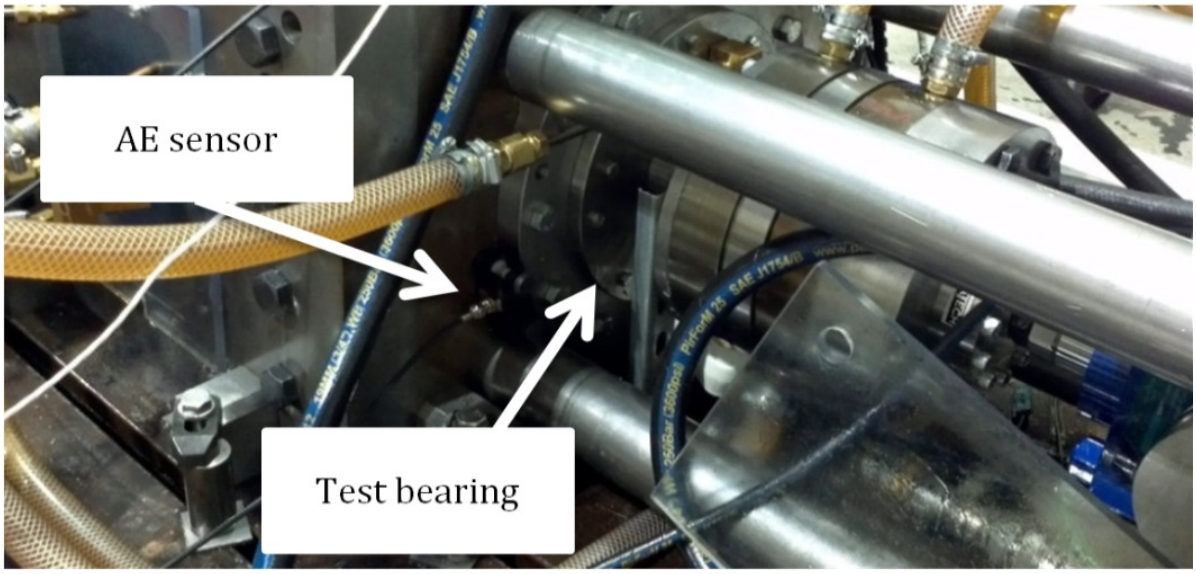

Figure 4-7: AE Sensor location.

4.3.3. Experimental procedure

A defect was artificially introduced in the outer race of the bearing by mechanical indentation using a drill. The defect dimensions were approximately 3mm along the race direction, 5mm width and 1mm depth. Figure 4-8shows an image of the defect obtained by endoscopic inspection.

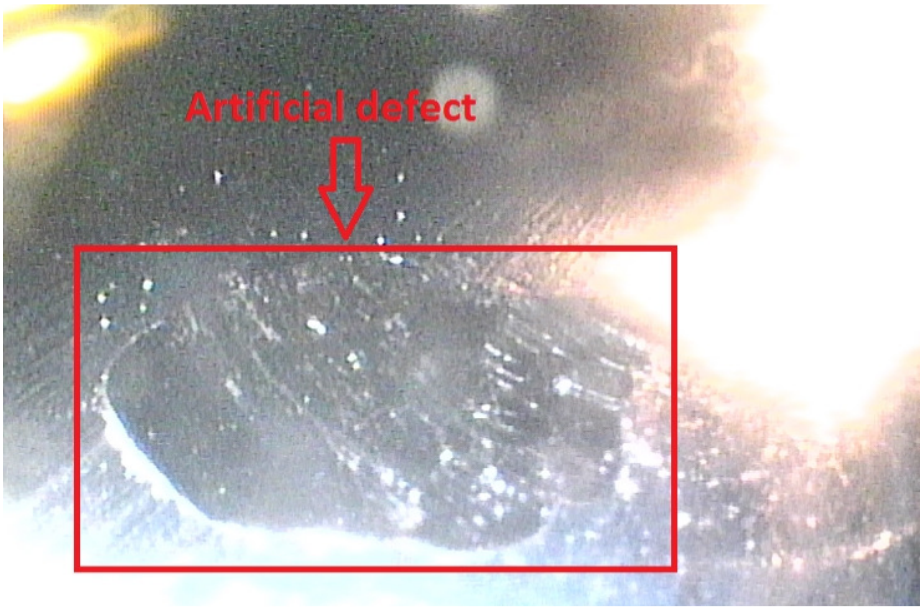

Figure 4-8: Outer race artificial defect (courtesy of Romax Technology Ltd.).

The test rig was operated at 1650 rpm and the radial and axial load was 40 kN and 140 kN respectively. It was in operation for 1 hour prior to the beginning of the data acquisition in order to reach thermal equilibrium. 18 data files were acquired, being the interval between two measurements of 10 seconds and the time window of the acquisition was 2 seconds.

In addition, prior to the introduction of the defect, several AE samples using the same setup and procedure were acquired in order to present a comparison of the AE signal with the defect and in the absence of outer race defect (section 4.3.4.1).

4.3.4. Selection of the optimal Wavelet parameters

4.3.4.1. Scalograms of the AE signal

The purpose of this section is to show the effect that is caused on AE signals due to the introduction of the defect in the bearing. AE signals are wideband and complex in terms of frequency components. For this reason, in order to understand the frequency components present in the signal, in both the frequency and time-domain, the scalogram obtained using the CWT is displayed for the bearing with a defect and for the signals acquired prior to the introduction of the defect. As a result, a clear picture of the effect on AE signals generated by the defect in the outer race is displayed. To show an intuitive plot, the scales of the wavelets have been transformed to frequency using the following equation[125]:

$$F_a = \frac{F_c}{a\Delta} \tag{4.14}$$

where a is the scale, Δ is the sampling period, Fc refers to the centre frequency of the wavelet in Hz and F_a is the pseudo-frequency corresponding to the scale a, in Hz.

A typical waveform acquired from the defected bearing is shown in Figure 4-9(a). In the time-domain signal, the bursts produced by the impact between the outer race defect and the rolling elements are not appreciable. This is the typical waveform expected for incipient defects in which the SNR is low. Figure 4-9(b) shows the time-frequency decomposition of the AE signal

in the scalogram. Only 50 ms of the waveform is shown of the 2 second signal acquired in order to make the AE burst generated by the impact visually appreciable. It clearly shows two different components in the signal:

- Continuous bearing noise generated by normal bearing operation in the frequency range between 70 and 250 kHz. Most of the energy of the signal is part of this noise. This is the sum of many different individual AE events that occur due to the friction within the bearing components and appears in the signal as continuous noise.
- AE bursts of high frequency and very low amplitude that are attributed to the impact between the outer race defect and the rolling elements. The equation to calculate defect frequency for the bearing under investigation (ball pass frequency of the outer race (BPFO)) is as follows[126]:

$$\mathrm{BPFO} = \frac{\mathrm{Nb}}{2} \cdot \mathrm{S}\left(1 - \frac{\mathrm{Bd}}{\mathrm{Pd}}\cos\emptyset\right) \tag{4.15}$$

where S is the revolutions per second or relative speed difference between inner and outer race, Bd the ball or roller diameter, Nb refers to the number of balls or rollers, Pd is the pitch diameter and Φ the Contact angle. It was calculated as 6.61X for the bearing under investigation, being X the rotating speed. As the rotating speed was 1650 rpm, the time interval between the burst produced by the defect impact in the AE signal was calculated as 5.5 ms, which coincides with the high frequency AE transients observed in the high frequency region in the Wavelet scalogram. These AE signals are generated in the defected area when the rolling elements impact on it, and propagate from the source (defect) to the sensor. AE frequency components of up to 500 kHz are generated by the impact between the rolling elements and the defect in the outer race.

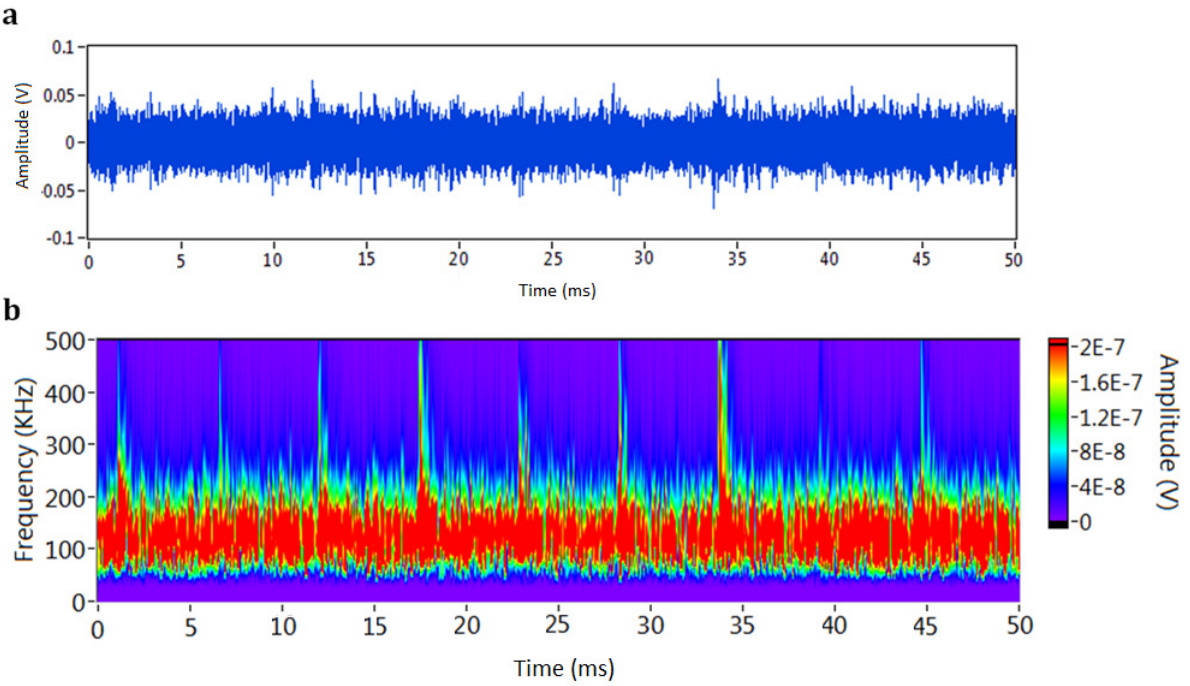

Figure 4-9: AE signal from defected bearing in (a) time-domain and (b) scalogram.

The AE signal captured prior to the introduction of the defect in the same operational conditions is displayed in Figure 4-10(a). It is clear that visually, the time-domain signal does not show any remarkable difference with the AE signal captured in the defected bearing (Figure 4-9 (a)). However, in the scalogram (Figure 4-10 (b)) the high frequency burst that the previous figure shows generated by the impact between the rolling elements and the outer race are not present. Thus, Figure 4-9 and Figure 4-10 present a time and time-frequency comparison of the change in the AE signal produced by an early stage defected bearing and a defect-free bearing. The scalograms shows clearly the frequencies excited by the normal bearing operation can be found up to 250-300 kHz. From these frequencies the power of the AE signal is extremely low.

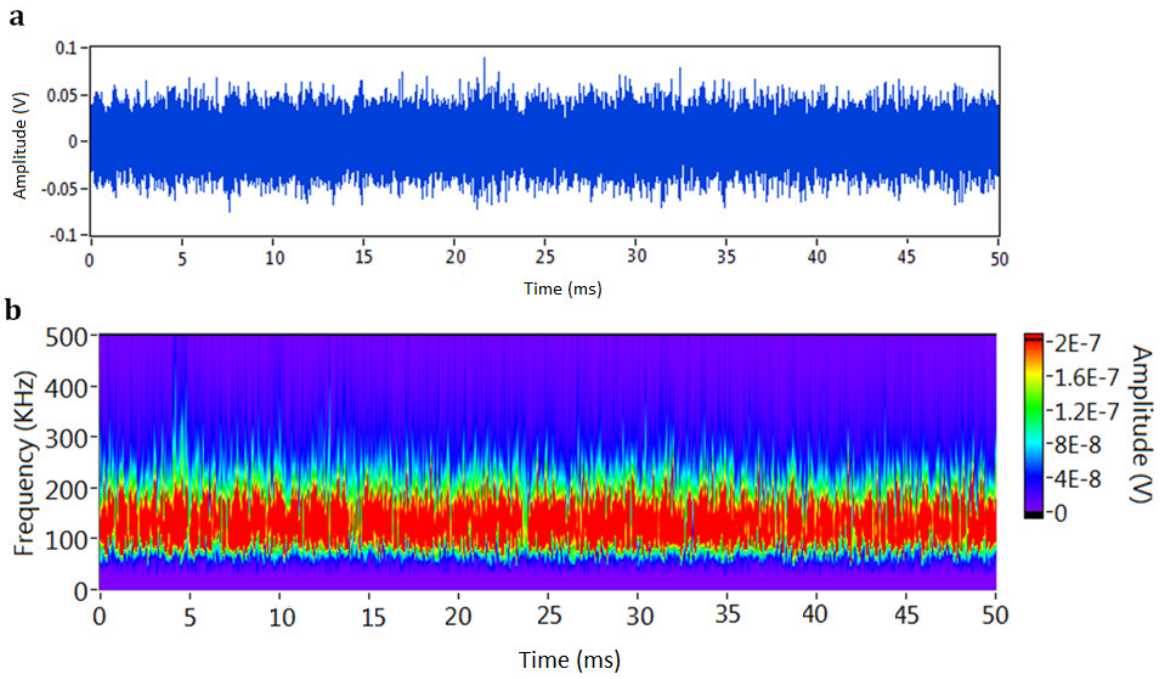

Figure 4-10: AE signal captured from non-defected bearing in (a) time-domain and (b) scalogram.

Thus, the AE signal carried more information about the defect in the high frequency range rather than in the low frequency range. For this reason, the WP, which offers higher resolution at higher frequencies than the DWT, has been selected as a pre-processor in the proposed method.

4.3.4.2. Optimal Wavelet packet decomposition level

The results of the spectrum generated by the proposed method, obtained using different WP level decomposition are presented in this section. The purpose of this is to find the WP node and decomposition level that offers optimum results in the de-noising process. The optimal level of decomposition and WP node are required for an efficient signal de-noising. Thus, with the objective of having a value that estimates the SNR of the output spectrum generated by the proposed method, the SNR of the WP-ACF spectrum is calculated as follows:

$$\mathrm{SNR(dB)} = 20\log\left(\frac{\text{Peak value (BPFO)}}{\mathrm{RMS_{noise}}}\right) \tag{4.16}$$

The different frequencies ranges associated with each wavelet nodes for different decomposition levels used in this section are presented in Table 4-1:

Table 4-1: Frequency range associated with each wavelet node for 1, 2, 3 and 4 decomposition level.

1 level decomposition		2 level decomposition		3 level decomposition		4 level decomposition	
Node	Freq. (kHz)	Node	Freq. (kHz)	Node	Freq. (kHz)	Node	Freq. (kHz)
1,0	0-250	2,0	0-125	3,0	0-62.5	4,0	0-31.25
1,1	250-500	2,1	125-250	3,1	62.5-125	4,1	31.25-62.5
-	-	2,2	375-500	3,2	187.5-250	4,2	93.75-125
-	-	2,3	250-375	3,3	125-187.5	4,3	62.5-93.75
-	-	-	-	3,4	437.5-500	4,4	218.75-250
-	-	-	-	3,5	375-437.5	4,5	187.5-218.75
-	-	-	-	3,6	250-312.5	4,6	125-156.25
-	-	-	-	3,7	312.5-375	4,7	156.25-187.5
-	-	-	-	-	-	4,8	468.75-500
-	-	-	-	-	-	4,9	437.5-468.75
-	-	-	-	-	-	4,10	375-406.25
-	-	-	-	-	-	4,11	406.25-437.5
-	-	-	-	-	-	4,12	250-281.25
-	-	-	-	-	-	4,13	281.25-312.5
-	-	-	-	-	-	4,14	343.75-375
-	-	-	-	-	-	4,15	312.5-343.75

The SNR value provides the ratio between the peak value of the BPFO (which is considered the valuable indicator of the presence of the defect), which is 6.61X for the bearing under investigation, and the noise floor in the vicinity of the BPFO peak. An example of the AE signal decomposed using the WP 3-level decomposition is shown in Figure 4-11. It clearly shows that for the different bands, the SNR of the AE signal generated by the impact between the defect and the defect varies. In the bands corresponding to lower frequencies ((3,0) and (3,1)) the AE signal produced by the defect is not visually detectable. However, in high frequency bands the

AE signal produced by the defect is visually noticeable, particularly in the band from (3,4) to (3,7) corresponding to different frequency bands from 250 and 500 kHz. In these bands, the impulse generated at the start of the burst rise clearly over the noise level with higher SNR. The frequency bandwidth for the application of de-noising technique based on WP is limited by the sampling rate used in the data acquisition. However, increasing the sampling rate increases the computational complexity. Thus, to find a compromise between both, it was selected 1Msample/sec as sampling rate, which provides 500 kHz bandwidth to the AE signal according to the Nyquist theorem.

It is worth noting the low amplitude in the high frequency WP nodes. The node with the higher SNR, (3,4) has a maximum amplitude of 9 mV, in contrast with the (3,1) node, in which higher amplitudes are present, up to 70 mV. Therefore, any unexpected source of noise, such as electrical noise coming from the power source, that can affect the measurement in the high frequency band, would have a significant impact on the detection due to the low amplitude of the AE signals in the high frequency region. Consequently, the performance of WP to de-noise the AE burst from the continuous AE signal would be deteriorated if unwanted sources of noise in the high frequency range are present. To overcome this obstacle, a resonant sensor, with peak sensitivity in the high frequency band can be used to increase the amplitude measured at high frequencies and increment the SNR. In addition, the importance of using couplant is critical since as described in section 2.5.2, the use of a couplant can greatly improve this transmission by around 10 times at 500 kHz.

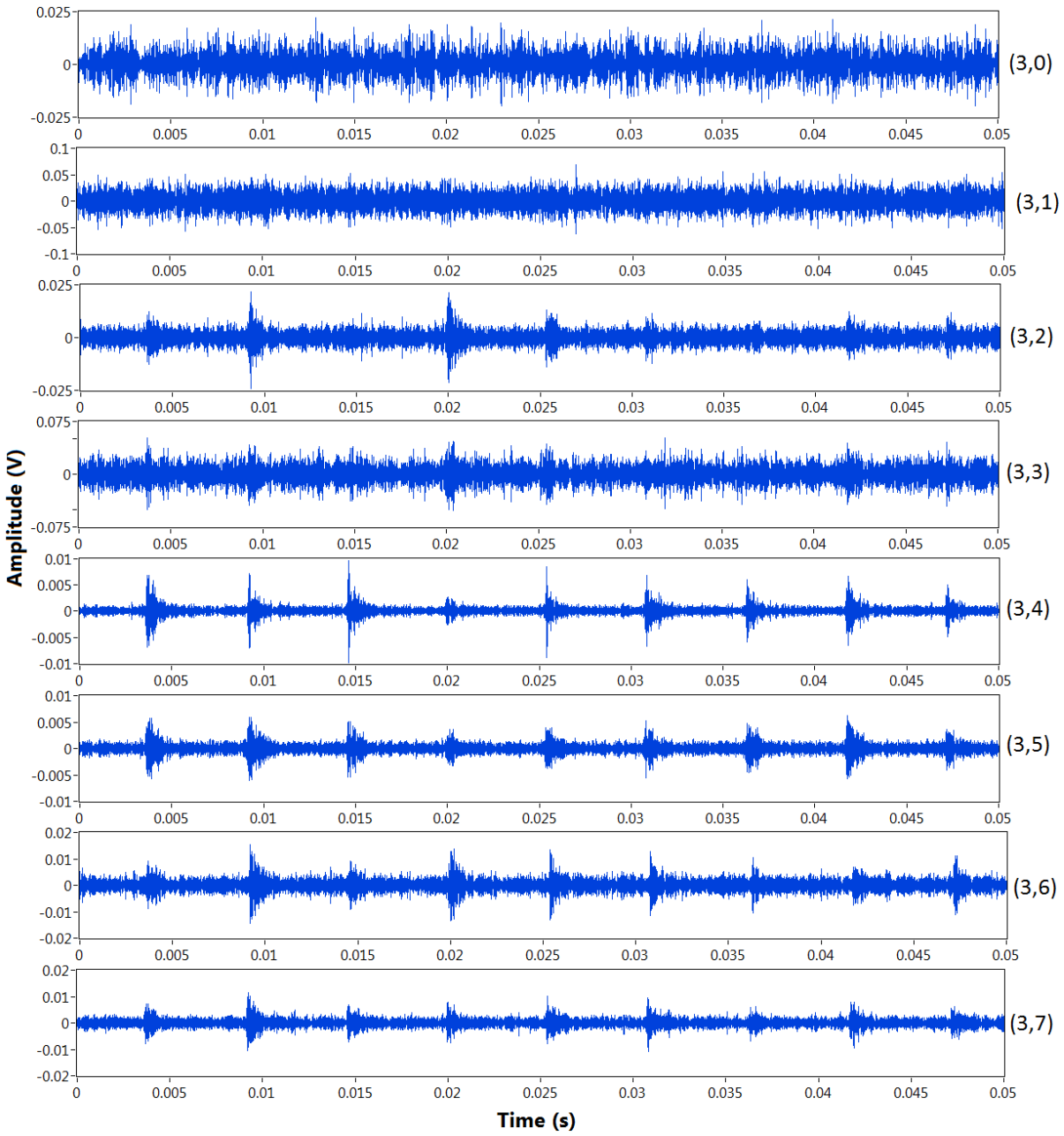

Figure 4-11: AE signal decomposed using 3-level WP.

The SNR of the WP-ACF spectrum obtained using different WP level decomposition and the wavelet Db11 is shown in Figure 4-12. To obtain consistent results, the figure shows the average obtained from the 18 samples acquired in the experiment. The highest SNR value corresponds to the (2,2) Wavelet node (57.63 dB) and (4,0) the lowest (29.39 dB). The frequency range of the (2,2) band corresponds to 375-500 kHz. The WP nodes (3,4) and (4,8) also show positive results with SNR values of 57.39 dB and 56.89 dB, respectively. The considerable variation of the SNR

for different WP parameters illustrates the importance of the parameter selection in the pre-processor.

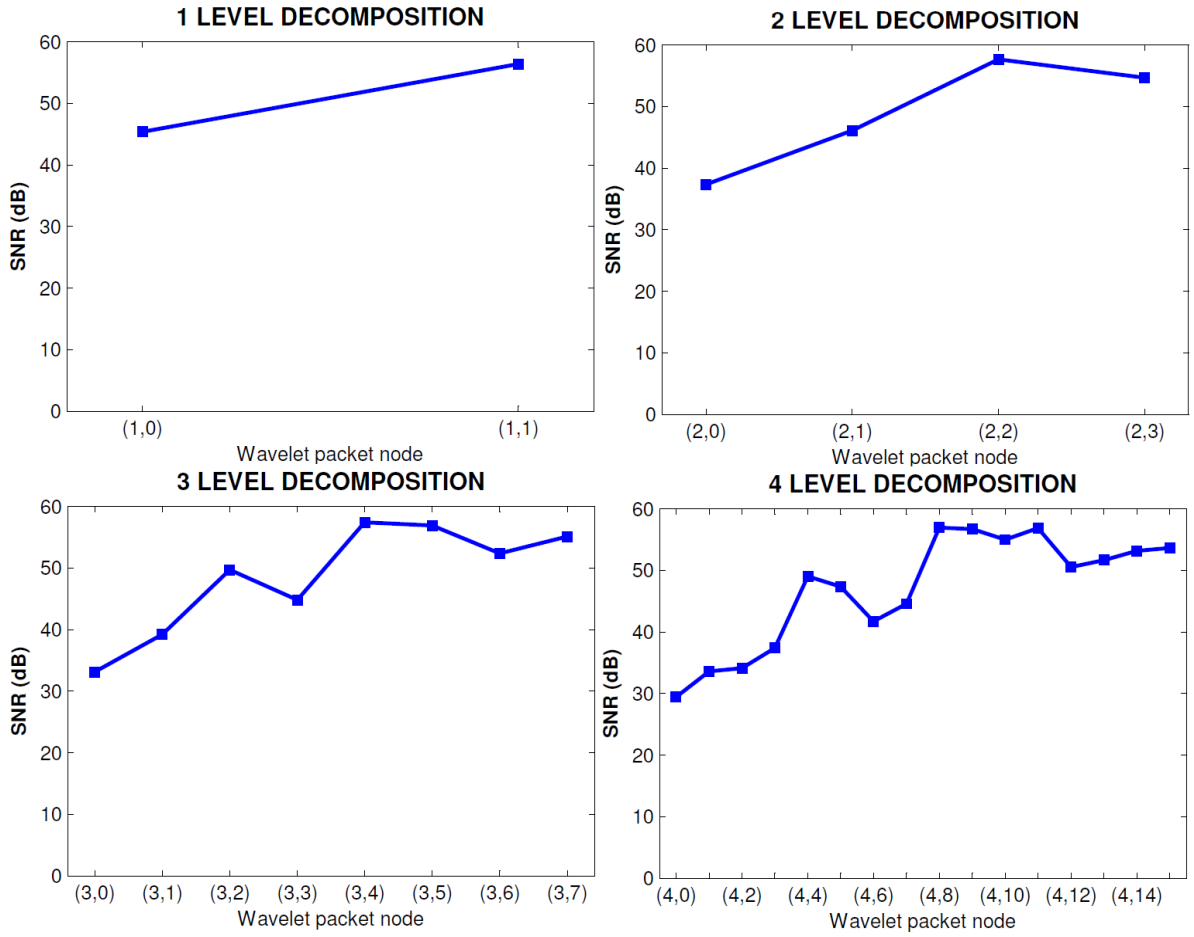

Figure 4-12: SNR for 1-4 level decomposition.

An example of the original signal and the signal obtained after the application of the WP 2 level decomposition (2,2) is presented in Figure 4-13. This figure shows that the periodic bursts in the signal are appreciable in the de-noised signal using WP (Figure 4-13(b)) but not in the raw signal (Figure 4-13 (a)). Thus, the WP used as a pre-processor in the WP-ACF method enhances the higher frequencies included in the AE burst and reduces the power of the signal attributed to continuous AE generated by normal bearing operation in the band 70-250 kHz. Moreover, the de-noised signal shows that the impacts do not produce the same amplitude with a considerable variation. It should be noted that the bursts are evenly distributed in time and the delay between them is constant (5.5 ms).

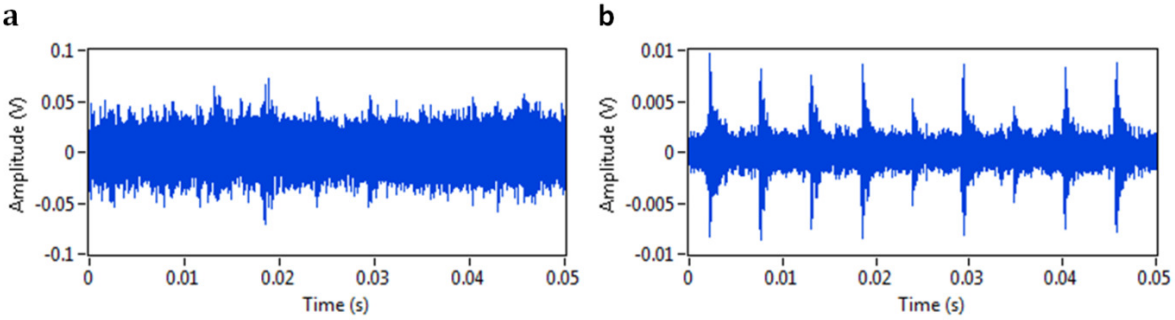

Figure 4-13: AE time-domain signal (a) before WP de-noise and (b) after WP de-noise.

4.3.4.3. Optimal Mother Wavelet selection

One of the most important steps to ensure a precise decomposition of the AE signal into frequency bands and signal de-noising is the selection of the mother Wavelet. Different mother Wavelets have different properties such as regularity, orthogonally, admissibility and vanishing moments [29]. These parameters affect the frequency band decomposition and therefore the de-noising capabilities. Furthermore, different types of wavelets have different time-frequency structures; the Wavelet whose time-frequency structure best matches that of the transient component in order to detect the transient component effectively [127]. This section evaluates the best mother wavelet empirically calculating the SNR using again equation 4.16. As described in the previous section the results obtained for the mother Wavelet selection are the average of the 18 AE samples acquired. The mother Wavelets utilised are the well-known Daubechies, Coiflet, and Symmlet.

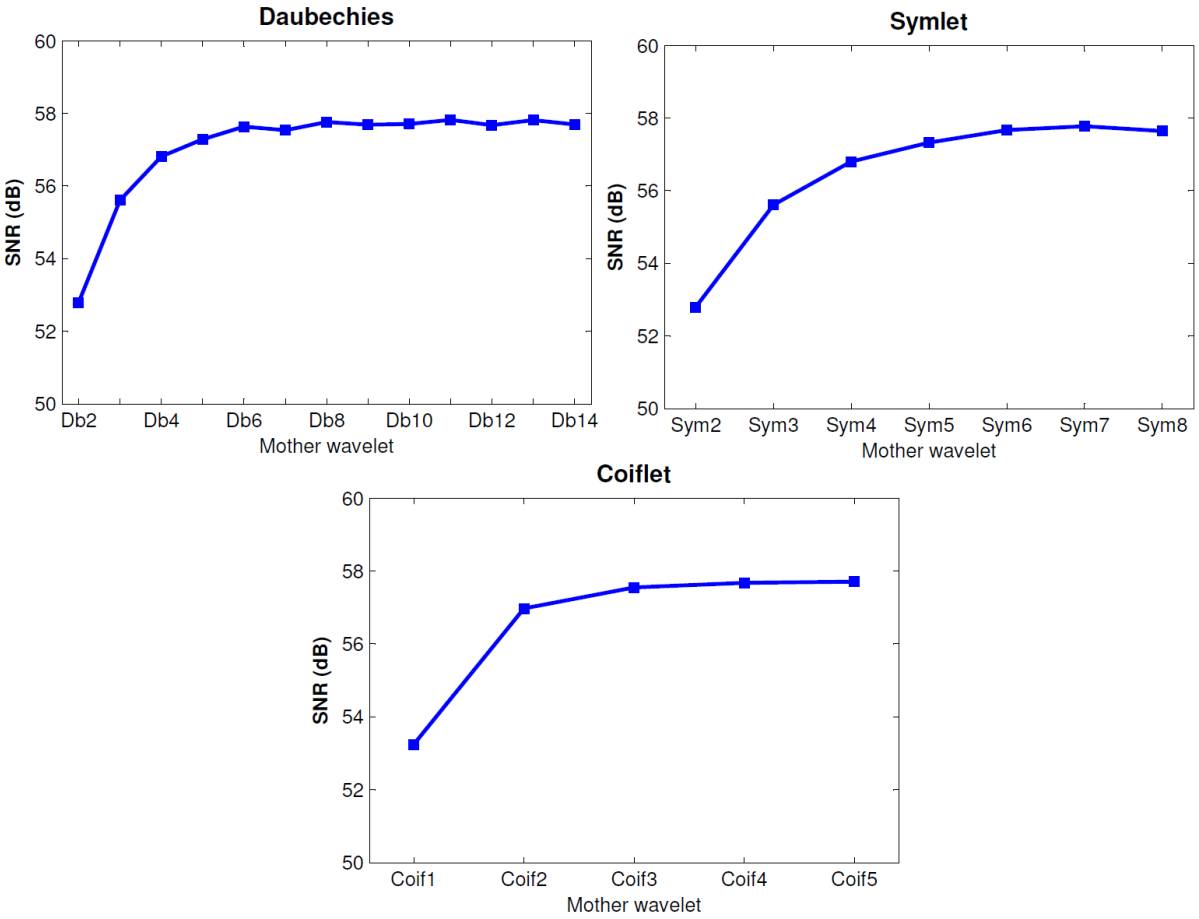

Figure 4-14: Calculated SNR for the WP-ACF spectrum using different mother Wavelets.

The results for the different the mothers Wavelets are shown in Figure 4-14. In the horizontal axis, the coefficient shown next to the mother wavelet represents the order for that particular mother wavelet. It clearly shows increasing SNR with increasing mother Wavelet order. Furthermore, the results obtained for the different mother Wavelets with high order are similar. The Db1 provides the lower result, 47.64 dB. The highest SNR was obtained with the Db11 with 57.82 dB. It should be pointed out the high influence of the selected mother Wavelet in the proposed method which produces a high impact on the SNR of the WP-ACF spectrum. To illustrate the significance of the choice of mother Wavelet, the WP-ACF spectrum using the mother Wavelets that provides the highest and the lowest SNR (Db1 and Db11) are shown in Figure 4-15. It is evident that the signal is significantly noisier using the Db1 mother Wavelet. Therefore, in the results presented in the following sections, the mother Wavelet and decomposition node used are Db11 and (2,2) respectively.

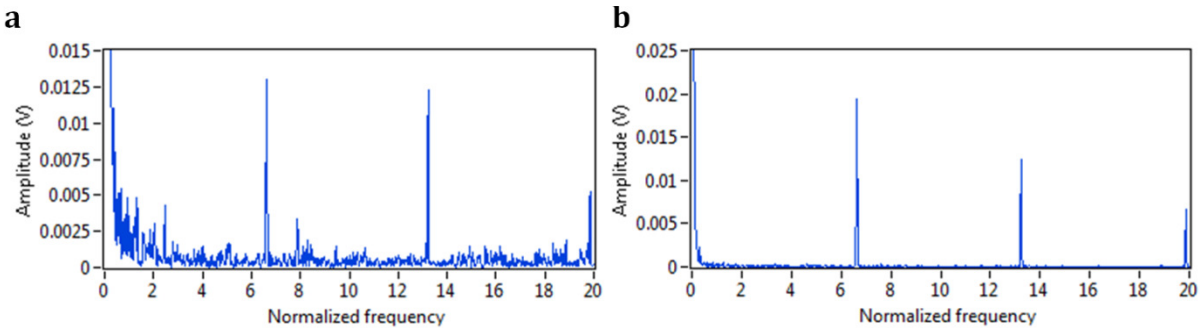

Figure 4-15: Comparison of the WP-ACF spectrum obtained with using the (a) Db1and (b) Db11 mother Wavelet.

4.3.5. Autocorrelation function

The autocorrelation function increases significantly the SNR of the WP-ACF spectrum. Due to the high frequency content of AE, and the fact that the AE signal pattern occurs only in the amplitude modulation, the ACF applied directly to the AE signals does not have the ability to find the patterns in the signal. For this reason, when the ACF is applied directly to the AE signal, the SNR of the WP-ACF is decreased and for this reason, not valid in for the proposed method. However, if the ACF is applied to the envelope extracted from the AE signal, instead of to the AE signal itself, there is a significant increase in the SNR of the spectrum. Figure 4-16 shows an example of the application of the ACF prior and after the extraction of the envelope.

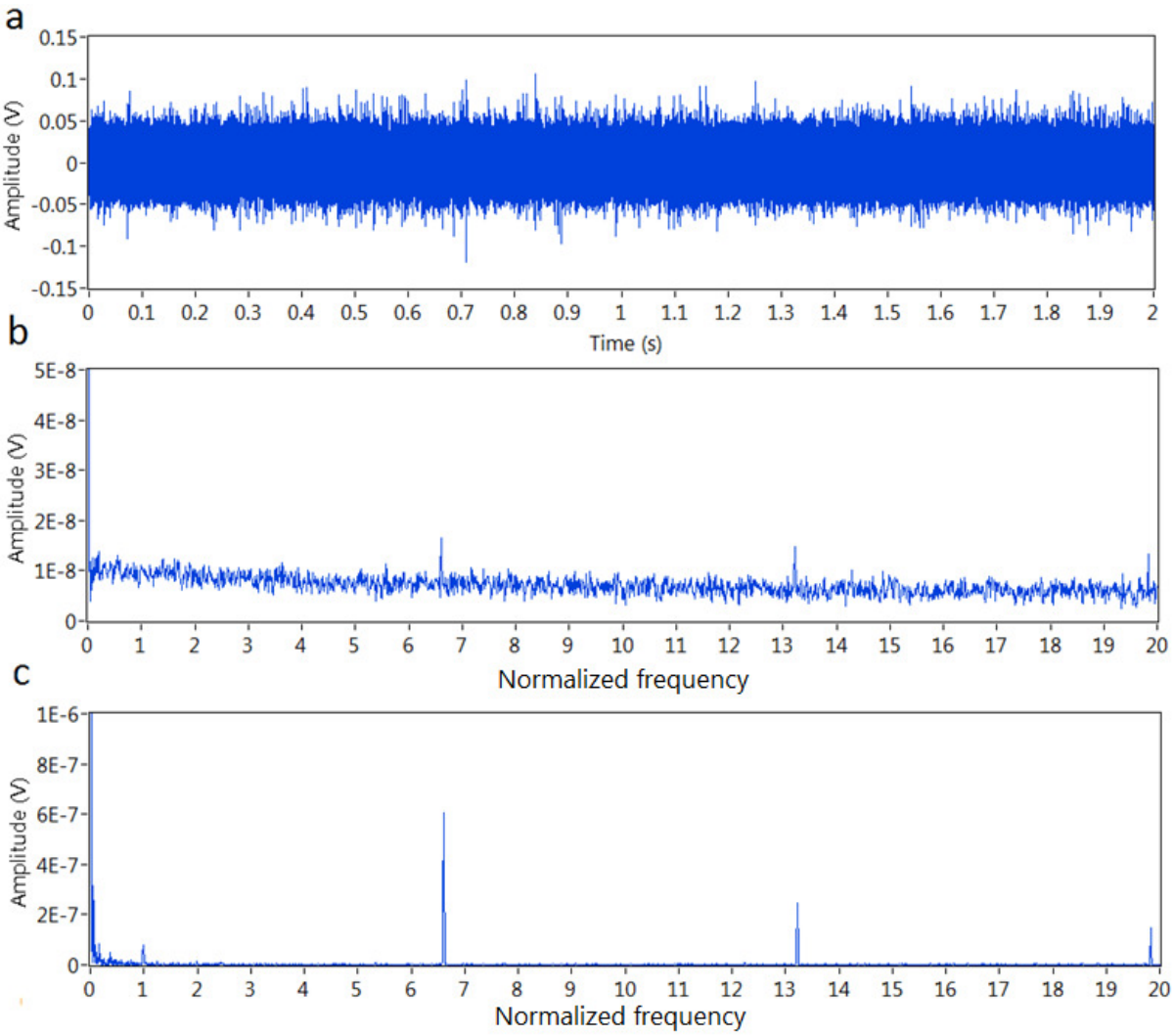

Figure 4-16: (a) AE time-domain signal and WP-ACF spectrum obtained with autocorrelation applied (b) prior and (c) after to the extraction of the envelope.

A comparison of the WP-ACF spectrum and the spectrum without applying the ACF is shown in Figure 4-17. The increase in the SNR with the ACF is evident. The noise floor is reduced significantly by applying the ACF to the AE enveloped signal.

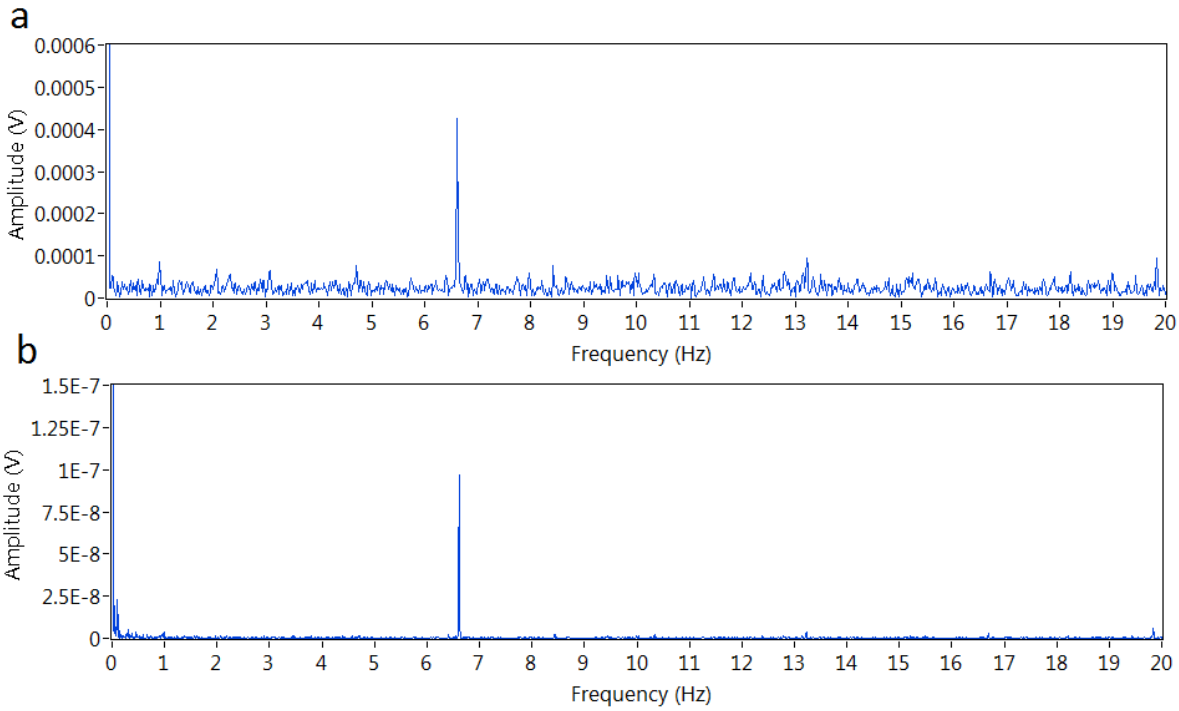

Figure 4-17: Spectrum without (a) the post-processor and (b) with post-processor.

4.3.6. Results of the proposed method

To illustrate the advantage and strength of the WP-ACF method, the spectrum generated by both traditional envelope and WP-ACF spectrum are shown in Figure 4-18. The BPFO calculated as 6.61X using equation 4.14 can be visually distinguished in both graphs. However, it is clear that the ratio between the peak at the BPFO (6.61X) and the noise floor is considerably higher in the WP-ACF spectrum. This is a major benefit for automated fault detection since it is usually carried out using a threshold detector. The method avoids false alarms produced by a threshold being crossed by noise instead of the spike at the characteristic frequency produced by the defect. Harmonics of the BPFO are also appreciable in the graph (2XBPFO and 3XBPFO).

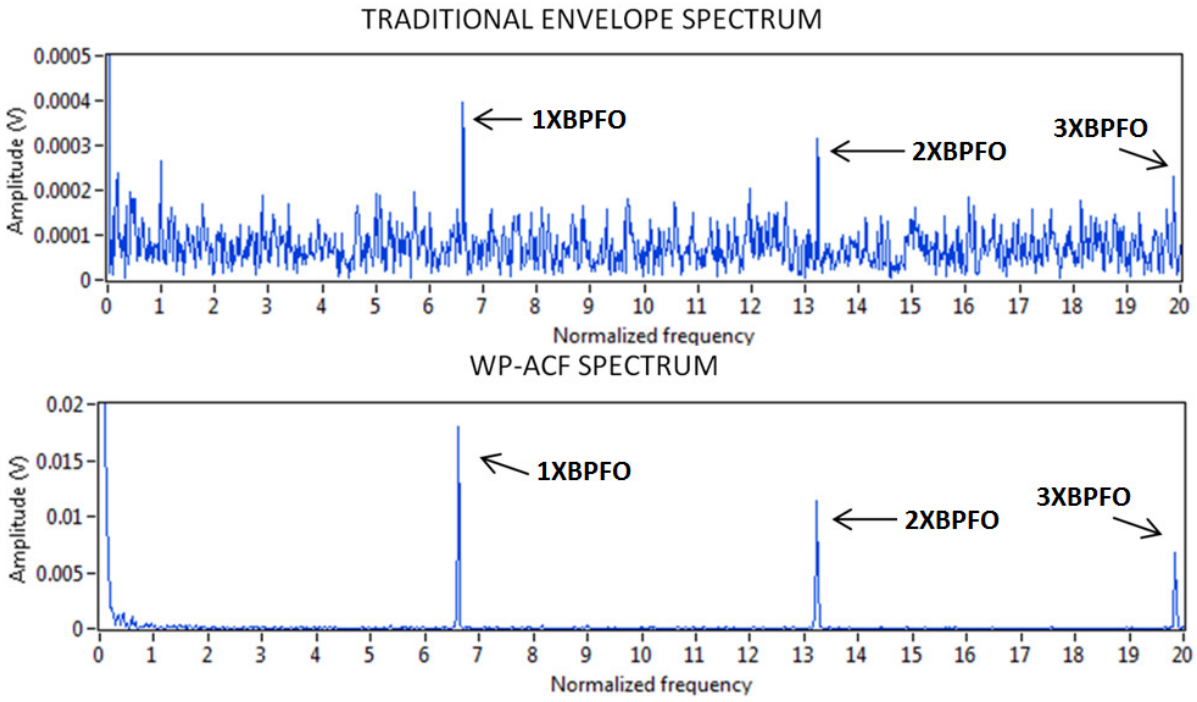

Figure 4-18: An example of the traditional envelope spectrum and the WP-ACF spectrum.

In order to evaluate the proposed method under extremely low SNR conditions, additional noise is superimposed on the signal. The frequency spectrum of the AE noise produced by normal bearing operation is not evenly distributed at all frequencies; the authors believe that adding white noise does not represent a real scenario. To obtain a more realistic scenario, the type of added noise was the AE signal acquired from the same bearing when it was in a healthy condition (defect free). These signals only include AE noise produced by normal bearing operation, but the bursts produced by the impact between the defect and the rolling elements are not present. Therefore, adding this noise to the AE signal captured in the defected bearing reduces the SNR ratio and simulates early stage defects, decreasing the ratio between AE bursts and continuous bearing AE noise. The noise was captured using the same experimental setup and operational conditions existing prior to the introduction of the defect.

The added noise to the AE signals was in the range between -21dB and 21dB in intervals of 3dB. The equation to calculate the added noise is as follows:

$$\text{Added noise (dB)} = 20\log\left(\frac{\text{RMS}_{\text{noise}}}{\text{RMS}_{\text{signal}}}\right) \tag{4.17}$$

Some examples of the AE signal captured from the defected bearing with 0, 6, 12 and 15dB added noise are presented in Figure 4-19. It shows a clear increase of amplitude caused by the increase of additional noise. The AE signals are highly affected by a significant amount of noise. As a result, the bursts produced by the defect are not visually distinguishable in any of the waveforms.

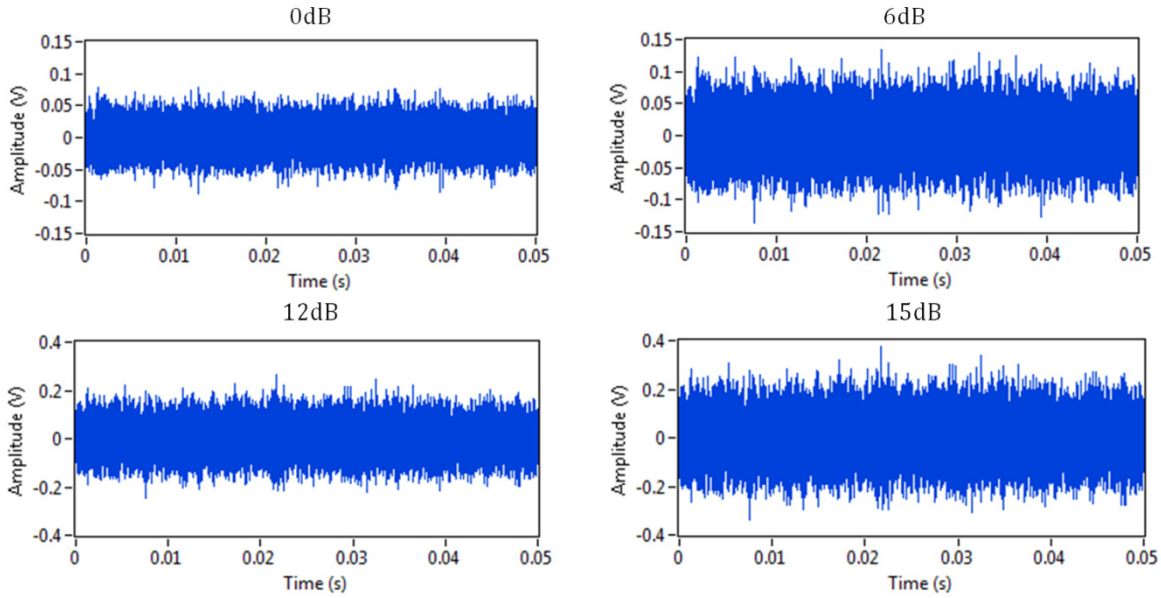

Figure 4-19: Some examples of the time-domain AE signal captured in the defected bearing with additional noise (0, 6, 12 and 15dB).

Figure 4-20 displays the de-noised signals using the (2,2) WP node and Db11 mother Wavelet, as previously selected as the most efficient for AE de-noising. The AE bursts produced by the outer race defect are only visible with 0dB of additional noise. However, for the rest of the AE waveforms, the AE transients are not visually evident. This is caused by an increase in amplitude due to the addition of noise. Thus, the WP de-noising technique is not sufficient under extremely noisy conditions. Therefore, further signal processing where the HT and the autocorrelation function are applied in order to unmask the defect. Therefore, although the noise is extremely high even when the de-noised signal possesses 6, 12 or 15dB additional noise, as it is presented later in this section, the WP-ACF spectrum is able to distinguish the defect and locate the fault frequency (BPFO).

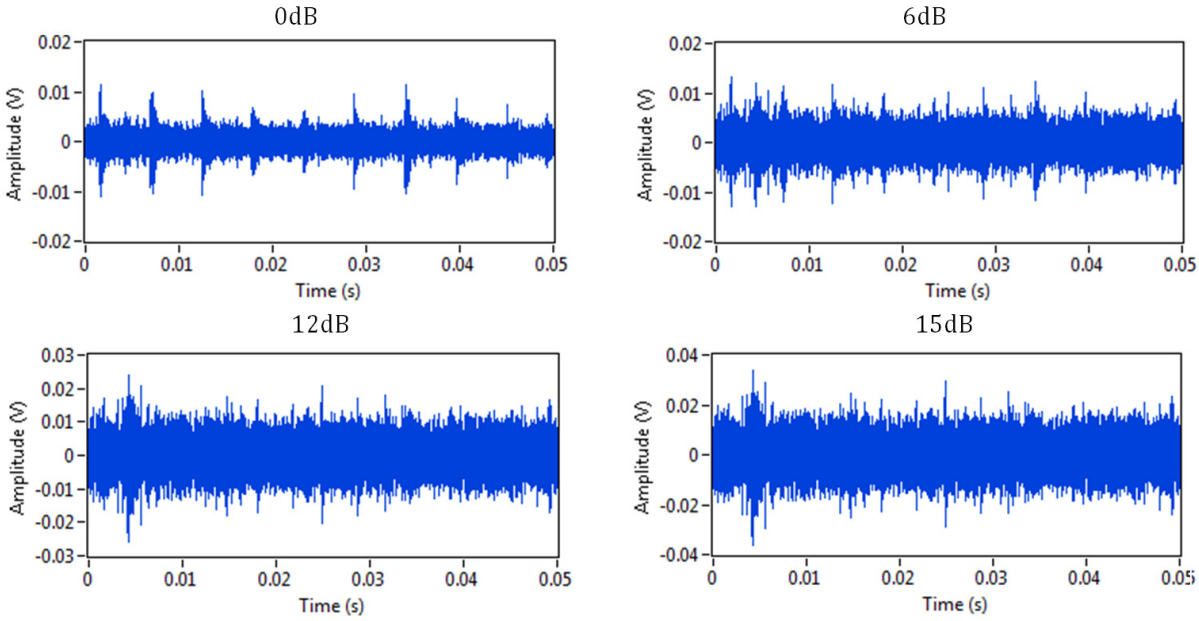

Figure 4-20: Some examples of the time-domain AE signal with additional noise (0, 6, 12 and 15dB) after de-noising.

The quantifier used to investigate the performance of the WP-ACF spectrum and the traditional Hilbert envelope is again the SNR value, calculated using in equation 4.16. In contrast with vibration analysis, the AE signals can be demodulated directly to reveal characteristic defect frequency without the need to determine the resonance frequency band. For this reason, the traditional envelope analysis has been applied to the AE signals without the application of any narrow band-pass filter prior to the extraction of the envelope.

The results of the traditional envelope analysis and the proposed method are presented in Figure 4-21. The horizontal axis shows the added noise in dB and the vertical axis displays the SNR values in dB. The difference in SNR between the proposed method and the traditional method is approximately 33dB with low added noise (<0dB). The graph shows that the noise up to -9dB has little impact in the SNR in both methods. From this value, there is a clear trend of decreasing SNR in both techniques. However, the WP-ACF spectrum identifies the defect up to 15dB added noise. From 15dB the SNR is so low that the peak cannot be distinguished from the noise floor using the proposed method. In contrast, with the traditional method, the defect cannot be detected from 6dB added noise due to the low SNR. The maximum difference in SNR

corresponds with 3dB added noise is 35.15**.** This result clearly shows the better performance of the WP-ACF spectrum detecting incipient defects in extremely low SNR conditions.

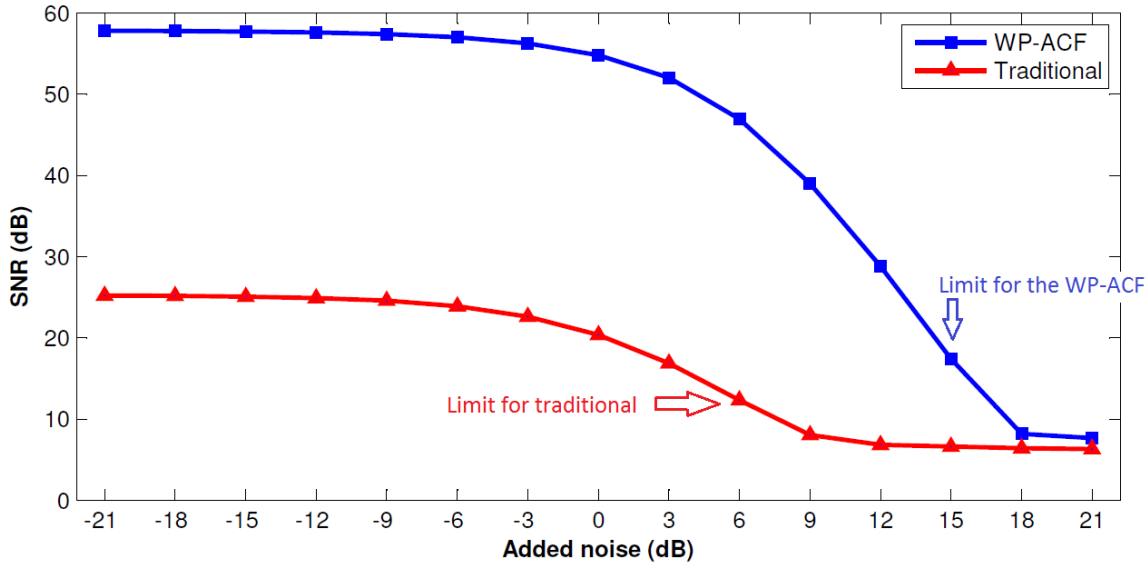

Figure 4-21: SNR calculated for the traditional and WP-ACF method for different noise conditions.

Figure 4-22 shows the spectrum generated by both methods with added noise. In the first case (0dB), both methods are able to identify the fault frequency at 6.61X (BPFO) and harmonics, indicating a defected outer race. However, the WP-ACF spectrum shows significantly higher SNR and the floor noise is diminished compared with the traditional envelope method. The results of both methods with 6 dB added noise show that using the traditional envelope analysis, the BPFO is hardly detected and the proposed method is still able to identify the peak at the BPFO with high SNR. This level of added noise is the limit for the traditional method to identify the defect. The next case (12dB) shows how the envelope analysis method is not able to identify the BPFO but it is still distinguishable with the WP-ACF method with high SNR. In the last figure (15dB added noise) the WP-ACF spectrum is able to identify the BPFO but, in this case, high noise at other frequencies is also present, whereas the traditional method is still not able to distinguish the fault frequency.

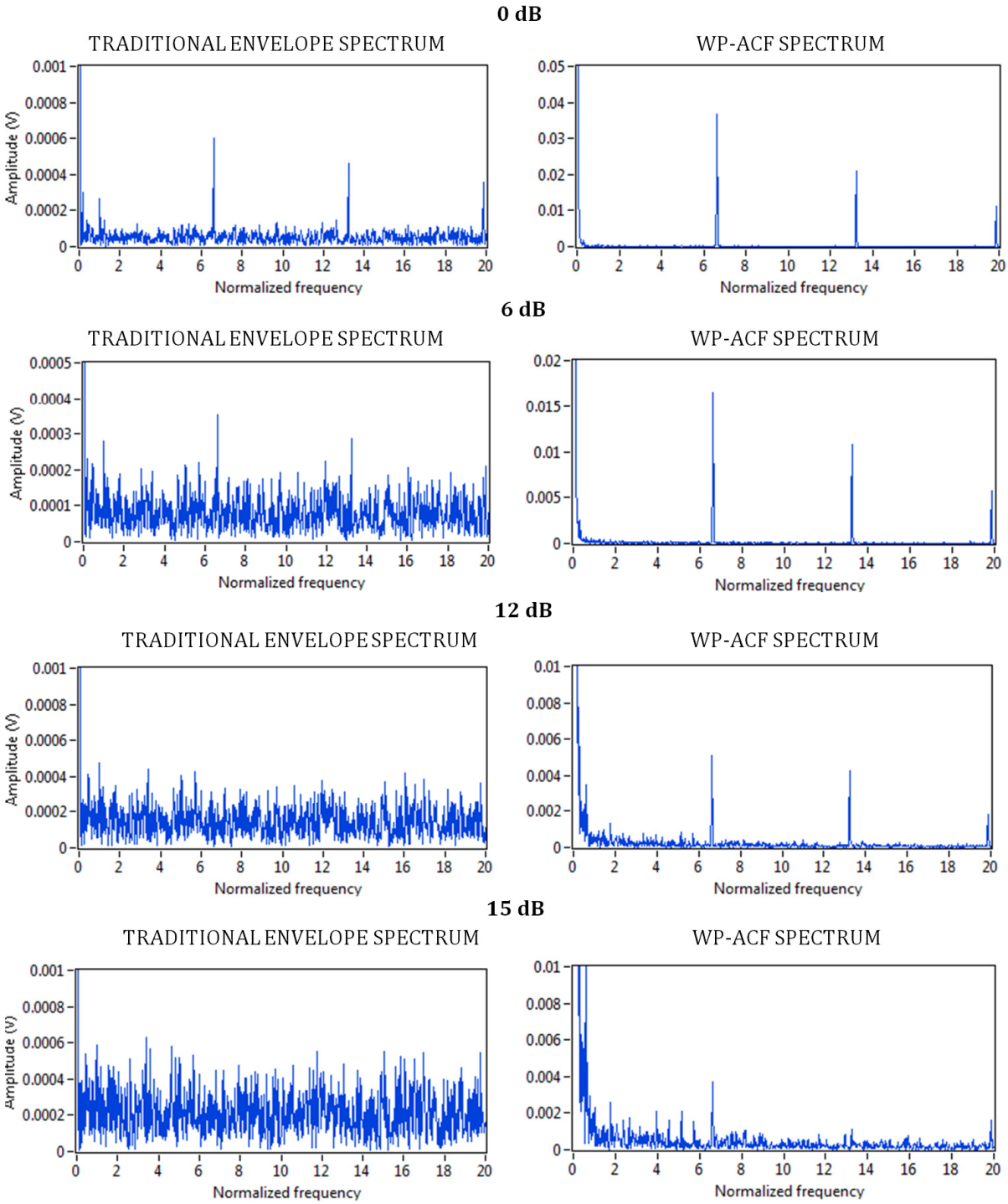

Figure 4-22: Examples of the results obtained with the WP-ACF method and the traditional envelope analysis with 0, 6, 12 and 15dB of added noise.

4.4. Summary

In this chapter a novel method for bearing incipient defect detection has been presented. The effectiveness of the WP-ACF spectrum was tested using experimental data. This investigation

shows promising results of the proposed method and better performance for localised defect detection in tapered roller bearings in both high and low SNR conditions compared to the traditional envelope analysis. The WP-ACF is able to identify the defect present in the bearing outer race under 9dB lower SNR conditions than traditional envelope analysis.

The most efficient mother Wavelet and WP node in the de-noising process have been investigated. The (2,2) WP node, which corresponds to the frequency band 375-500 kHz, show the best results for AE signal de-noising. However, this frequency band could be enhanced due to the fact that frequencies in excess of 500 kHz cannot be investigated due to the sampling rate used (1 MSsamples/sec). In the next chapter, the optimal frequency band for localised defect detection in helical gears and spherical roller bearings is further investigated increasing the sampling rate to 5 MSsamples/sec. In addition, the effect of the optimum frequency band varying the distance of the sensor to the defect is further explored. The optimal mother wavelet for signal de-noising was dB11; however, the rest of mother families investigated show similar results and the performance for AE signal de-noising clearly improves increasing the wavelet order.

The research presented in this chapter has been published in the peer reviewed journal, Applied Acoustics.

Chapter 5

Further validation of the WP-ACF method

5.1. Introduction

In order to further validate the WP-ACF algorithm described in chapter 4 in different conditions, further experiments were carried out to evaluate under which conditions the proposed method is applicable. For this task, two different test scenarios were investigated. Firstly, the detection of a naturally developed defect in the outer race of spherical roller bearings

using the WP-ACF method was investigated. The test rig was operated in different operational conditions in order to evaluate the impact of speed and load on the detection. The importance of this experiment lies with the fact that the vast majority of the studies carried out for defect detection using AE have been performed using artificially defected bearings[55]. Thus, very few studies have targeted the detection of naturally degraded bearings. Secondly, the detection of gear defects using the WP-ACF method was explored. Gear fault detection is of high importance in numerous fields such as automotive and wind energy industry[128]. Thus, a test rig was utilised to artificially generate a defect in a straight bevel gear and the AE signals acquired from the gearbox case were processed using the WP-ACF algorithm. This is the first known attempt to detect faults in bevel gears using AE.

5.2. WP-ACF for the detection of a naturally developed defect

The following investigations were carried out in this experiment:

- Investigate the performance of the WP-ACF for detection of a naturally developed defect
- Investigate the performance of the WP-ACF for defect detection in spherical roller bearings.
- Investigate the optimum frequency range using higher sampling rate (5MSamples/sec) which provides an enhanced bandwidth to further investigate the WP de-noising capabilities at higher frequencies.
- Study the impact on the defect detection using the WP-ACF method produced by the change of operational conditions (load and speed).
- Investigate how distance from the defect to the AE sensor position impacts on the optimal WP node for signal de-noising. For this reason, two different sensors were installed in the bearing case at different distances from the defect.

5.2.1. Instrumentation

In this experiment, two different AE sensors were used. The purpose of using two sensors is to is to study the optimal WP node for different distance from the defect to the sensor. The sensors utilised were Vallen VS900RIC AE. These include an internal preamplifier with a 34dB gain and are capable of operating in a range from -40 to 85 °C. The signal was band-pass filtered from 100 kHz to 1000 kHz. The first sensor (AE1) was installed at the top region of the bearing, close to the defected area. The second sensor (AE2) was installed at the bottom of the bearing, at 40 cm approximately from the defect. A graphical description of the sensor arrangement is presented in Figure 5-1. The preamplifier was powered through a decoupling box connected to a linear power supply. The decoupling box was connected to a commercial data acquisition card through a coaxial cable. The data acquisition card used was ADlink PCI-9816, with a maximum sampling rate of 10 MSamples/sec, 16-bit resolution and ±5V input range. The sampling rate was set at 5 Msamples/sec. Following to the acquisition, the data was downsampled to 2 Msamples/sec to avoid unnecessary signal processing without loss of significant information. The data were acquired, saved and processed using LabView® 2012.

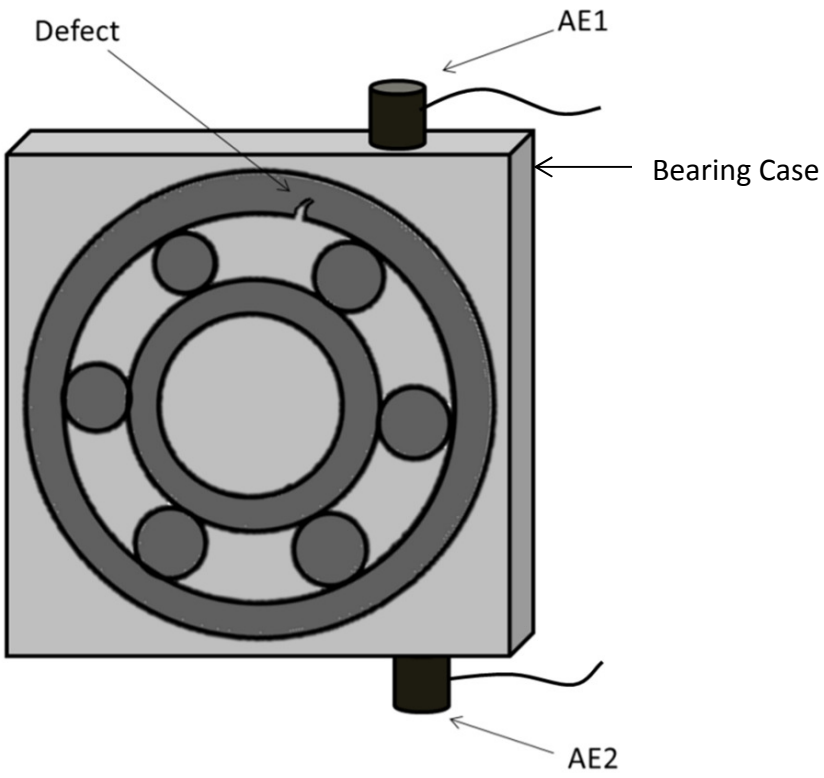

Figure 5-1: Sensor arrangement.

5.2.2. Experimental procedure

The test rig used in this investigation is the same that was used for the experiments described in section4.3. The picture of the defect captured by endoscopic inspection is shown in Figure 5-2. The size of the spall is approximately 5x10mm. The test bearing is a spherical roller bearing from SKF model 22234 CC. The BPFO for this bearing provided by the manufacturer is 8.17X where X corresponds to the rotating speed. This bearing was used as radial slave bearing to transmit the force from the radial hydraulic actuator to the shaft in order to simulate different load conditions. The region where the spall originated was in the top area of the bearing outer race, where the radial hydraulic actuator pushes the bearing to produce the radial load in the shaft. This is the region where the defects are expected to originate due to the high stress generated by the radial load produced by the hydraulic actuator. The test rig was operated for 1 hour prior to the beginning of the data acquisition in order to reach thermal equilibrium. The test rig was operated at 9 different conditions of load and speed in order to study the effect of the operational conditions in the fault detection (Table 5-1).

Figure 5-2: Outer race natural spall.

Table 5-1: Operational conditions of the test rig during the experiments.

Condition	**Speed (RPM)**	**Axial load(KN)**	**Radial load (KN)**
C1	500	1	8
C2	1000	1	8
C3	1650	1	8
C4	500	8	68
C5	1000	8	68
C6	1650	8	68
C7	500	34	138
C8	1000	34	138
C9	1650	34	138

18 data files were acquired, being the interval between two measurements of 10 seconds and the time window of the acquisition was 2 seconds.

5.2.3. Experimental results and observations

Typical time-domain AE signal acquired in C6 is shown in Figure 5-3. It shows an amplitude modulated AE signal that is attributed to misalignment which produces modulation at 1X. This was further investigated in Chapter 6. It is clear that the impact between rolling elements and defect is not evident in the AE waveform. However, The SNR of the AE signal generated by the impact between the rolling elements and the AE signal produced by normal bearing operation changes drastically for different operational conditions. As displayed in Figure 5-4, the raw AE signal in C8, in which the AE burst generated by the defect is clearly seen above the noise level, is opposite to the observation in other conditions such as 1,2,3,4,5,6,7. Thus, the high load and high rotating speed combination generates higher SNR. Particularly, C8 and C9 show very high SNR. Thus, this scenario offers a good potential for testing the WP-ACF in different SNR conditions due to the different SNR produced by the change in load and rotating speed.

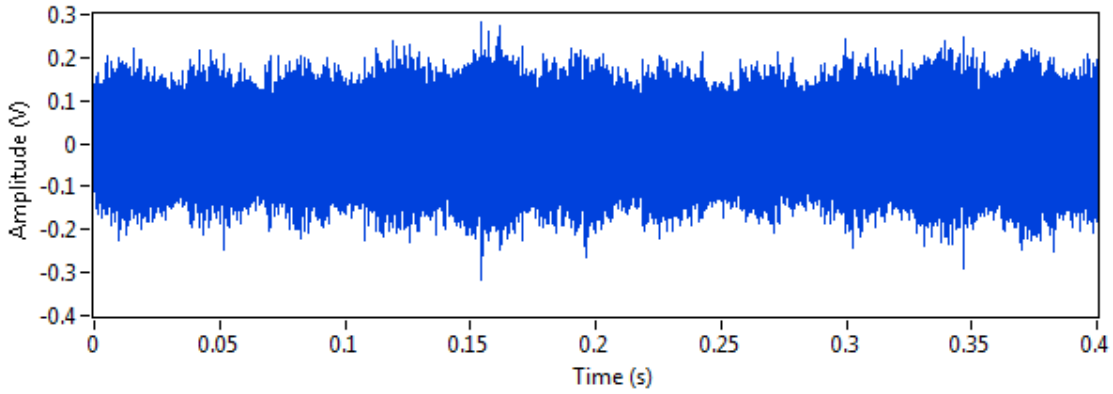

Figure 5-3: Raw AE signal acquired in C6.

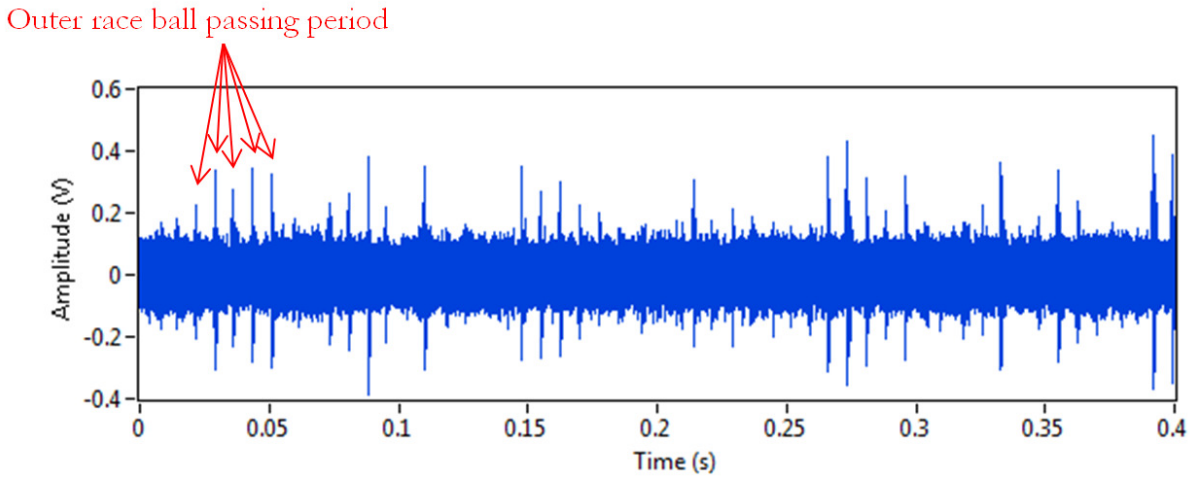

Figure 5-4: Raw AE signal acquired in C8.

The frequency spectrum of the recorded AE signals from both AE1 and AE2 sensor show similar results (Figure 5-5). The AE activity is concentrated between 70 and 400 kHz with peak value at around 100 kHz. The energy of the signals at frequencies above 700 kHz is extremely low.

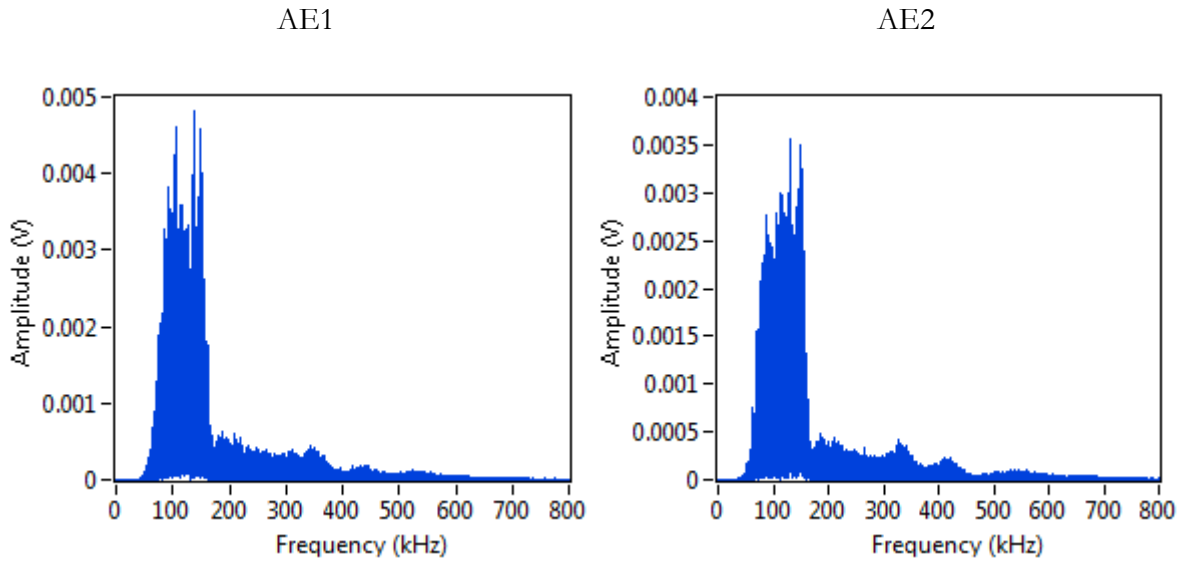

Figure 5-5: Frequency content of the AE signals captured in the experiment.

Figure 5-6 displays the signals from both AE1 and AE2 showing one of the burst generated by the outer race defect. The waveforms show how the sensor installed closer to the defect (AE1) receives this AE burst before AE2, installed in the opposite side of the bearing case. Therefore, the AE signal generated in the defect has to travel further to reach the sensor AE2. This time

difference is approximately 150 μs. The effect of the distance travel by the AE signal from the defect to the sensor is further studied in the next section.

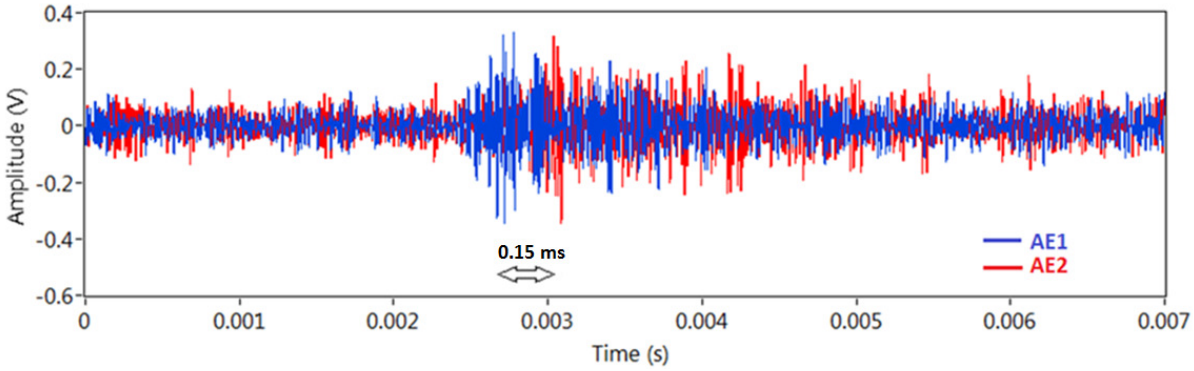

Figure 5-6: AE burst produced by the outer race defect showing different arrival time for both AE sensors.

5.2.3.1. Optimal WP node

The optimal WP-node was investigated in this section. This study aims to determine the effect of the distance from the defect to the AE sensor on the selection of the optimal WP node. In addition, the effect of different operational conditions in the SNR is presented. The SNR of WP-ACF spectrum was estimated using equation 4.16. Due to the higher sampling rate used in this experiment in comparison with the experiment presented in chapter 4, the optimal WP node can be investigated in more detail, offering the possibility to evaluate the SNR with frequencies up to 1 MHz, instead of 500 kHz. Although the sampling rate was 5Msamples/sec, which would theoretically give the possibility to analyse signals up to 2.5 MHz, according to the Nyquist–Shannon sampling theorem. However, to reduce computational complexity, the signals were downsampled to 2 Msamples/sec. The different frequencies range associated with each wavelet nodes for different decomposition levels used in this section are presented in Table 5-2.

Table 5-2: Frequency range associated with each wavelet node for 1, 2, 3 and 4 decomposition level.

1 level decomposition		**2 level decomposition**		**3 level decomposition**		**4 level decomposition**	
Node	Freq (kHz)	Node	Freq (kHz)	Node	Freq (kHz)	Node	Freq (kHz)
1,0	0-500	2,0	0-250	3,0	0-125	4,0	0-62.5
1,1	500-1000	2,1	250-500	3,1	125-250	4,1	62.5-125
-	-	2,2	750-1000	3,2	375-500	4,2	187.5-250
-	-	2,3	500-750	3,3	250-375	4,3	125-187.5
-	-	-	-	3,4	875-1000	4,4	437.5-500
-	-	-	-	3,5	750-875	4,5	375-437.5
-	-	-	-	3,6	500-625	4,6	250-312.5
-	-	-	-	3,7	625-750	4,7	312.5-375
-	-	-	-	-	-	4,8	937.5-1000
-	-	-	-	-	-	4,9	875-937.5
-	-	-	-	-	-	4,10	750-812.5
-	-	-	-	-	-	4,11	812.5-875
-	-	-	-	-	-	4,12	500-562.5
-	-	-	-	-	-	4,13	562.5-625
-	-	-	-	-	-	4,14	687.5-750
-	-	-	-	-	-	4,15	625-687.5

The SNR of WP-ACF using different WP levels and nodes for the signals captured with AE1 and AE2 are presented in Figure 5-7. In both AE1 and AE2, the WP nodes which correspond to high frequencies show higher SNR than the ones corresponding to low frequencies.

It is also evident that that the SNR of the signals captured from AE1provide higher SNR using the high frequency WP nodes. This is attributed to the distance from the sensor to the defect. The signals generated in the spall have to travel a longer distance to reach the sensor AE2. As

the attenuation of AE increases with frequency[129], higher frequencies attenuate faster than low frequency signals to reach AE2. AE1 is very close to the defected area so the attenuation of the high frequency content of the AE1 signal is lower than AE2. As a result, the SNR in the high frequency band is higher using the signals from AE1. The WP nodes that present higher SNR are (2,3) (38.73 dB) and (2,1) (37.09 dB) for AE1 and AE2 respectively. Similar results are obtained for the nodes (1,1) and (3,6) for AE1 and (3,2) for AE2.

On the other hand, in the low frequency range (0-250 kHz) the calculated SNR with AE1 is lower than AE2. This is attributed to the higher load produced by the radial actuator at the top of the bearing close to the area where AE1 is installed. Due to the higher load, the continuous AE generated is higher in that area (refer to section 3.5.1). As the continuous AE noise is present in the low frequency range, the signals captured with the sensor AE1 contain more of this continuous AE noise due to its position closer to the loaded area. For this reason, the SNR of the WP-ACF obtained with the wavelets nodes that correspond to the low frequency range are lower using sensor AE1 than AE2.

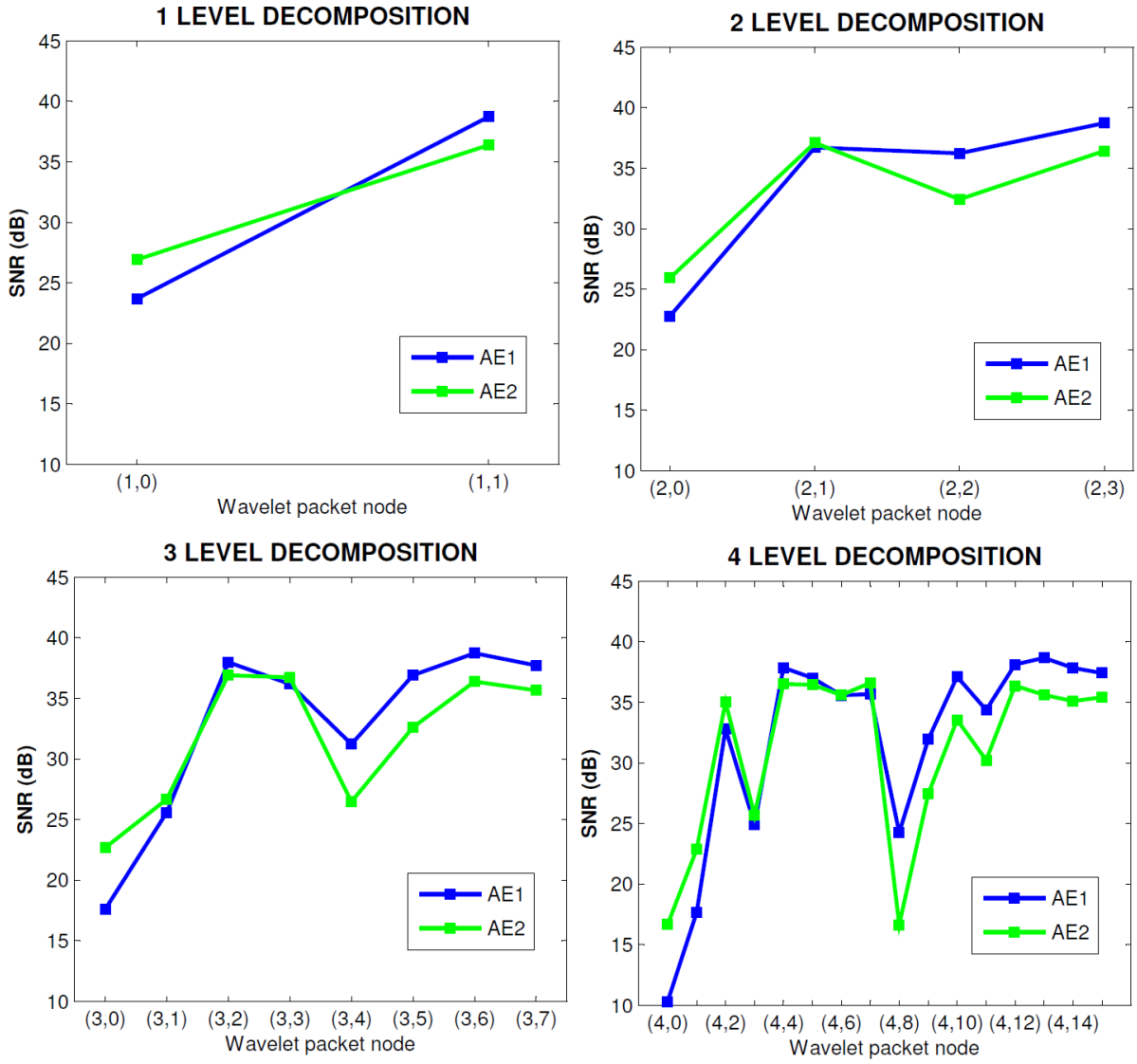

Figure 5-7: SNR for 1-4 level decomposition.

5.2.3.2. Effect of operational conditions

The different operational conditions of load and speed at which the test rig has been operated produce different SNR in the AE signals. The SNR calculated with equation 4.16using the WP-ACF and traditional envelope analysis is shown in Figure 5-8. This graph shows the high impact of operational conditions on the SNR in both traditional envelope analysis and WP-ACF. It is evident that using the WP-ACF the SNR is higher in all conditions. The difference between them differs from 24.49dB in C8 to 2.35dB in C3. There is no clear trend between varying speed and SNR value. While increasing speed increases SNR in C7, C8 and C9 (high load), the same

trend is not observed in C1 to C6 (low and medium load). This divergence is also observed in the variation of SNR with load. However, in general higher loads correspond to higher SNR values. The highest SNR values are obtained in C7 to C9, which correspond to the highest load conditions (8 and 68 kN axial and radial load respectively).

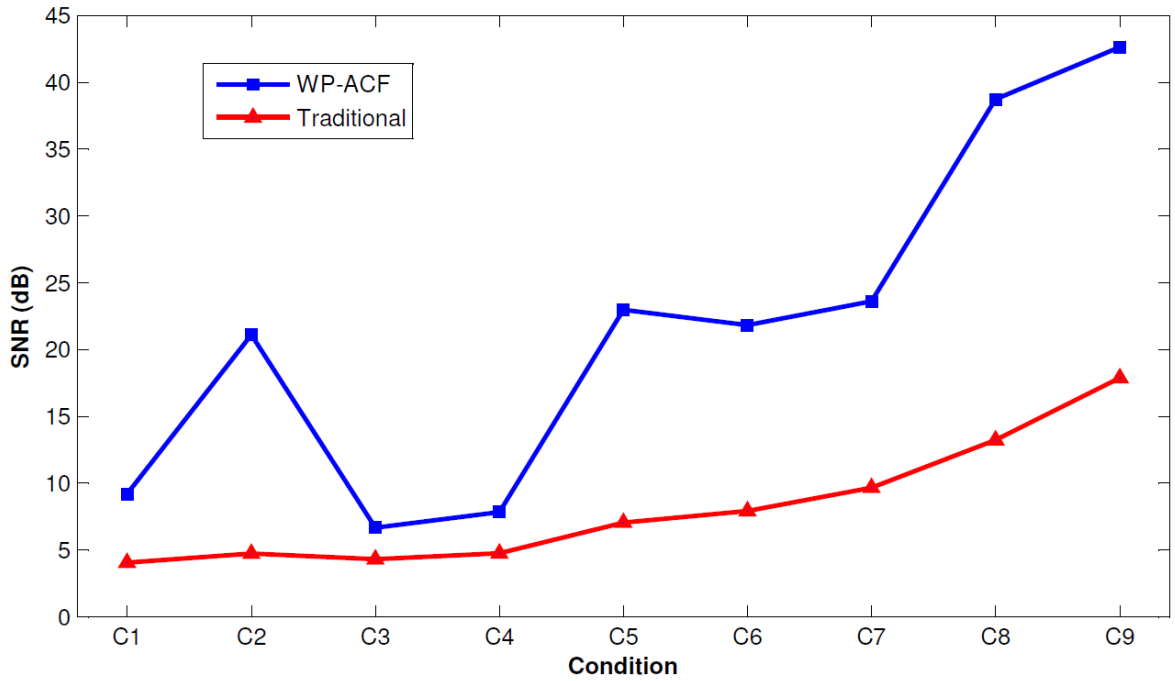

Figure 5-8: SNR of the WP-ACF and traditional envelope analysis for different operational conditions.

The spectra of several samples for C1 to C5 and C6 to C9 are displayed in Figure 5-9 and Figure 5-10 respectively. It is evident that the spectrum of both WP-ACF and traditional envelope analysis varies significantly with operational conditions. The WP-ACF spectra shows how the peak at the BPFO (8.17X) which provides the information regarding the defect is present in all conditions except in C3. In C1 to C7 the main peak in the WP-ACF is 1X, which is attributed to SAM. Further information regarding this peak at 1X attributed to SAM can be found in section 6. However, in C8 and C9 the peak at BPFO becomes dominant in the WP-ACF with high SNR. Furthermore, 2X is shown in C3, C5 and C6 in both WP-ACF and traditional envelope analysis which is also attributed to misalignment. 1X sidebands around the BPFO are evident in C7 and C8 in the WP-ACF spectrum. Sidebands are attributed to modulation of the AE burst generated due to the impact between bearings and rolling elements at the rotating speed

produced by the displacement of the shaft produced by misalignment. The displacement of the shaft is shown in section 6.4.1using the signals captured from proximity sensors installed on the shaft.

In the spectrum using traditional envelope analysis 1X is the main source of modulation in all conditions. In C1 and C2 2XBPFO is also present which might be indicative of the defected outer race. However, the main indication of the defect is the peak at BPFO which is not found in the spectrums of C1 and C2. Using the traditional envelope analysis, the BPFO peak is only presents in C6, C8 and C9.

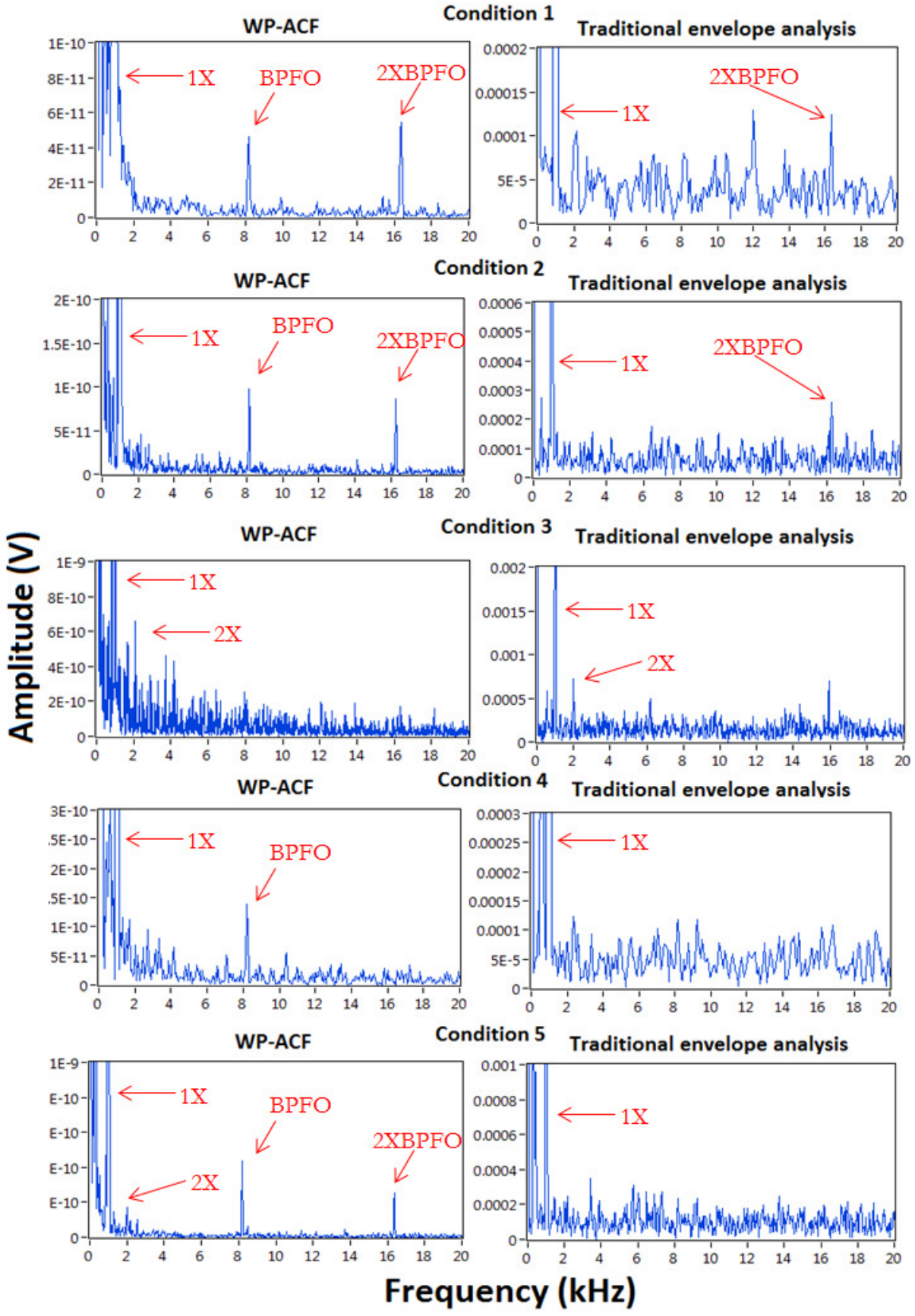

Figure 5-9: WP-ACF spectrum and traditional envelope spectrum for C1 to C5.

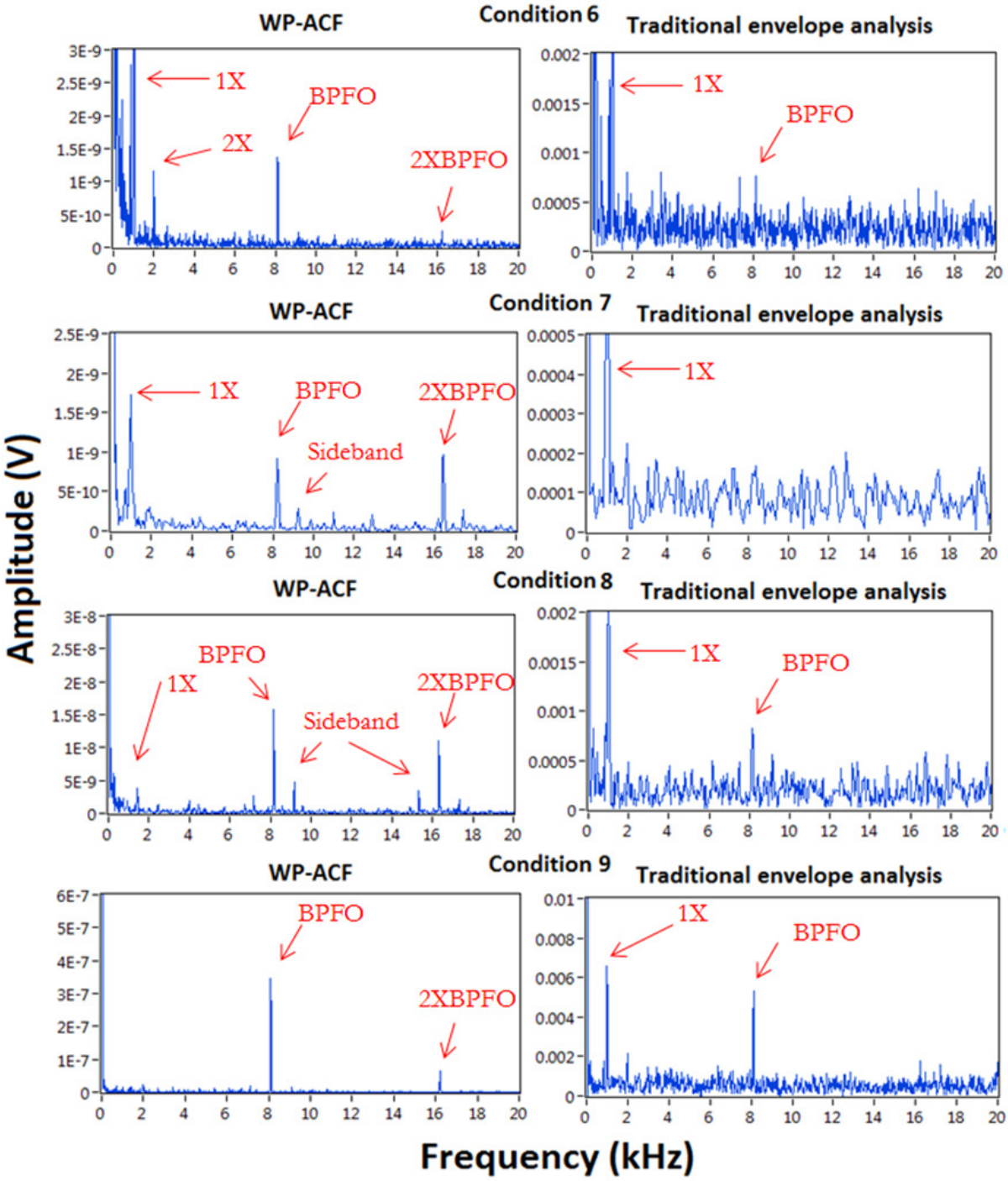

Figure 5-10: WP-ACF spectrum and traditional envelope spectrum for C6 to C9.

5.3. WP-ACF for the defection of gears defects

A seeded defect test is performed to assess the effectiveness of WP-ACF for the identification of seeded defects on straight bevel gears. The difficulty for gear defect detection using AE lies with the fact that the AE sensors are usually installed on the casing due to the complicated access to

the gears. The path between the gears and the case is usually very complex. The signal has to travel from the gears to the shaft, then to the bearings to reach the case. For this reason, the amplitude of the AE generated in the gear mesh when they reach the sensor is extremely low. The gear mesh frequency (GMF) peak and sidebands around it provides significant information regarding the condition of the gears and is very valuable for detection gearbox faults. The difficulty to detect the variation in the gear mesh falls on the high attenuation of the AE signals generated in the gear mesh to the bearing housing. Singh et al. [13] observed an attenuation of 19 dB across the gear mesh and a total loss of up to 45 dB was noted from the gear mesh to the bearing housing. For these reasons the AE signal generated in the gear mesh is of very low SNR and de-noising is of high importance. Also the high complexity of gearboxes, which usually contain a high number of bearings, contributes to an extremely noisy scenario since bearings also generate AE which is considered noise when looking at gear defects[130].

To validate the WP-ACF, AE waveforms were acquired from a gearbox in both defected and non-defected condition. The results are compared with the traditional envelope analysis.

5.3.1. Experimental setup

The AE measurements were carried out with a Machinery Fault Simulator manufactured by SpectraQuest, Richmond, VA, 1997[131]. The Machinery Fault Simulator allows for the measurement of AE data under a variety of fault conditions and is displayed in Figure 5-11 and Figure 5-12 (side view). It consists on a 745 W motor coupled to the gearbox which is connected to a generator to produce the load and increases the torque in the shaft. The motor speed is controlled through a variable frequency drive. A seeded defect was created in one of the pinion teeth to evaluate the performance of the WP-ACF method. The gearbox consists of three-way accessible straight cut bevels with 1.5:1 ratio (Figure 5-13). Further specifications of the gearbox are presented in Table 5-3.

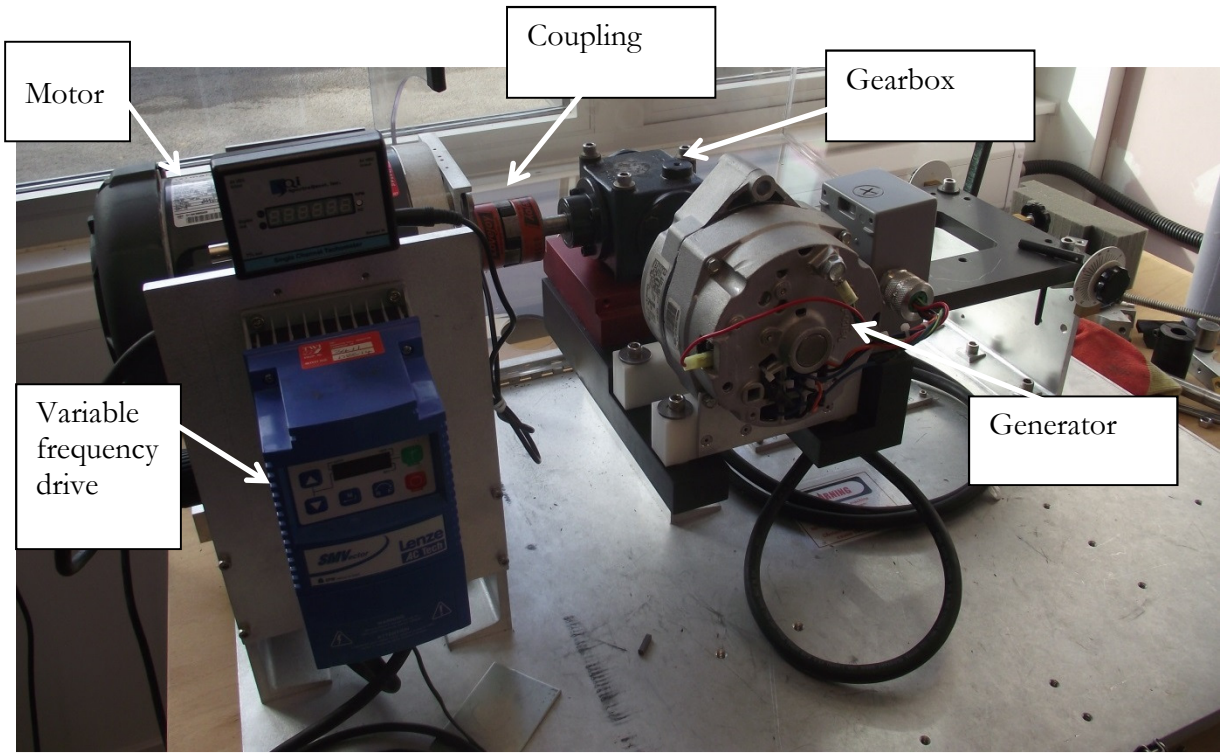

Figure 5-11: Test rig.

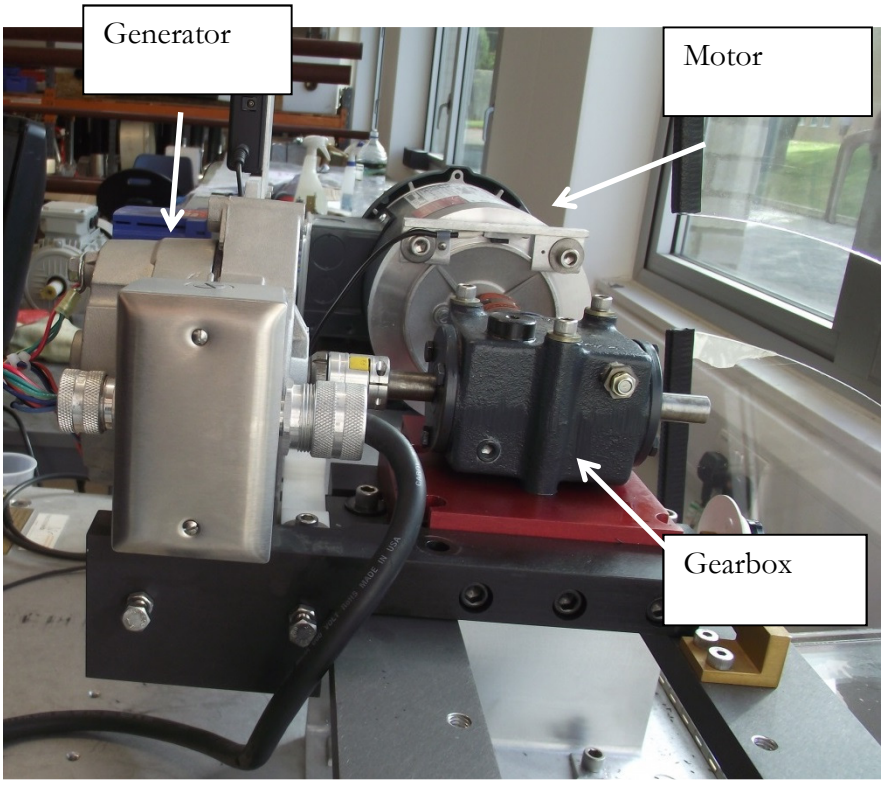

Figure 5-12: Test rig side view.

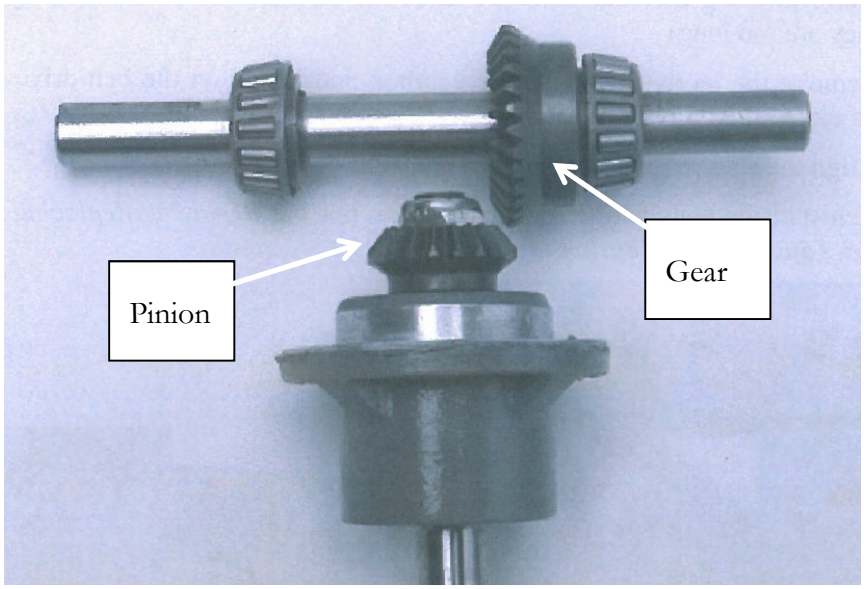

Figure 5-13: Gear arrangement [132].

Table 5-3: Gearbox specifications.

	Value
Gearbox Model	Hub City M2
Ratio	1.5:1
Gear type	Straight cut bevel
Pitch angle gear	56° 19’
Pitch angle pinion	33° 41’
Pressure angle for gear and pinion	20°
Material	Forged steel
Backslash tolerance	25.4-127μm
Pitch diameter pinion	28.57 mm
Pitch diameter gear	42.86 mm
Number teeth pinion	18
Number teeth gear	27

5.3.2. Instrumentation

A Vallen VS900RIC AE transducer was employed with a bandwidth from 100 kHz up to 1 MHz. It includes an internal preamplifier of 34dB gain and was capable of operating from -40 to 85 °C. The signal was band-pass filtered from 70 kHz to 1000 kHz. The AE sensor was attached

to the test gearbox housing using a magnetic holder as shown in Figure 5-14. The paint of the gearbox was removed prior to the experiments and treated with a degreaser to avoid attenuation of the signals. The preamplifier was powered through a decoupling box connected to a linear power supply. The decoupling box was connected to a commercial data acquisition card through a coaxial cable. The data acquisition card used was ADlink PCI-9816, with a maximum sampling rate of 10 MSamples/sec, 16-bit resolution and ±5V input range. The sampling rate was set at 5 Msamples/sec. The acquired data was downsampled to 2 Msamples/sec to reduce the computational load without loss of significant information. The data was acquired, saved and processed using LabView® 2012.

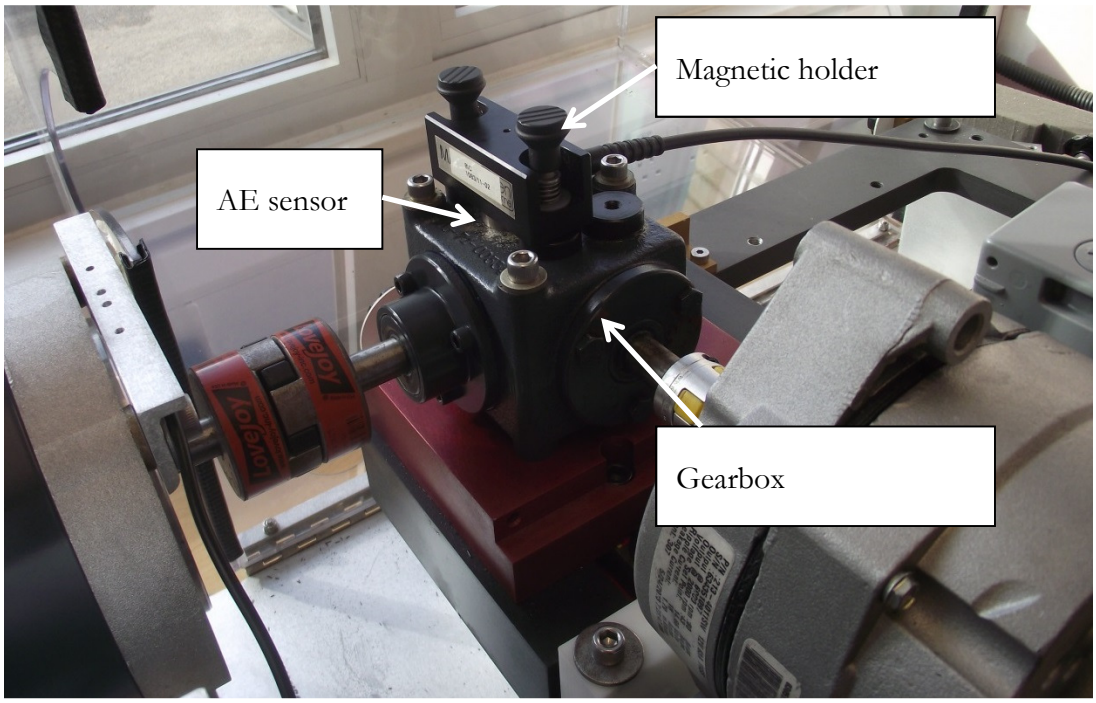

Figure 5-14: Sensor installation on the gearbox.

5.3.3. Experimental procedure

Prior to the introduction of the defect, 12 AE waveforms were acquired to observe the results obtained using the WP-ACF from a healthy gearbox and compare it with the results obtained with the AE data captured from the defected gearbox. The waveforms were acquired at 6000 rpm. For the experiments, the generator was disconnected so the shaft rotated unconstrained. The interval between two acquisitions was set at 10 seconds and the time window of the

acquisition was 1 s. The gearbox was then stopped and dismantled. A defect was artificially introduced in one of the pinion teeth using an engraving machine [57]. The defect size was approximately 2 by 6 mm (Figure 5-15). The gearbox was then operated again at 6000 rpm and 12 AE waveforms were acquired.

Figure 5-15: Seeded defect on the pinion tooth.

5.3.4. Experimental results and observations

A typical waveform associated with the defect-free condition is presented in Figure 5-16. Continuous type AE is dominant but several AE discrete events are also present in the signal. It is worth noting the complex pattern, contrary to what was observed in the AE signal captured from the healthy bearing (Figure 4-10) in which the continuous AE signal dominates with no remarkable AE discrete transients present. The period of the AE transient displayed in the AE signal show a random pattern with no fixed period between them. Figure 5-17 shows the raw AE signal associated with defect condition. The signal displays similar shape to that shown for the non-defected condition. Figure 5-18 shows the frequency spectrum of the AE signal calculated in both the defected and non-defected condition. It shows that the energy of the signal is concentrated between 70 and 350 kHz with no particular difference between them.

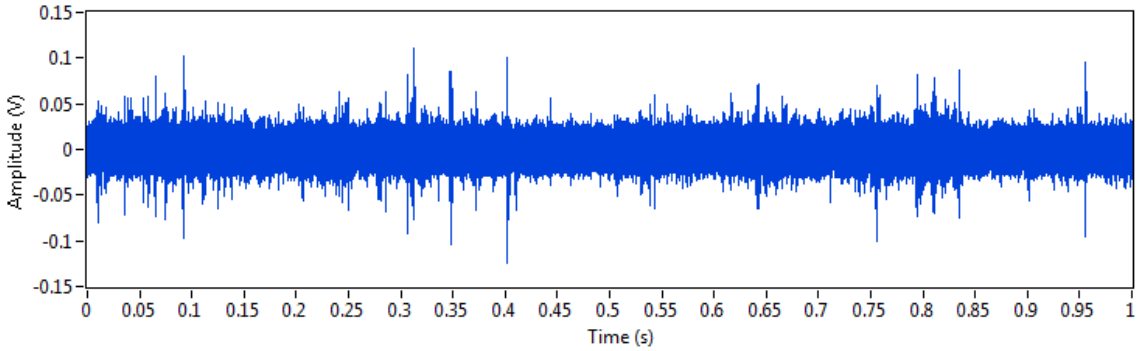

Figure 5-16: AE waveform acquired in defect-free condition.

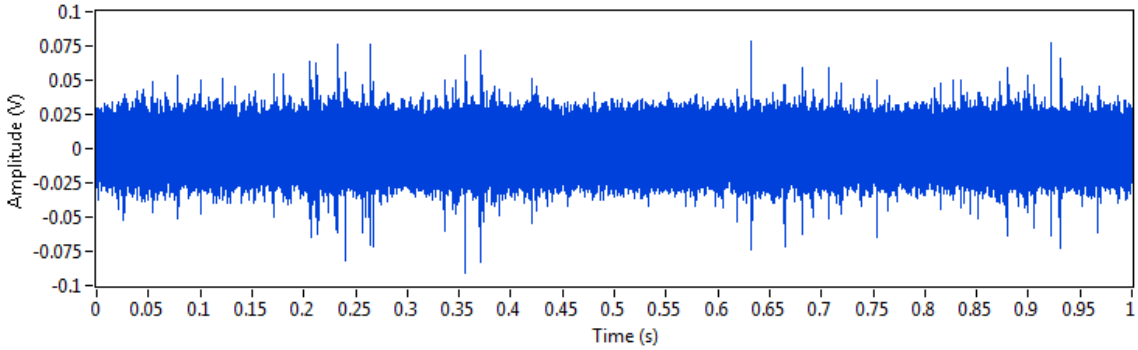

Figure 5-17: AE Waveform acquired in defected condition.

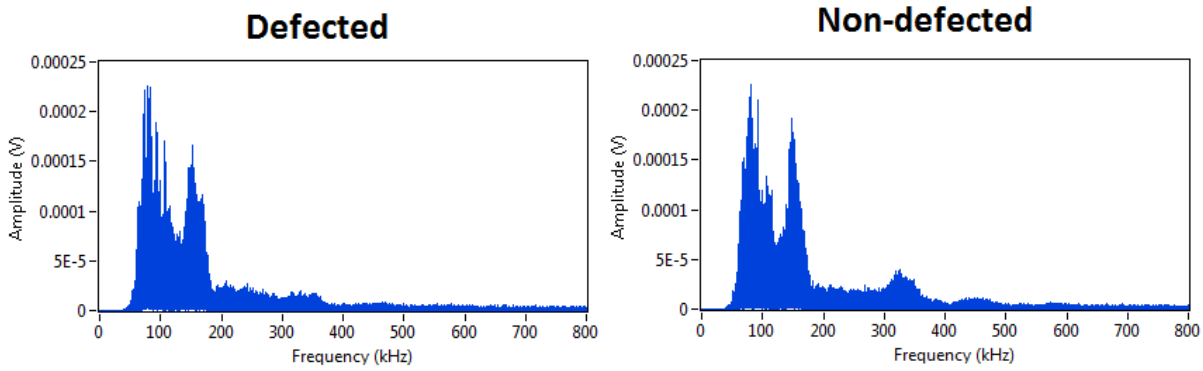

Figure 5-18: AE frequency spectrum associated with defected and defect-free condition

Figure 5-19 shows the AE time-domain signal and time-frequency decomposition using WT associated with the defect free condition. As observed with the AE signals captured from bearings, continuous AE noise dominates in the frequency range between 70 and 250 kHz. However, in contrast to the observations in the AE signals captured from bearings, even in defect-free conditions, several AE discrete events with peak frequencies up to 600 kHz are present in the scalogram. The AE time-domain signal and time-frequency decomposition of the signal captured in defected condition is shown in Figure 5-20. It displays similar shape as

observed in defect free condition with continuous AE noise and numerous discrete AE events. It is worth noting, the AE events in both defected and defected-free conditions show random and non-periodic pattern opposite to the observations in the AE signals associated with non-defected bearings. This is attributed to the higher complexity of gearboxes in comparison with a single bearing as the gearbox under investigation includes three bearings and two gears. Therefore, the AE events could originate in any of the gearbox parts.

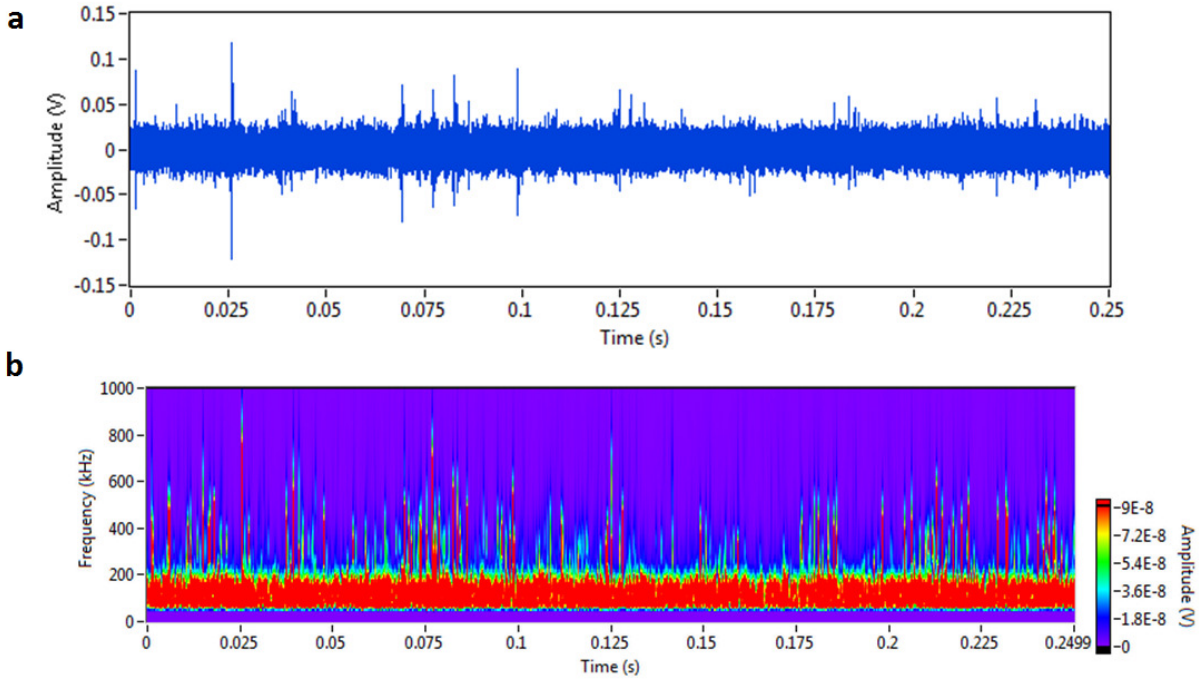

Figure 5-19: AE signal from the gearbox in defect-free condition in (a) time-domain and (b) scalogram.

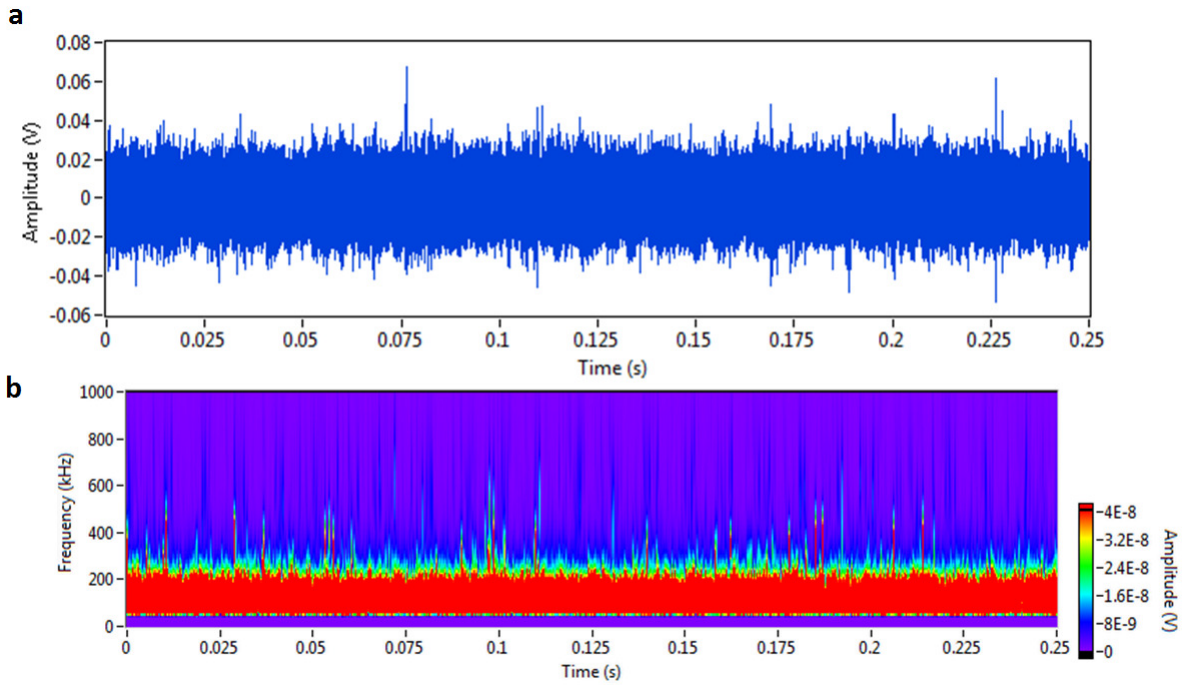

Figure 5-20: AE signal from the gearbox in defected condition in (a) time-domain and (b) scalogram.

Figure 5-21 shows the decomposition of the AE signal in defected condition using WP. The signal was decomposed using Db11 wavelet and 3 levels. The levels corresponding to the higher frequencies were discarded due to the high amount of electronic noise as the AE signal at frequencies above 500 kHz is extremely low as shown in Figure 5-18. Thus, only (4,0) to (4,7) nodes are shown which correspond to the bands between 0-500 kHz (Table 5-2). A portion of 0.1 s of the signal is shown, which corresponds to 10 rotations of the shaft at 6000 rpm. Similar to the results obtained for bearings, the nodes corresponding to the high frequency bands de-noise the signal and show the discrete AE events with higher SNR than low frequency nodes. The performance of the nodes (4,2), (4,6) and (4,7) is particularly efficient in de-noising the AE discrete events from the continuous background noise. However, in this case, the periodicity of the AE events is not uniform as shown for bearing defects and cannot be correlated with the defect generated in the gear tooth. If the AE events were generated by the defect the AE events periodicity should be at 1X of the gear (0.66X of the pinion speed) as for every rotation the defects enter once in the gear mesh. However, this is not visually discernible in the decomposed signal using WP.

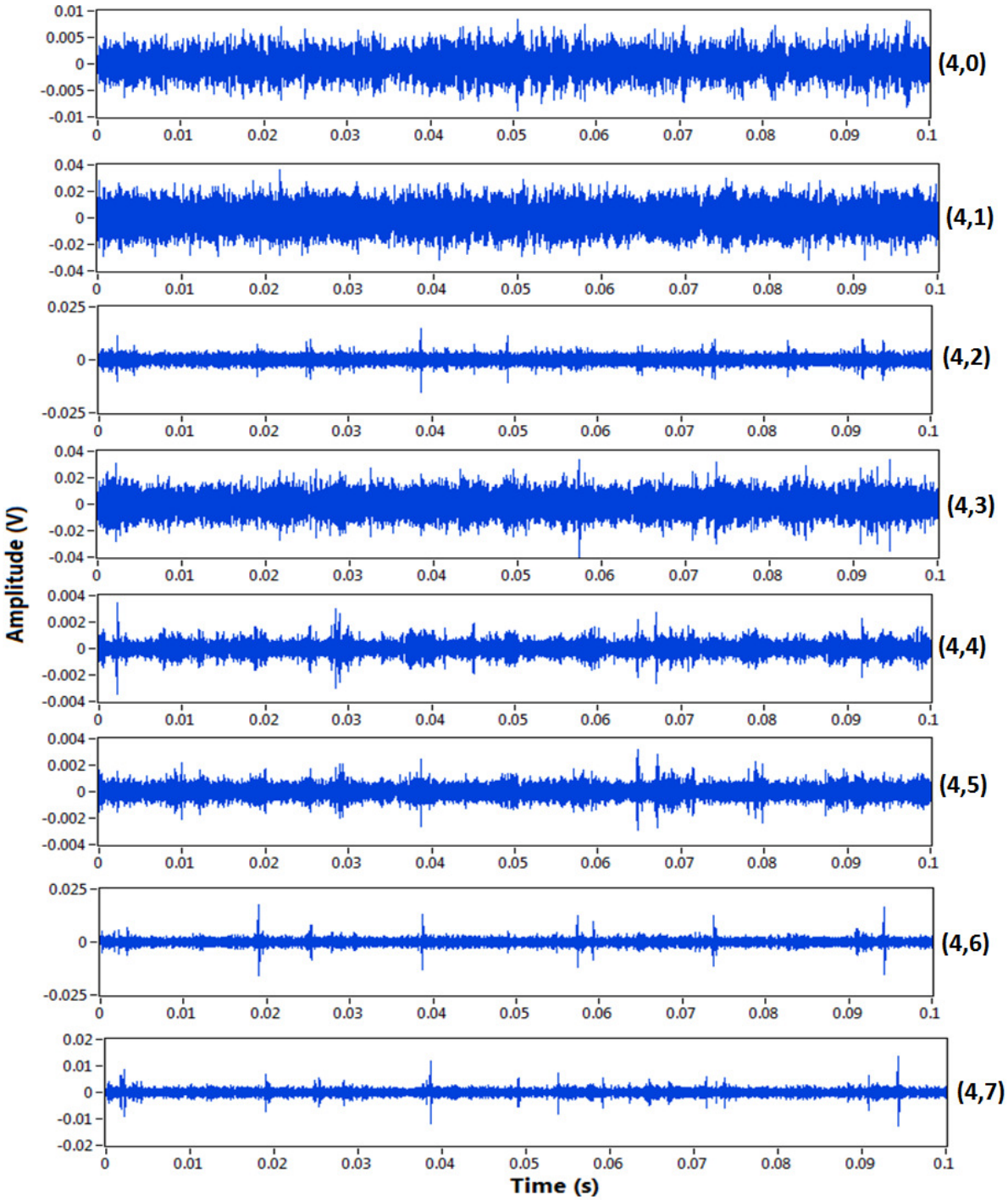

Figure 5-21: 4-level WP decomposition of the AE signal associated with defected condition.

Figure 5-22shows the WP-ACF spectrum applied to the AE signal associated with defect-free condition. The WP was applied using Db11 wavelet and the (2,1) (250-500 kHz) wavelet has been selected as it offers the highest SNR for the GMF .The GMF corresponding to 18X of the pinion and 2XGMF is dominant in the spectrum. The source of AE activity that produces these

peaks is asperity interactions between gears in mesh. The WP-ACF shows high sensitivity to de-noise these AE events. It is worth noting that sidebands are not present around the GMF, which indicate a healthy condition of the gears. Figure 5-23, displays the traditional envelope analysis in which the GMF and 2XGMF are also present. However, the SNR of both peaks are much lower than the WP-ACF peaks. This suggests that the traditional envelope analysis is less sensitive than the WP-ACF to the AE burst generated by asperity contact in gear mesh than the WP-ACF spectrum.

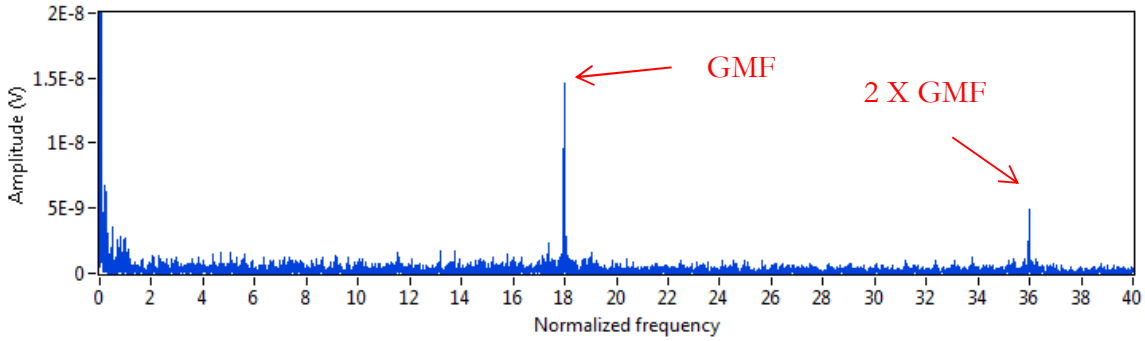

Figure 5-22: WP-ACF spectrum in defect-free condition.

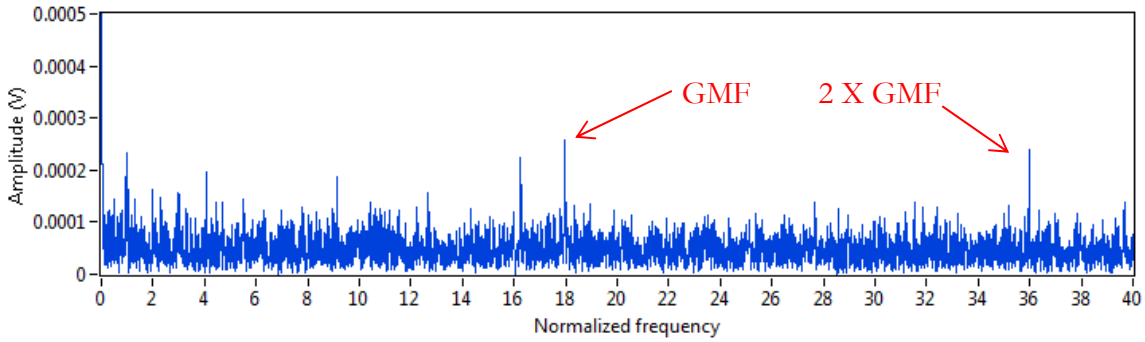

Figure 5-23: Traditional envelop analysis spectrum in non-defected condition.

Figure 5-24 shows the spectrum obtained using the WP-ACF associated with the defected condition. It clearly shows higher number of frequency components excited in the spectrum. The main peak is the GMF and 2XGMF is also present. There are also prominent peaks at 1X and 2X of the gear and 1X of the pinion. It is worth remarking the presence of sidebands of 1X of the pinion rotating speed around the GMF. Usually, the presence of meshing frequency harmonic sidebands and their amplitudes can prove to be very valuable when diagnosing gear

defects[133].The increment in the number and amplitude of such sidebands may indicate a fault condition[134]. As observed in Figure 5-22 the sidebands were not present before the introduction of the seeded defect. Thus, the appearance of these sidebands in the WP-ACF around the GMF suggests amplitude modulation around the GMF which could be attributed to defected pinion tooth[135]. Furthermore, the spacing of the sidebands is related to their source[136]. The fact that the sidebands are spaced 1X of the pinion rotating speed, where the defect was seeded and not 1X of the gear rotating speed, strongly indicate that the sidebands are caused by the amplitude modulation in the GMF produced by the seeded defect introduced.

Figure 5-25 shows the spectrum obtained with the traditional envelope analysis. In this case, the main peak is not GMF as observed in the WP-ACF spectrum, but the peak at 1X of the pinion rotating speed. The GMF peak is present with extremely low SNR as observed in the non-defected condition. However, the sidebands around the rotating speed are not visible using the traditional envelope analysis, attributed to the low SNR. As a result, the sidebands are below the noise level and are not discernible. In addition, 1X and 2X of the gear rotating speed are also present in the spectrum.

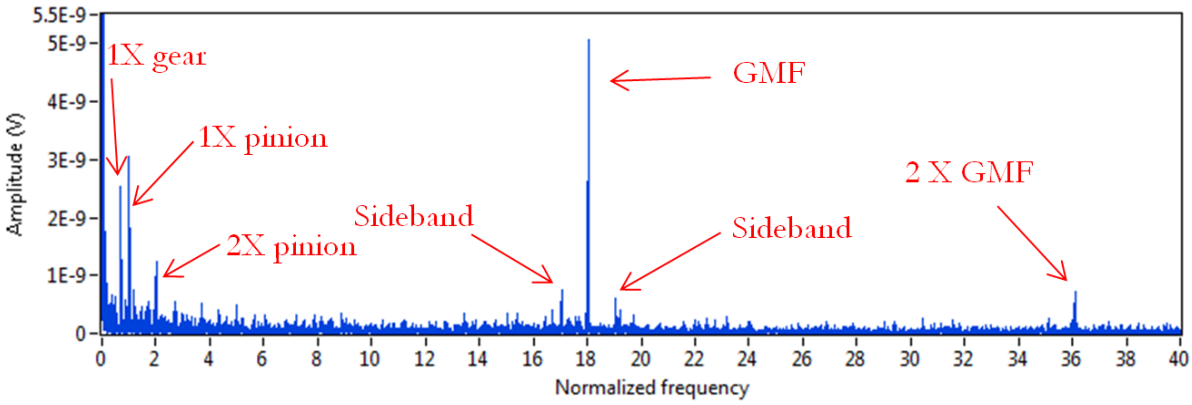

Figure 5-24: WP-ACF spectrum in defected condition.

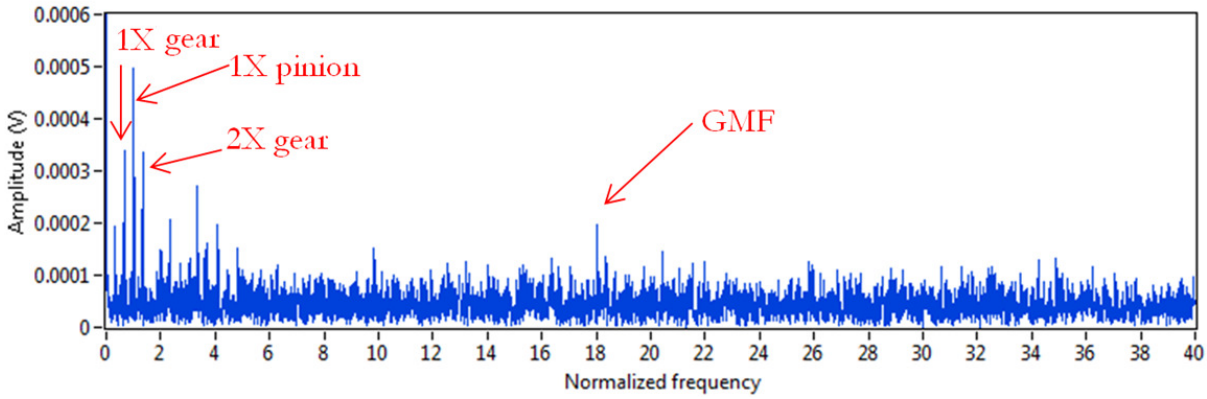

Figure 5-25: Traditional envelop analysis spectrum in defected condition.

5.4. Summary

5.4.1. On the naturally defected spherical bearings

The WP-ACF method has been validated for the detection of a naturally developed defect in the outer race of spherical roller bearings. This experiment allows validating the method in a situation closer to a real industrial condition than the experiments presented in chapter 4.

The high sampling rate used in the experiments (5 Msamples/sec) allows further investigating the WP as a pre-processor with higher frequency range than the experiments presented in chapter 4. The WP nodes corresponding to the high frequency range provides higher SNR and they show higher sensitivity to the natural defect as they were also observed in the experiment with seeded defects in the previous chapter. In particular, for the sensor AE1, the WP node (2,3) (500-750kHz) displays the highest SNR. In addition, the node (1,1)(500-1000kHz) and (3,6) (500-625kHz) showed slightly lower SNR. For the sensor AE2 the node (2,1) (250-500 kHz) offers the highest SNR for this sensor with similar results for (3,2) (375-500kHz). Although the optimum frequency range varies slightly between the scenarios with seeded and natural defects, the medium - high frequency range shows better de-noising potential and consequently higher SNR.

Another interesting finding is the significant impact of operational conditions on both WP- ACF traditional envelope analyses. While the SNR using the WP-ACF is 42.62dB in C9, in C3 it is as low as 6.67dB. Thus, the detection of the defect is highly influenced by operational conditions.

The sensor installed closer to the defect (AE1) exhibits optimal SNR results at higher frequencies than AE2 sensor which are 500-750 kHz and 250-500 kHz respectively. This is attributed to the higher attenuation of the high frequency signals and they have to be transmitted further to reach AE2.

Comparison of the WP-ACF and traditional envelope analysis results demonstrate that the WP-ACF is more sensitive in detecting the natural incipient bearing defect than traditional envelope analysis in all conditions but C3 in which the BPFO peak is present neither in the WP-ACF spectrum nor in the traditional envelope analysis. Thus, the detection of the fault cannot be achieved.

5.4.2. On the seeded defected Bevel gears

Preliminary experiments on the application of WP-ACF for straight bevel gear defect detection have been presented. This is the first known attempt to detect defects in bevel gears using AE. The spectrum calculated from the AE signals captures from the gearbox using both WP-ACF and traditional envelope analysis show an increase in spectral components in the defected condition particularly in the gear and pinon rotating speed range. However, the most important component in gear fault diagnosis is GMF and its harmonics, together with sidebands produced by modulation. The increment in the number and amplitude of such sidebands indicates a fault condition[134]. Thus, the higher SNR of these peaks shown using the WP-ACF shows the higher sensitivity and the potential use of this method for gear defect detection.

Chapter 6

Shaft angular misalignment detection using AE

6.1. Introduction

To date, the most common technique applied to detect shaft misalignment is vibration analysis and in particular, vibration spectrum; however, the speed, the coupling type and the stiffness have a strong effect on the vibration spectrum that may lead to an inaccurate diagnosis [96]. In addition, vibration signals are usually acquired using accelerometers installed in the bearing

housing or on the machine case. Thus, the signal measured is in fact a response to those forces that are transmitted from the rotor to the stationary parts of the machine such as the bearing case [137].

Although several AE studies have been conducted to detect crack onset and propagation, spalls, pitting and wear in different components of rotating machinery using AE technique[117][28][55], the detection of rotor-dynamic faults such as misalignment using AE technique has not been fully investigated. For this reason, the main aim of this study is to develop an approach based on AE signal analysis in order to detect SAM and study the effect of operational conditions. This experimental study uses proximity sensors to accurately characterise the periodic displacement of the shaft produced by SAM. Then, the detection of the shaft displacement using AE and acceleration signals is accomplished using sensors installed in one of the bearing housing. The results obtained using these two techniques are compared and discussed.

6.2. Proposed method for SAM detection

Misalignment produces periodic changes in the lubricant film thickness and the frictional moment between the bearing and the shaft [138][139]. These phenomena cause frictional rubbing between the shaft and stator components which causes a release of AE energy that propagates from the rub source to the sensor installed in the bearing housing [140]. Thus, the signals captured by the AE sensors are modulated due to the periodic variation of rubbing. The WP-ACF method has been investigated to detect misalignment fault. However, as the modulation produced by misalignment does not produce rapid transient AE produced by interaction between defect and rolling elements, the method is not efficient in this case. On the contrary, the modulation produced by misalignment is a smooth modulation of the background continuous AE noise that was considered noise in the previous chapters. Therefore envelope analysis is applied to the AE signals to detect this variation of AE generated by misalignment (Figure 6-1). Envelope analysis has been traditionally used to identify bearing and gear

defects[141]. Nevertheless, in this study, the effect of SAM in the AE envelope spectrum under varying operational conditions is investigated.

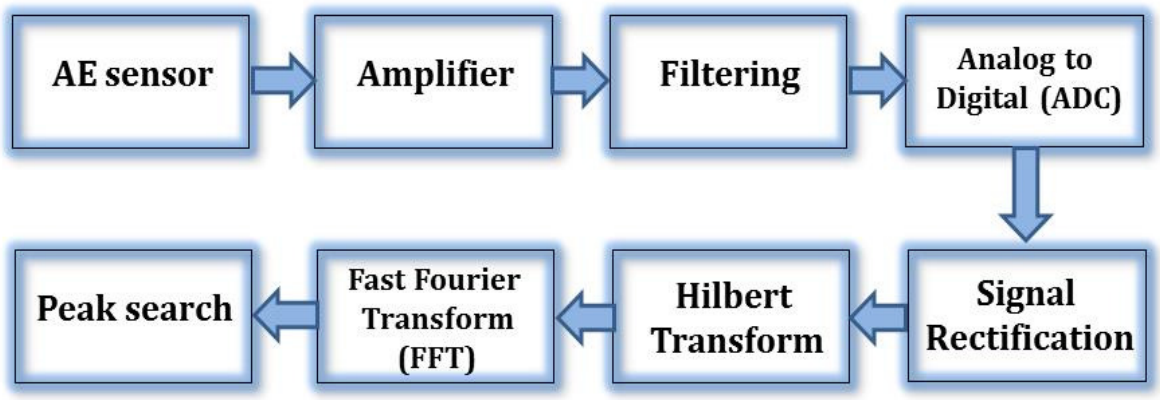

Figure 6-1: Schematic of the proposed method for misalignment detection.

The signal acquisition is carried out, using an AE sensor, followed by amplification, filtering and analog to digital conversion. More detailed information about the data acquisition procedure is presented in section6.3.2.1. Subsequent to the signal acquisition, envelope analysis is applied. This technique has been traditionally used in vibration to detect a broad range of faults in rotating machinery; however, it also has been successfully developed for bearing and gearbox defect detection using AE [55][83]. The process of extracting the envelope of a signal has two different steps: signal rectification and a HT. Further information about envelope analysis can be found in section 3.2.4.

Subsequent to the envelope extraction, the time-domain signal is transformed into frequency domain using the FFT to obtain the frequency spectrum of the enveloped AE signal.

6.3. Experimental setup and measurements

6.3.1. Test rig

The test rig used in this work (Figure 6-2) was developed by Romax Technology Ltd. in order to investigate bearing skidding and its effect on the bearing useful life. The test rig was designed to represent the shaft arrangement in a typical 2 MW wind turbine. The shaft was supported by

three test bearings; one spherical roller bearing and two tapered roller bearings. Gear load was simulated by hydraulic actuators, applying axial and radial loads through the slave bearings. A thrust bearing was used as the axial slave bearing and a spherical bearing as the radial slave.

A 30 kW motor was used to power the test rig with a nominal speed of 1650RPM. It was controlled through a variable frequency drive that modified the rotational speed. The rated axial and radial load of the rig was 40 kN and 140 kN, respectively. The test rig is capable of reproducing a wide range of dynamic loads typically experienced by wind turbine drive trains.

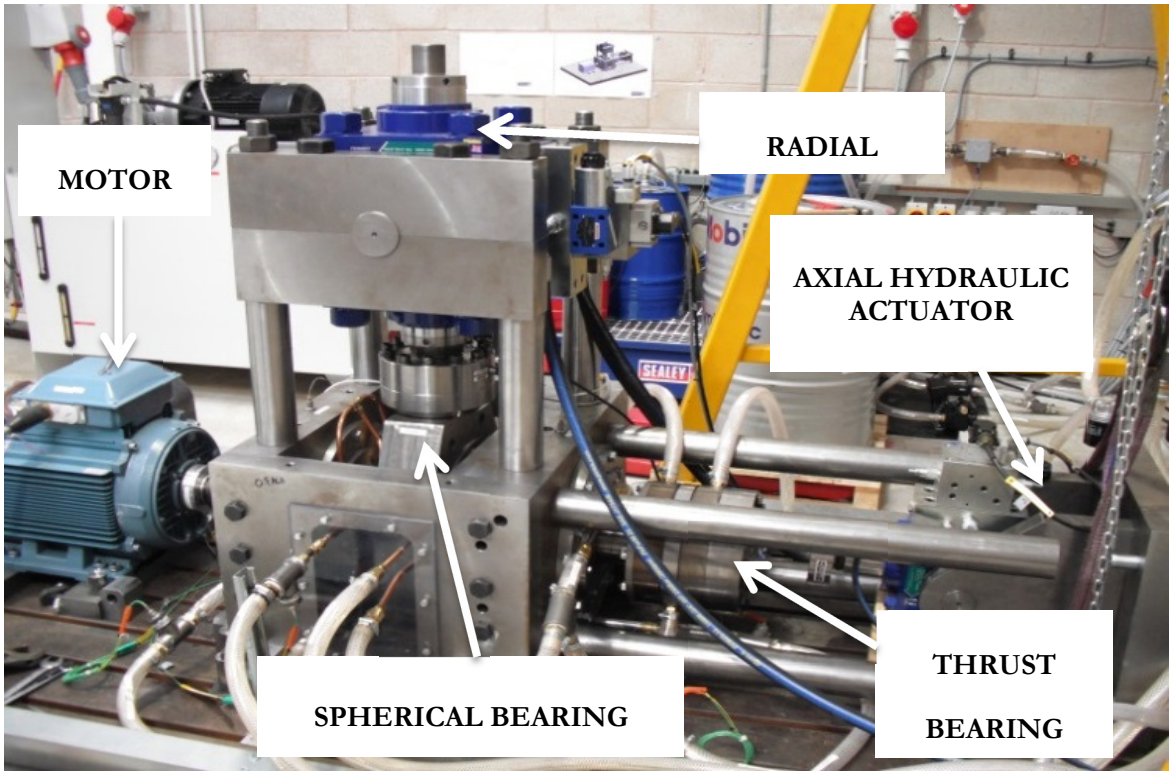

Figure 6-2: Test rig used in the experiment.

6.3.2. Instrumentation

Three different types of sensors were utilised in this investigation (Figure 6-3):

- One AE sensor,
- One accelerometer to compare the results obtained using AE and acceleration spectrum,

- Two proximity sensors to measure accurately the displacement of the shaft produced by the SAM and correlate it with the AE envelope spectrum and the acceleration spectrum.

6.3.2.1. AE

One Vallen VS900RIC AE transducer was employed with a bandwidth from 100 kHz up to 1000 kHz. It includes an internal preamplifier with a 34dB gain and is operative in a range of -40 to 85 ^{0}C. The signal was band-pass filtered from 100 kHz to 1000 kHz. The sensor was attached to the spherical slave bearing that supported the radial load produced by the hydraulic actuator (Figure 6-3). The preamplifier was powered through a decoupling box connected to a linear power supply. The decoupling box was connected to a commercial data acquisition card through a coaxial cable. The data acquisition card used was ADlink PCI-9816, with a maximum sampling rate of 10MSamples/sec, 16-bit resolution and ±5V input range. The sampling rate was set as 5Msamples/sec and the data was acquired, saved and processed using LabView® 2012.

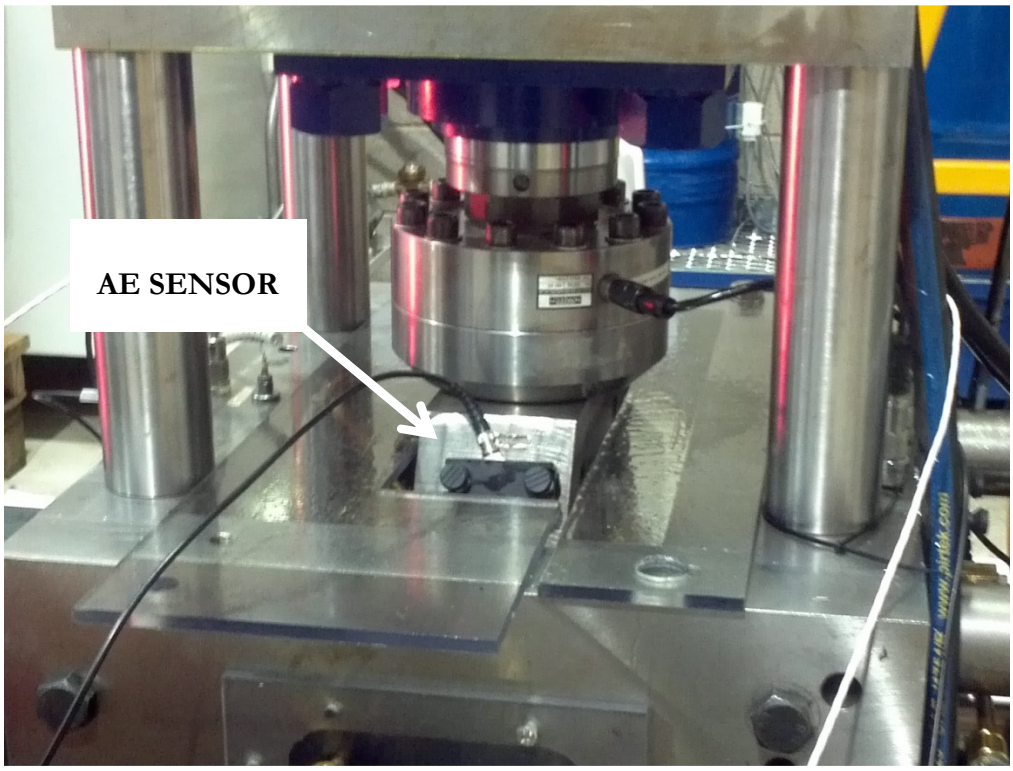

Figure 6-3: AE sensor location.

6.3.2.2. Accelerometers

The accelerometer employed was 4519-003 from Brüel & Kjær offering a response from 0.5Hz to 20 kHz and 100 mV/g sensitivity. It was installed in vertical direction of the spherical bearing. The acceleration signal was continuously acquired during the whole test using the NI 9234 data acquisition card and CompactRIO platform from National instruments. The NI 9234 data acquisition offers 51 kSamples/sec as maximum sample rate, accurate 24-bit resolution conversion, ±5 V input range and includes antialiasing filter. The acceleration signal was sampled at 20 kSamples/sec.

6.3.2.3. Proximity sensors

Proximity sensors provide a direct measurement of the shaft position. Two proximity sensors were installed in vertical and horizontal direction in order to analyse the shaft displacement in both axes. The proximity sensors were installed next to the spherical bearing where the accelerometer and AE sensor were installed. The proximity sensor used was a Baumer model IWRM 12 U9502 and the signal was sampled at 300 Samples/sec using the data acquisition card NI 9205 from National Instruments. It offers 250 kSamples/sec maximum sample rate with 16-bit resolution.

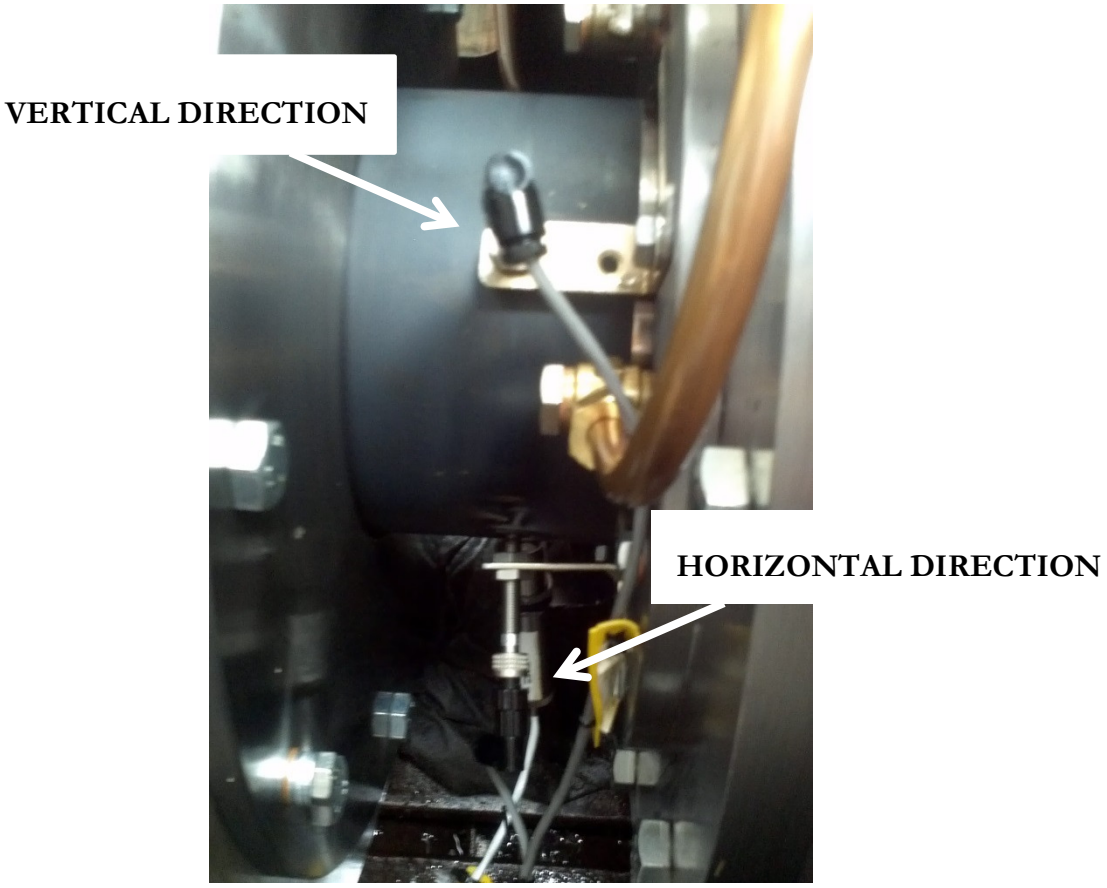

Figure 6-4: Proximity sensor location

6.3.2.4. Measurements

The test rig was operated continuously for 1 hour prior to the beginning of the data acquisition in order to reach thermal equilibrium. The measurements were carried out in 9 different operational conditions of varying axial load, radial load and rotational speed in order to study the impact on AE and acceleration signals (Table 6-1). 18 AE data files were acquired for each condition. The time between two measurements was set at 10 seconds and the time window of the acquisition was 2 seconds. A total of 162 AE data files were acquired. The signals from the accelerometers and proximity sensors were acquired and recorded continuously.

Table 6-1: Test rig operating conditions.

Condition	Speed (RPM)	Axial load(kN)	Radial load (kN)
C1	500	1	8
C2	1000	1	8

C3	1650	1	8
C4	500	8	68
C5	1000	8	68
C6	1650	8	68
C7	500	34	138
C8	1000	34	138
C9	1650	34	138

6.4. Experimental results and observations

6.4.1. Proximity sensor signals results and observations

A direct displacement measurement was carried out in order to correlate the shaft displacement with AE and acceleration signals. The accurate characterisation of the shaft displacement produced by SAM is carried out through the displacement signals acquired from the proximity sensors. The signals generated by these sensors provide precise information about the shaft displacement in all different operational conditions. The time-domain signals obtained from the proximity sensors in both vertical and horizontal direction are presented in Figure 6-5 (C2), displaying a sinusoidal shape in both directions. The displacement obtained in the other conditions is similar as shown in Figure 6-5. The DC offset in both graphs was caused by the distance of the proximity sensors to the shaft.

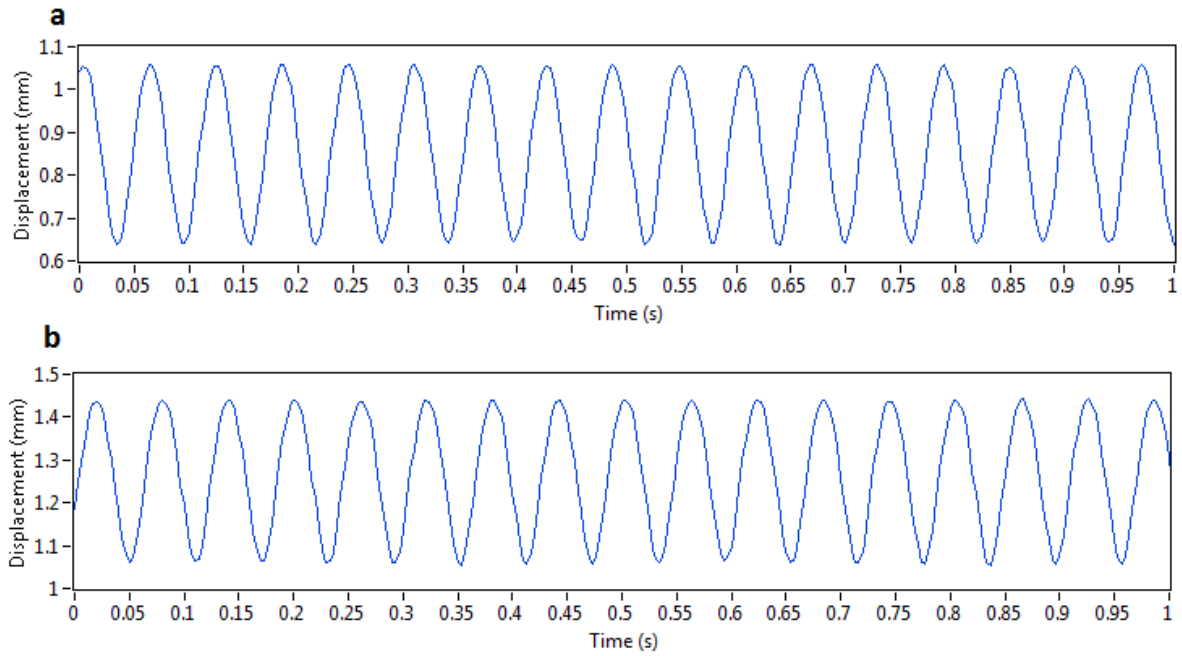

Figure 6-5: Horizontal (a) and vertical (b) displacement measurement of the shaft in the condition 2, using proximity sensors.

The displacement signals in the frequency domain calculated using FFT is presented in Figure 6-6. This is calculated in order to characterise the displacement of the shaft and correlate it to the rotational speed. The graph shows the frequency domain signals acquired from the proximity sensors in C2 in horizontal (a) and vertical (b) direction. The X-axis indicates the normalised frequency (times the rotational speed) and the Y-axis denotes displacement (mm). It shows dominant 1X behaviour that is also obvious in the other conditions. The amplitude of 1X is slightly higher in the horizontal than in the vertical direction. The results exhibit also the 2X component of shaft displacement but the amplitude of this displacement is significantly lower than the 1X amplitude and it is almost twice as important in the vertical direction compared with the horizontal direction. 1X is 16.6 and 28.57 times higher than 2X amplitudes in vertical and horizontal direction respectively in C2. It is similar under the other operational conditions. 3X component is also present but the amplitude is extremely low in comparison with 1X.

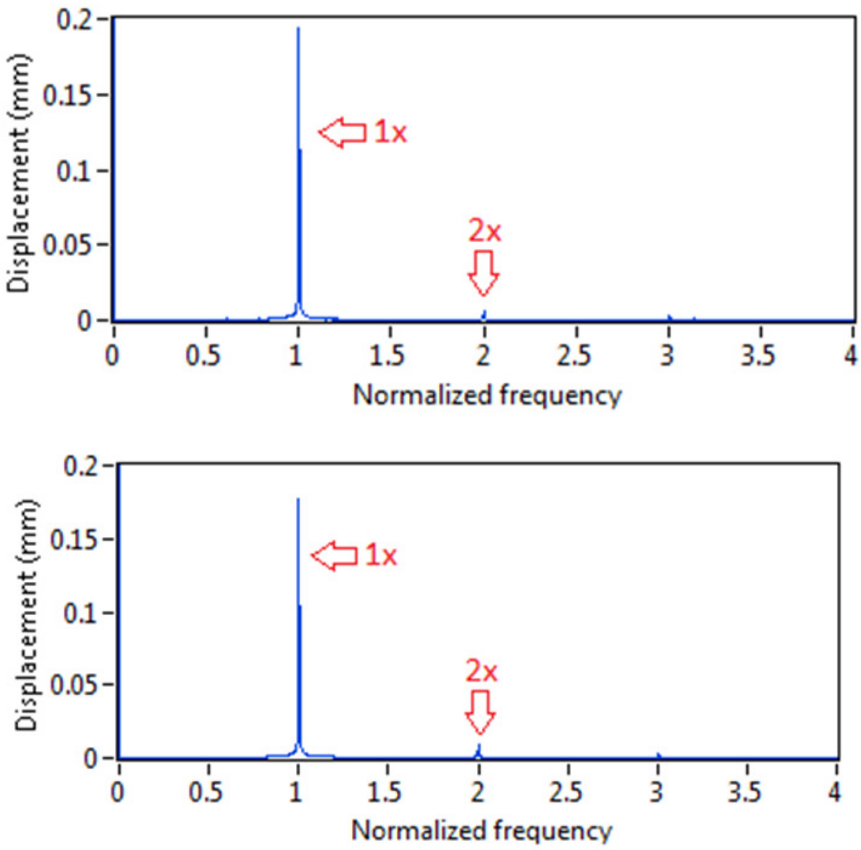

Figure 6-6: Horizontal (a) and vertical (b) displacement measurement on the shaft in C2 in the frequency domain.

The frequency spectrum of the proximity sensor signals shows that SAM produce a main 1X peak and a smaller 2X peak that agrees with the SAM characterization reported in [92] and[93]. On the other hand, imbalance and looseness can generate high 1X and moderate 2X amplitudes in the shaft displacement. However, they can be discarded due to the following reasons:

- Looseness generates harmonics (2X, 3X, 4X, etc.), which are usually of higher amplitude and not as low as presented for the proximity sensor signals and the noise floor would be raised[142].
- Unbalance is discarded due to the high vibration measured in the axial direction (1X and 2X) with the accelerometers shown in the next section. Misalignment generates high axial vibrations, sometimes even higher than radial vibrations. Unbalance does not produce significant vibrations in axial

direction[143][144]. Furthermore, when SAM is present, the measurements in vertical direction are slightly smaller than vertical direction as displayed in Figure 6-6 (1X peak) [143].

6.4.2. Acceleration signals results and observations

A typical acceleration waveform acquired in C1 is displayed in Figure 6-7.

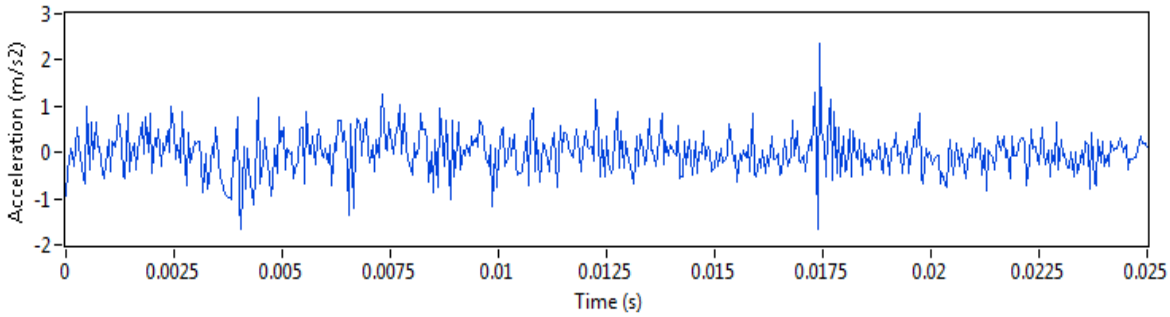

Figure 6-7: Example of acceleration signal acquired during the test (C1).

FFT analysis was applied to 25 seconds of the acceleration signal to obtain the frequency components of the 9 operational conditions. Only the low frequencies are shown in the acceleration spectrum because this is the interesting range for the investigation of misalignment detection (Figure 6-8). Peaks at 1X and 2X are distinguishable under all conditions. Under C1 and C2 the peak at 2X shows greater value than 1X in contrast to the results shown in the displacement signals. It is also evident that the underlying background noise is significantly higher than the displacement signals shown in the previous section. In the operational C3 to C9, the peak at 1X becomes dominant over the other peaks. Several peaks related to unknown sources of vibration are also present in the spectrum at different frequencies. In addition, the noise floor level changes for the different conditions. This spectrum noise floor and SNR of the acceleration signals are further investigated in section6.4.6.

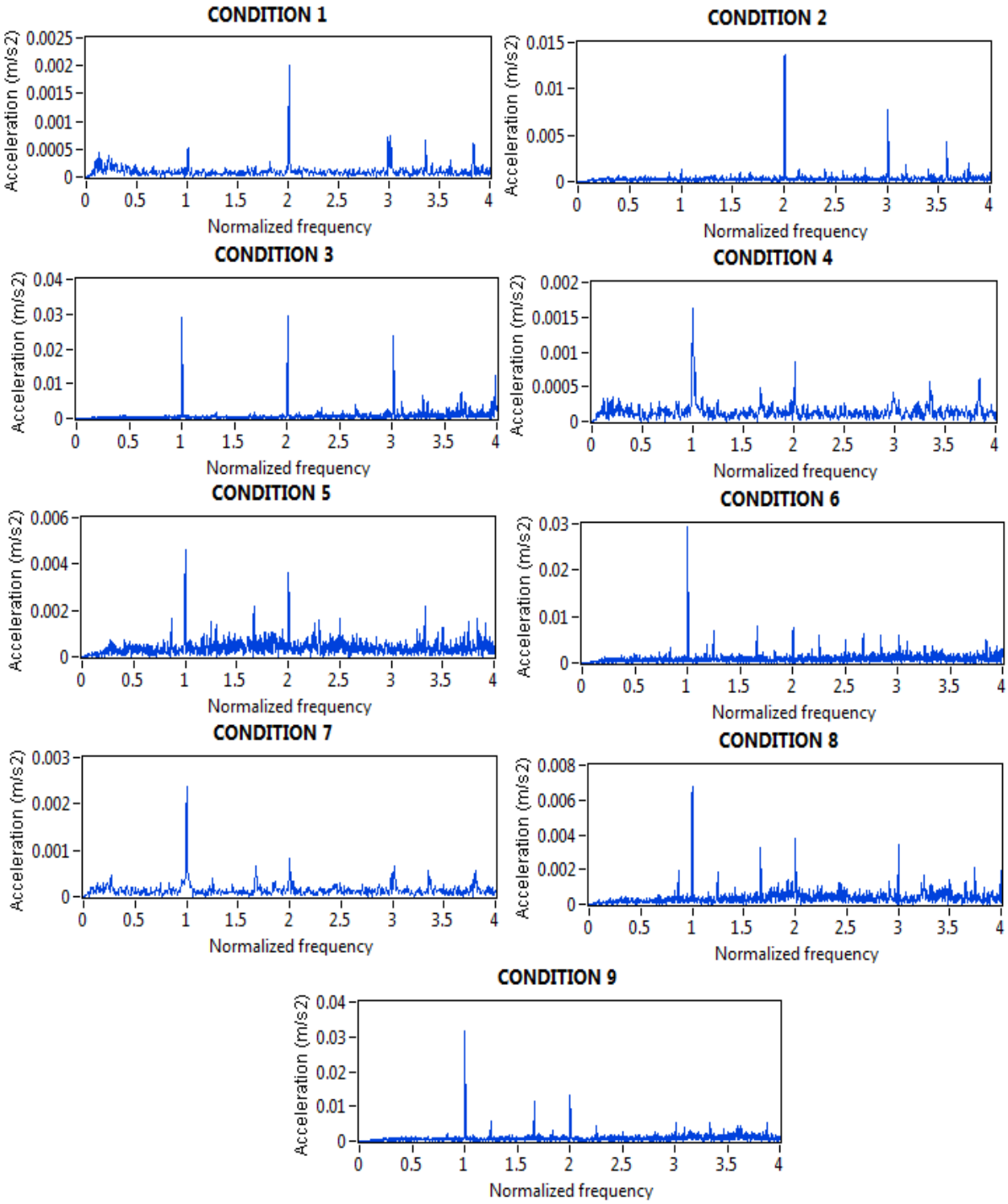

Figure 6-8: frequency spectrum of the acceleration signals. Peaks at 1X and 2X are visible in all conditions.

In order to show the high axial vibrations to discard the presence of unbalance described in the previous section, the acceleration spectrum in the axial direction is shown in Figure 6-9 (C9). It displays higher 1X and similar 2X vibrations than radial direction vibrations (Figure 6-8, C9).

This discards the potential of unbalance fault. Only C9 is displayed in the figure, however, the rest of the conditions also display higher 1X peak values in axial direction than radial direction.

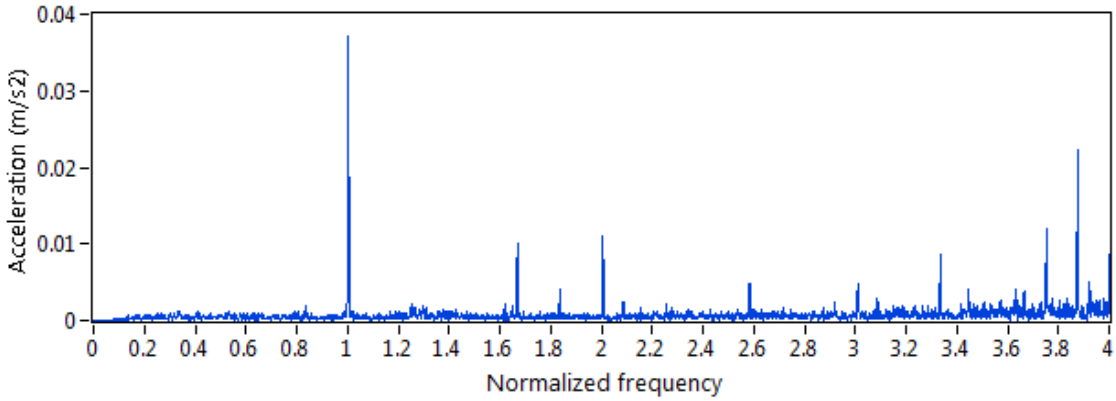

Figure 6-9: acceleration spectra in axial direction in C9.

6.4.3. AE signals results and observations

The AE waveforms for all 9 operational conditions under investigation are presented in Figure 6-10. The periodicity of amplitude modulation in the time-domain signal is more evident under low load than under high load conditions (C7, C8 and C9). The variation of amplitude modulation frequency in the AE signals is caused by the change of rotational speed. This variation is very clear in condition C1, C2 and C3. The change in AE signal level with both increasing load and speed is also evident. It is worth remarking that some random AE transients are visible under some conditions, which are attributed to unknown AE sources which could be cracking in any of the bearing components.

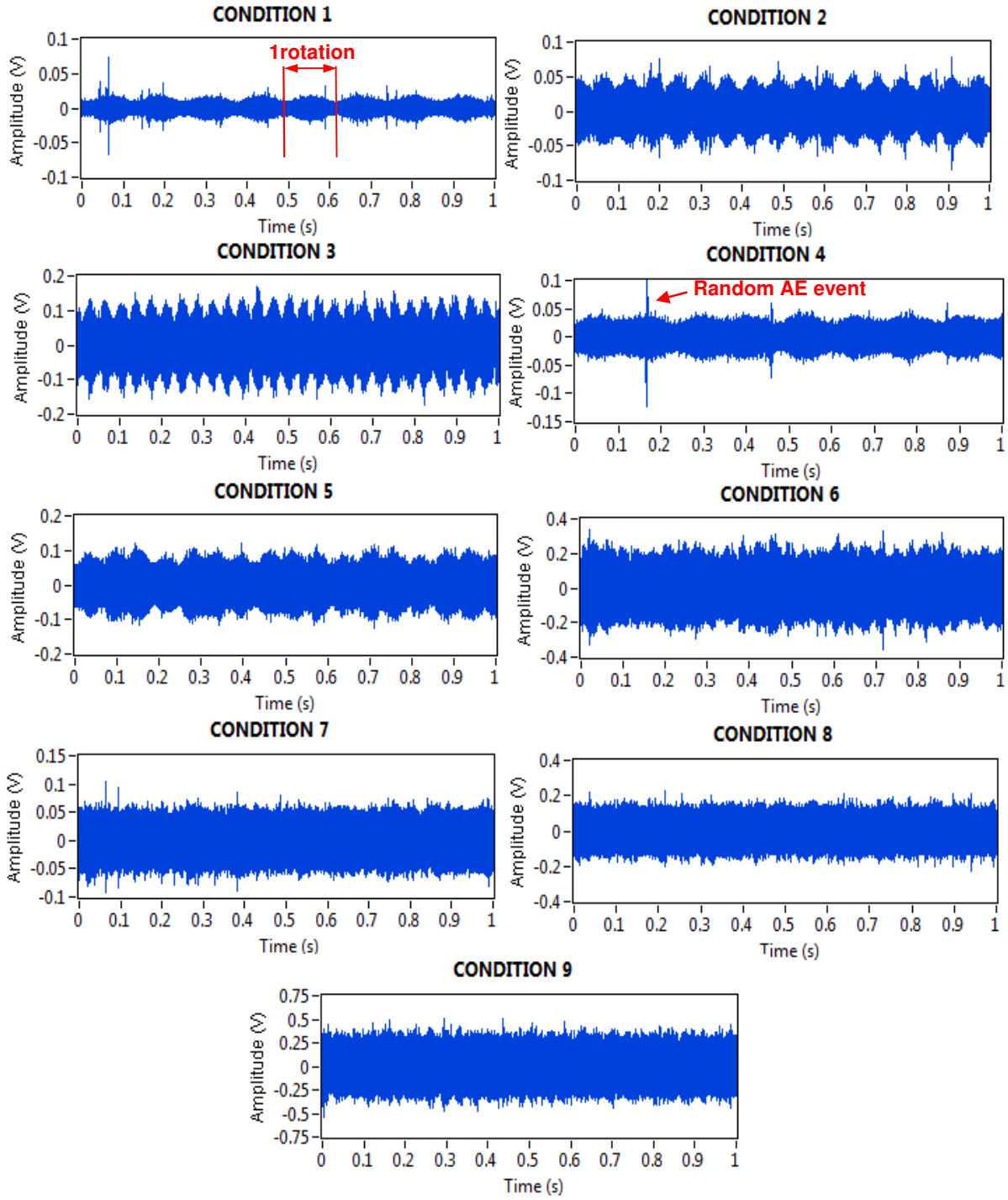

Figure 6-10: AE waveforms for all 9 conditions. Amplitude modulation is obvious under most of the conditions.

In order to analyse the frequency components of the amplitude modulation in the AE signals, envelope analysis was applied. The envelope was estimated using the Hilbert transform following

a full signal rectification and FFT as described in section 6.2. The AE envelope spectrum resulting from this analysis is presented in Figure 6-11.

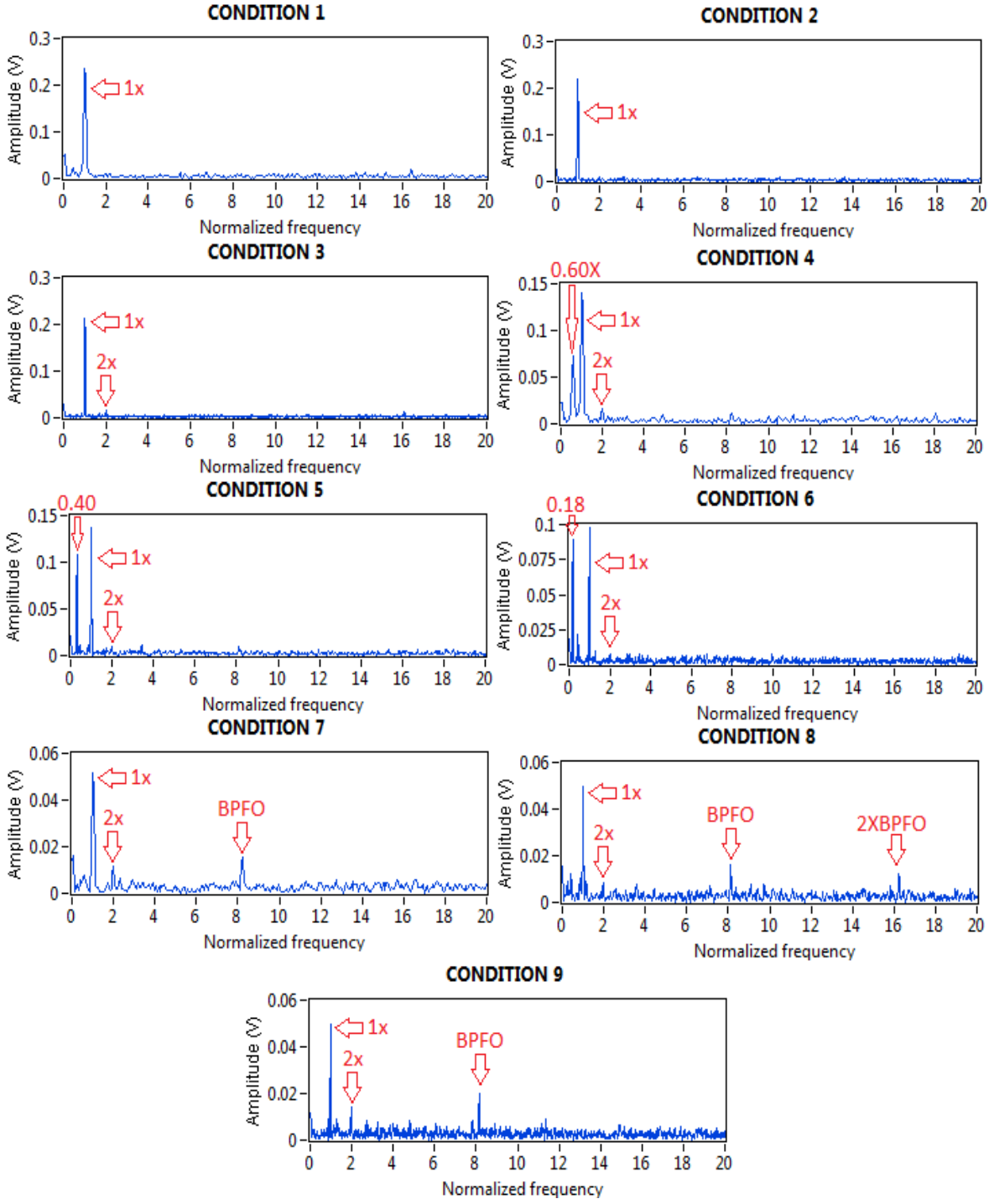

Figure 6-11: AE envelope spectrum for all 9 conditions.

The 1X peak is clearly the main peak in all conditions and samples. However, peaks at 2X are not obvious under C1 and C2. This is attributed to the low displacement of the shaft at 2X, observed in the proximity sensor results. Thus, the modulation of AE signals in the 2X peak is masked in some samples by the AE background noise. It is remarkable that under C7, C8 andC9, peaks at 8.17X and 16.34X are also present. They correspond to the BPFO and twice this frequency (2XBPFO) respectively [145]. Modulation at the BPFO in the AE signals is generally present when outer race defects are present [146]. However, the presence of a defect in the outer race cannot be confirmed because the bearing was not inspected before the experiments. Moreover, peaks at non-synchronous frequencies are also present in C4 andC5 and C6 at 0.60X, 0.40X, 0.18X respectively. The source of these peaks is further investigated in section 6.4.5.

6.4.4. Influence of operational conditions

The impact of load and speed in the displacement, AE and acceleration signals is described in this section. The effect of operational conditions on the detection of rotor-dynamics faults, i.e. misalignment is of high importance because of a high variability in the signature produced in AE or acceleration signals can be an obstacle for the correct diagnosis of this fault.

6.4.4.1. Influence on shaft displacement

The 1X and 2X peak values in both vertical and horizontal direction are shown in Figure 6-12 and Figure 6-13. These four graphs are generated by calculating the peak value of 1X and 2X under the 9 different conditions of load and speed for horizontal and vertical direction. As observed in these graphs, the variation of the shaft displacement behaviour is rather low (less than 20%) and it is evident that the speed and load do not significantly affect the values, particularly for the main behaviour of the shaft, 1X. The ratio 1X peak/2X peak under C2 is 16.6 and 28.57 for vertical and horizontal direction, respectively, which is similar for the other operational conditions. Thus, the 1X peak is by a considerable margin the major component of the shaft displacement signature.

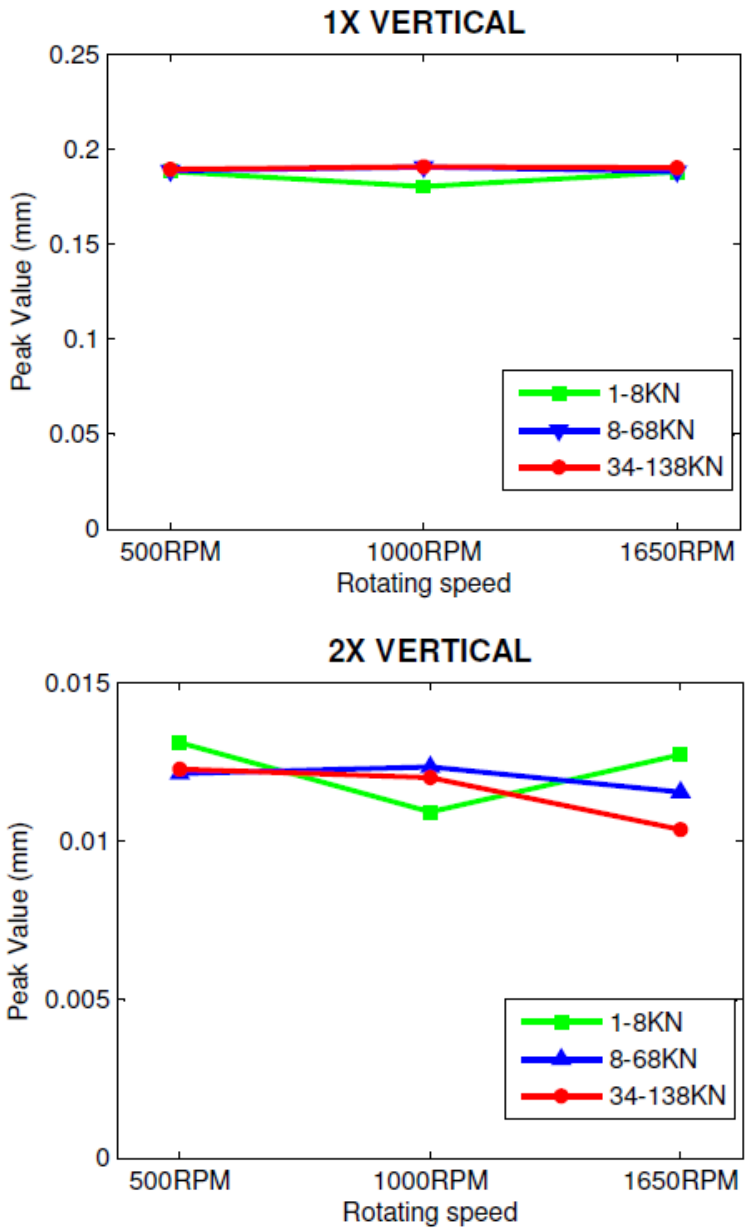

Figure 6-12: 1X and 2X peaks of displacement signals in vertical direction.

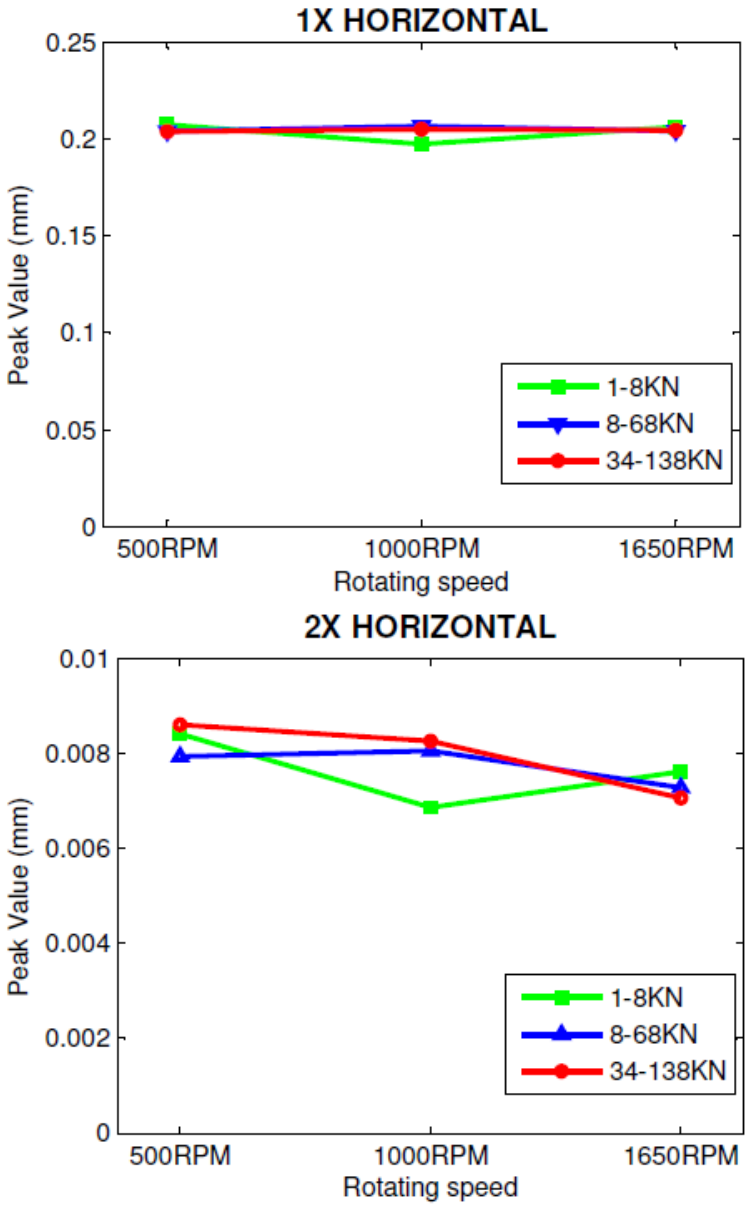

Figure 6-13: 1X and 2X peaks of displacement signals in horizontal direction.

6.4.4.2. Influence on acceleration signals

As previously presented for the proximity sensor signals, the 1X and 2X peak values in the acceleration spectrum are shown in Figure 6-14. The 1X peak values have a pronounced increase with increasing rotational speed. An illustrative example is the change in peak values when moving from C1 to C3 (changing rotational speed at constant load), which is 50 times higher (0.00052 m/s2 to 0.028995 m/s2). On the other hand, the load has little impact on the peak at 1X. With respect to the peaks values at 2X, they show a similar trend as the 1X peak. However,

in the lowest load conditions (C1, C2 and C3) the 2X peak value is significantly greater than in the higher load conditions. There is also a remarkable increase of 2X in 1-8KN load condition at 1000 and 1650 RPM.

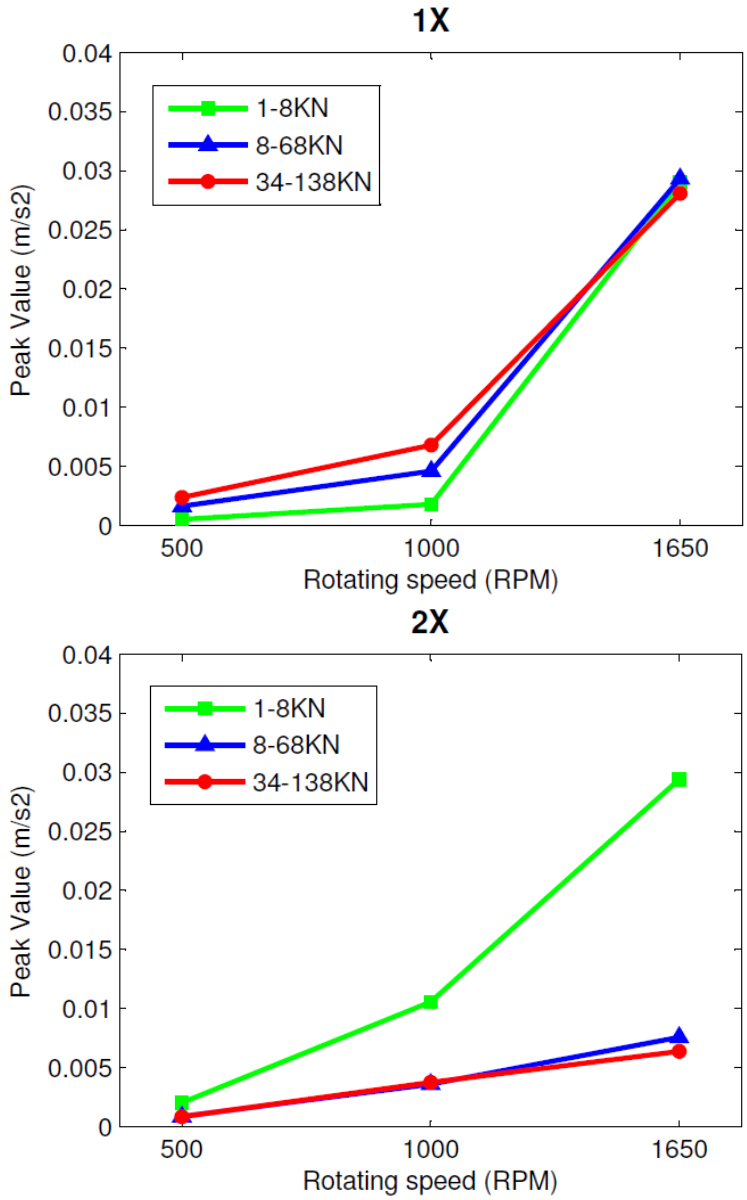

Figure 6-14: Peak amplitude at 1X and 2X of acceleration spectrum.

6.4.4.3. Influence on AE signals

The peaks in the AE envelope spectrum at 1X and 2X were calculated by averaging the values from the 18 samples acquired for each condition (Figure 6-15). The 1X peak values clearly rise with increasing speed. In contrast, there is no significant impact of load variations on the 1X

peak. The 2X peaks have a similar trend as the 1X peaks with increasing speed. However, in contrast to 1X, the 2X peak is slightly more affected by load, particularly under 34-138KN load. It is should be noted that the value of the 1X and 2X peaks rise with increasing speed and this effect was also observed in the acceleration spectrum.

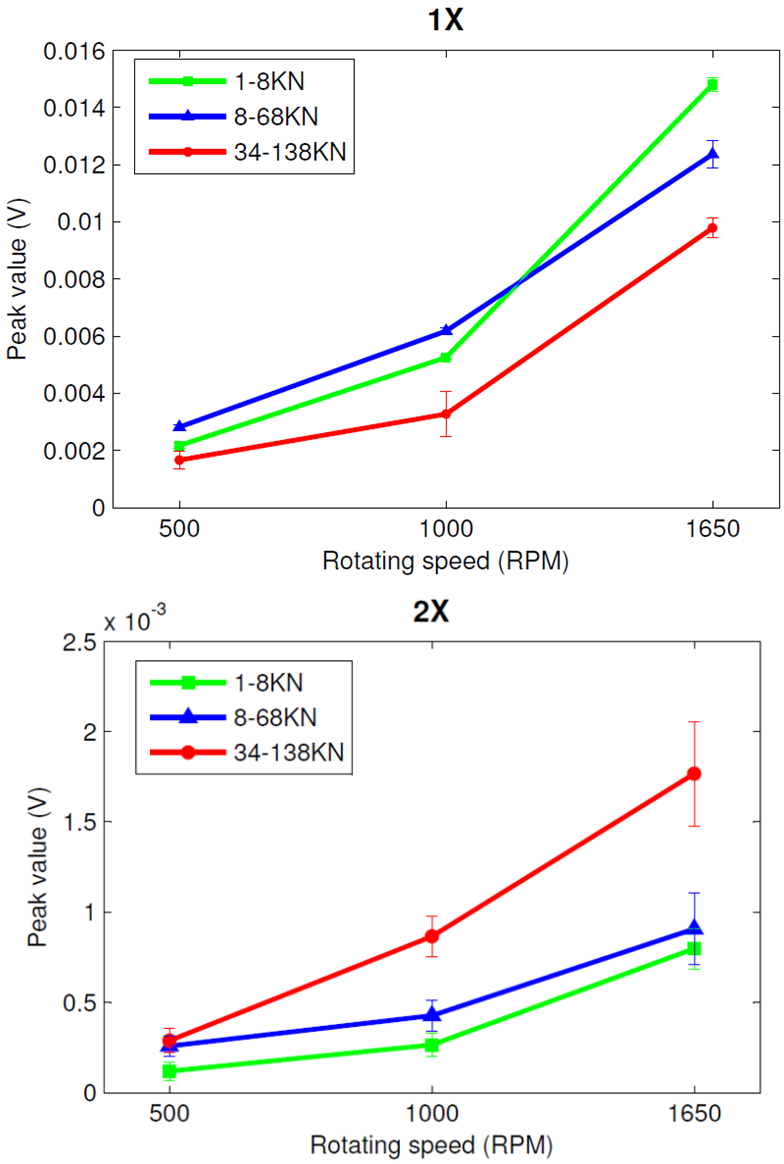

Figure 6-15: Peak amplitude at 1X and 2X in AE envelope spectrum.

6.4.5. Observations of non-synchronous peaks

In the AE envelope spectrum C4, C5 and C6 display a prominent peak at a non-synchronous frequency (5 Hz). This peak does not vary in frequency with rotational speed. It can be found in the AE envelope spectrum under C4, C5 and C6 at 0.6X, 0.3X and 0.18X, respectively (Figure

6-11). The source of that modulation is the control loop frequency of the hydraulic actuators. The control loop produces a ripple in the load applied to the rig in the radial and vertical direction with a frequency of 5 Hz. It was detected using the load transducer installed in the rig. Figure 6-16 shows the FFT spectrum of the signal acquired from the radial load transducer. It shows a prominent peak at 0.18X that corresponds to 5 Hz at the maximum rotational speed (1650RPM). Although the ripple is of low amplitude compared with the constant load, which is 68 kN in radial direction (5.8%), this periodic fluctuation of the load affects the shaft displacement spectrum and modulates the AE signal as shown in Figure 6-17(a)-(b) respectively. The Y-axis of the displacement signals is displayed on a logarithmic scale due to the small displacement of the shaft produced by the ripple of the load. It is worth noting that the impact of this load variation on the AE signals is significantly higher than displacement spectrum and the peak is comparable with 1X. On the other hand, as shown in Figure 6-16 (c) the load fluctuation is not evident in the spectrum.

Studies in elasto-hydrodynamic lubrication have shown that the thickness of an oil film is influenced by the load [147]. As the main source of AE in rotating machinery is attributed to asperity contact between surfaces in relative motion, the change in film lubricant thickness with varying load leads to a change in AE amplitude. Thus, the periodic variation of load is detected using envelope analysis. The increase of the AE amplitude with increasing load has been reported by other authors [57]. Thus, the combination of AE signals and envelope analysis was capable of detecting small variations of radial load in the shaft. This was not the case for acceleration spectrum.

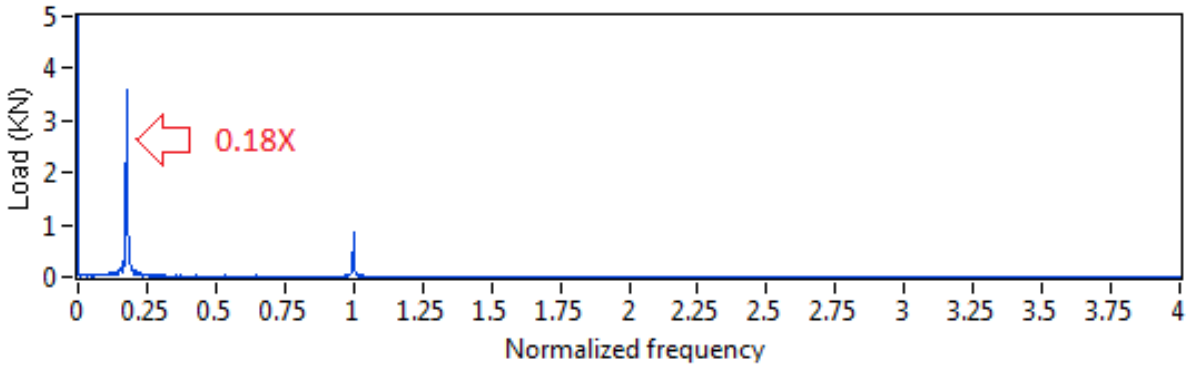

Figure 6-16: FFT spectrum of the signal acquired from the radial load transducer (C6).

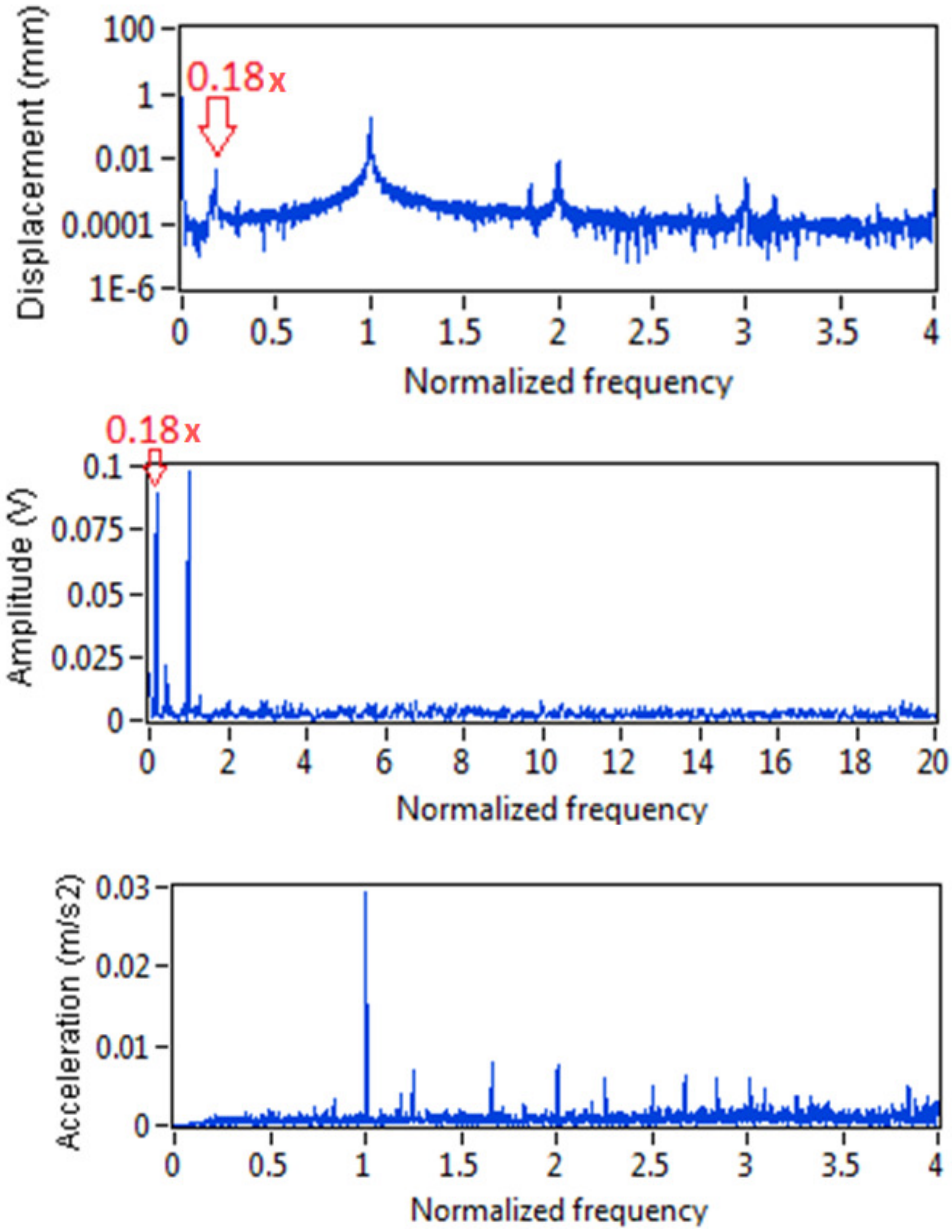

Figure 6-17: Spectrum of (a) vertical proximity sensor, (b) enveloped AE and (c) vibration (C6).

6.4.6. Signal to noise ratio

In order to compare the performance of AE and acceleration in the detection of SAM faults, the SNR was defined as the ratio of the peak of the 1X to the RMS noise level calculated over the range 0.7X -4X, expressed in dB:

$$\mathrm{SNR_{dB}} = 20\log\left(\frac{\text{Peak value(1X)}}{\text{RMS noise(0.7X}-\text{4X)}}\right) \tag{6.1}$$

The harmonics of the fundamental frequency (2X, 3X, etc.) are not considered to be noise and are not included as noise in SNR calculations. The range 0.7X -4X was used for the noise calculation in order to allow a direct comparison of the SNR of AE and acceleration signals. The reason for selecting the first value was in order to eliminate the subsynchronous peaks described in section 6.4.5. The higher limit was set as 4X because it was considered that the high frequency noise does not influence diagnosis and detection of the peaks in the low frequency spectrum (1X, 2X, 3X, etc.).

The SNR of the acceleration spectrum for all the operational conditions is presented in Figure 6-18. It shows that this SNR does not follow a linear trend with increasing rotational speed. The intermediate speed presents a lower SNR than the other two. The highest speed presents the greatest SNR ratio. On the other hand, the SNR clearly increases with increasing load.

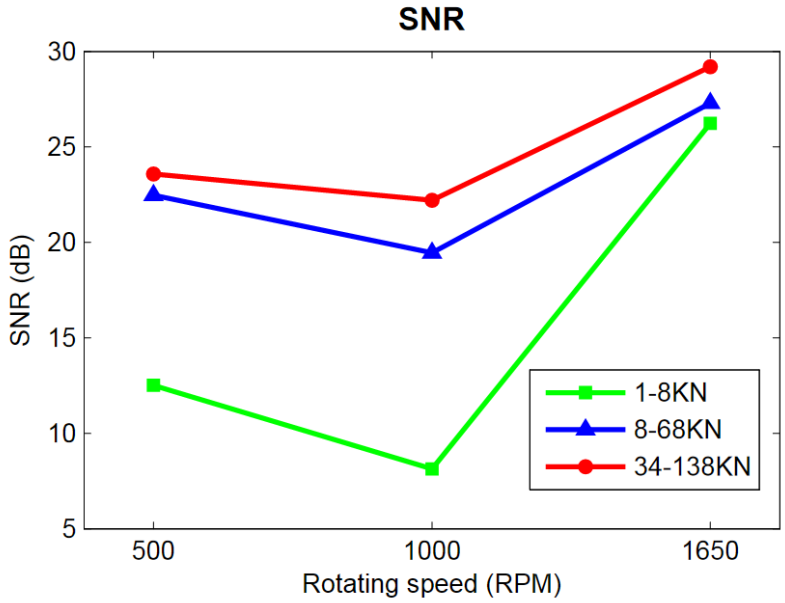

Figure 6-18: SNR of 1X in acceleration spectrum.

The 1X SNR of the AE envelope spectrum for all operational conditions (Figure 6-19) was determined using the same equation used for the acceleration signals (equation 2). A clear trend of reduction of SNR value with increasing load can be observed. On the other hand, there is no linear trend in SNR variation with changing rotational speed. These values of SNR are higher in all conditions than the obtained for acceleration signals.

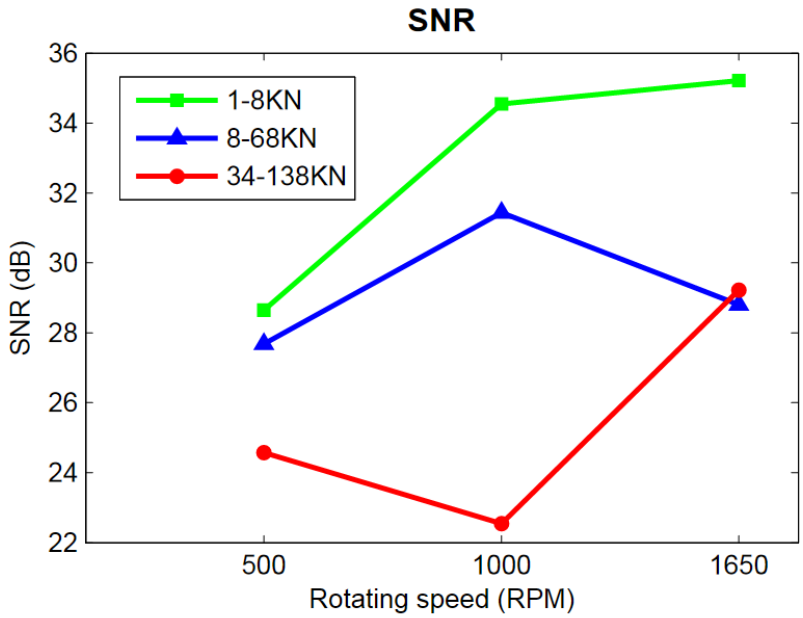

Figure 6-19: SNR for the 1X peak in the AE envelope.

6.5. Discussion

As presented and described in section 6.4.1, SAM produces shaft displacement principally at 1X in all operational conditions. It is 16.6 and 28.57 times more than the 2X peak as shown in the displacement signals. However, the acceleration spectrum shows the 1X peak clearly lower than the 2X peak under C1 and C2 which could lead on to an inaccurate diagnosis of SAM. Figure 6-20 shows the spectrum of the AE envelope (a) and acceleration (b) under C2. The 1X peak is clearly lower than the 2X peak in the acceleration spectrum, while AE shows a prominent 1X peak, which represents the main behaviour of the shaft measured, using proximity sensors. On the other hand, AE shows a prominent 1X peak in all the 9 operational conditions, clearly of greater amplitude than 2X and other sources of modulation such as BPFO and 2XBPFO. Therefore, as shown in the results presented here, the signature of SAM generated in the AE using envelope spectrum is more stable with changing operational conditions than the acceleration spectrum signature. The high impact in acceleration spectrum with varying operational conditions was also concluded by Toht and Ganeriwala in [97].

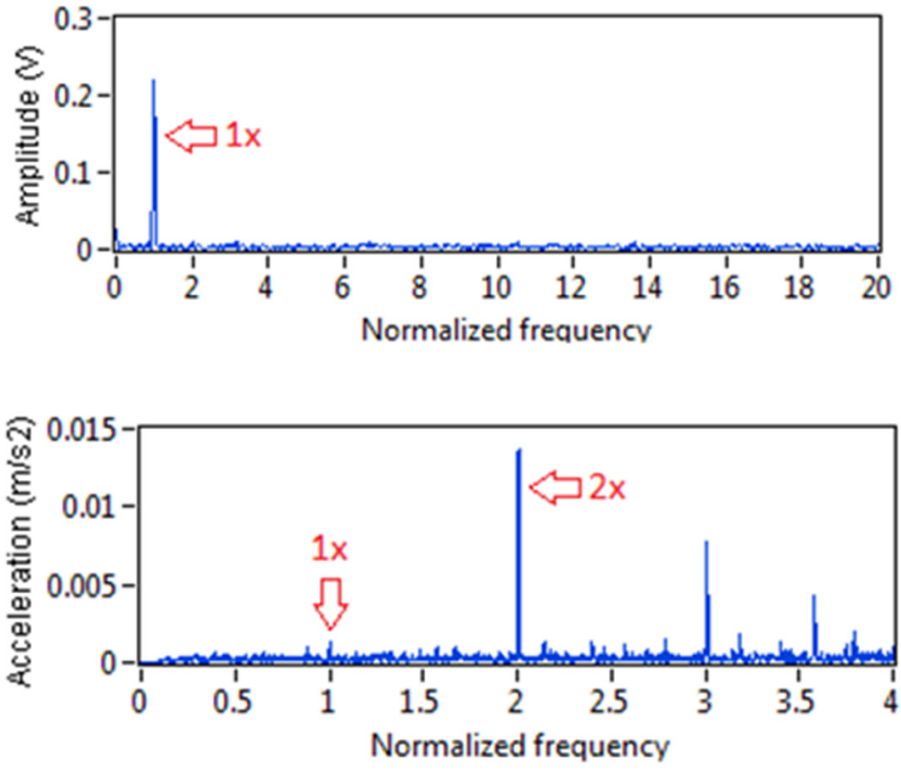

Figure 6-20: Results of (a) AE envelope spectrum and (b) acceleration spectrum under C2.

The shaft displacement has been shown to be slightly affected under all operational conditions, while in AE and acceleration measurements the impact is significantly higher. AE and acceleration signals are both highly affected by rotational speed. However, the impact of load on the 1X and 2X spectrum components is not as influential as rotational speed in both techniques. AE envelope spectrum offers higher SNR than acceleration spectrum in all conditions. AE and acceleration spectrum have opposite behaviour on the impact of operational conditions on the SNR of 1X peak. While increasing load increases the SNR of the acceleration signals, the SNR of the 1X peak in the AE envelope spectrum decreases. On the other hand, the SNR does not follow a linear trend with varying speed of both techniques.

6.6. Summary

In this chapter, the detectability of SAM using AE and acceleration signals with variable operating conditions has been presented. This is the first attempt to evaluate the detection of SAM using AE technique with varying operational conditions. The shaft displacement detected with proximity sensors has been compared with vibration analysis and AE technique. AE combined with envelope analysis has shown the capability and reliability to detect SAM. Traditionally, vibration analysis has been used to detect misalignment fault in rotating machinery. However, the results show that AE offers more stability and higher SNR in the detection of SAM under varying operational conditions.

As shown in section 6.4.5 while AE has shown high sensitivity to the periodic fluctuation of radial load produced by the hydraulic actuator on the test bearing, acceleration spectrum does not show any indication of this problem. This indicates a high sensitivity of AE technique to radial load variation. Fluctuations of bearing load greatly affect rolling fatigue life, seizure performance and the stiffness of the shaft support system [148].

It is worth noting that although the displacement spectrum shows that the shaft displacement keeps nearly constant with changing load and speed, the impact of load and speed in AE and particularly in acceleration spectrum is rather high.

The research presented in this chapter has been published in the peer reviewed journal Applied Acoustics.

Chapter 7

Conclusions and recommendations for further work

Rotating machinery is extensively used in a range of mechanical transmission systems and its reliability is key aspect of many domestic and industrial applications. The detection of faults at an early stage in rotating machinery is of high importance to avoid unexpected breakdowns, saving resources and increasing safety in industrial plants. The AE technique shows improvements for

early fault detection in rotating machinery in previous studies. However, it presents some drawbacks that have to be overcome for it to be applied as a reliable solution, mainly in processing, interpreting and classifying the information. Noise reduction is a vital aspect for fault detection at an early stage as the signals are frequently noisy and the attenuation of the signals generated by the defect is extremely high as the AE signals have to travel to the sensors, usually installed in the component housing. The main objective of this thesis has been the investigation of two different approaches to enhance AE technique to detect faults in rotating machinery. Firstly, the detection of localised defects at an early stage in bearings and gears using AE has been improved combining WP as a pre-processor and ACF as postprocessor to the envelope analysis. Secondly, the detection of SAM using AE has been explored, finding superiorities to the well-known acceleration spectrum in detection of the fault in different operational conditions.

The topic of the research and the background in which this thesis was established is described in Chapter 1. The aim of this research is provided in this chapter as well as the main contributions to the knowledge.

Chapter 2 introduces the theoretical background of AE technique, emphasising the application of AE for rotating machinery fault detection. This section also describes the applications of AE, the types of AE sensors and the typical defects that are encountered in bearings and gears associated with rotating machinery industrial environments.

Chapter 3 presents a literature review of signal processing techniques used in rotating machinery fault detection using AE with a detailed description of time-domain methods, WT, classification methods, envelope analysis and cyclostationarity analysis.

Chapter 4 describes a novel signal processing technique applied to AE signals for incipient defect detection in bearings. A mathematical formulation describing the method is presented in this chapter. Subsequently, an experimental study was conducted to validate the method of detecting a seeded defect in the outer race of a bearing, applying noise baseline in addition to simulate extremely low SNR conditions. The proposed method has shown to perform better than the

traditional envelope analysis and it is able to detect localised defects at lower SNR conditions providing a significant advantage in bearing defect detection in low SNR conditions with 9dB lower SNR than the traditional method. This scenario, in which the SNR is extremely low, is typically present in defects at an early stage. These significant improvements can be implemented into currently available commercial equipment, and so can be used by CM systems to detect defects in rotating machinery at an earlier stage in several fields including marine, nuclear and mining. The enhancement for early stage defect detection of bearings provided by this method is beneficial in planning the maintenance in advance, reducing the machinery down-time and consequently reducing the costs associated with bearing breakdown. The WP-ACF spectrum is simple to implement in an automated system by applying a threshold detector in the spectrum to find the peaks which are related to bearing and gear faults. In addition, the proposed method can be applied to real-time monitoring as it is computationally efficient.

The literature proposes initial concepts as to how to de-noise the AE signal using DWT prior to applying envelope analysis signal [18][98]. However, WP offers advantages in signal de-noising particularly if the information is present in the high frequency components. For this reason, the use of WP transform as pre-processor for envelope analysis was investigated. The optimal WP node and wavelet family in a wide range of frequencies were studied to obtain the most efficient performance of detecting localised defects in gears and bearings. The result for the optimal WP node presented by Feng showed that the optimal WP for bearing fault detection was [20-30 kHz] [52]. However, the total bandwidth analysed was 0-40 kHz. In the present investigation the bandwidth analyses was 70-500 kHz for the seeded defect in the outer race of the bearing and 70-1000 kHz for the naturally developed defect in the bearing outer race and seeded defect in straight bevel gears. This provides wider bandwidth to estimate the optimal WP node for AE signal de-noising. The results of this investigation show that the optimal bandwidth for AE signal de-noising varies between scenarios. However, in general, mid-high frequencies (250-750 kHz) allow for optimal signal de-noising. In addition, an investigation was conducted in Chapter 5 to clarify the impact of the distance from the defect to the AE sensor on the optimal WP node.

The results show that the higher the distance from the AE sensor to the defect, the optimal WP node for signal de-noising shifts to lower frequencies. The optimal mother wavelet for AE signal de-noising has shown to be Db11. However, other families such as Coiflet and Symlet offer similar results using higher order mother wavelets.

Due to the low amplitude of the AE signals in the optimal bands (250-750 kHz), the lower frequencies of any unexpected sources of noise, such as electrical noise transmitted through the power source or any electromagnetic interference, that can affect the measurement in this frequency band, would have a significant impact on the detection using the WP-ACF. Thus, the performance of WP to de-noise the AE burst from the continuous AE signal would be deteriorated. As described in section 2.5.2. the use of couplant can greatly improves the transmission from the bearing case to the sensor by about 10 times at 500 kHz. Thus, the use of couplant is of high importance to obtain an optimal SNR, applying the WP-ACF method as it analyses the mid-high frequency components of the AE signals.

The WP-ACF method requires *a priori* knowledge of the bearing and gear to identify the fault frequencies, and sometimes the access to this information presents some difficulties or is not possible. This is an intrinsic shortcoming of any algorithm derived from envelope analysis.

Chapter 5 presents a validation of the WP-ACF method in two different scenarios. First, the detection of a naturally developed defect in the outer race of a spherical roller bearing is investigated. The results obtained in this investigation show the high impact of operational conditions in the detection of the defect on the WP-ACF method. The same tendency is observed using the traditional envelope analysis. In general, an increase in load increases the sensitivity of the WP-ACF for defect detection. The impact of rotational speed in the WP-ACF SNR does not show any evident relationship.

Secondly, an experimental study was conducted on the detection of a seeded defect on one of the gear tooth of a bevel gear. This is the first known attempt to detect defects in bevel gears using AE. The results of this investigation again show better performance of WP-ACF over

traditional envelope analysis in de-noising the GMF. The increment or presence of sidebands around this characteristic frequency produced by amplitude modulation can inform about the presence of localised defect in any of the gear tooth and tooth wear. Thus, it can be concluded that the WP-ACF method offers advantages to AE for gear defect detection.

In chapter 6, an experimental investigation of the detection of SAM using AE and acceleration signals with variable operating conditions is presented. Other researchers have identified the modulation on the AE signals produced by misalignment [98][99][37]; however, their investigations did not target the detection of misalignment and the impact of operational conditions on the detection of misalignment using AE. Therefore, this is the first attempt to evaluate the detection of SAM using AE technique with varying operational conditions. The shaft displacement produced by SAM detected using proximity sensors installed in the shaft has been compared with acceleration spectrum and AE technique. AE combined with envelope analysis has shown the capability to detect SAM. Acceleration spectrum has been traditionally used to detect misalignment fault in rotating machinery. However, this research has shown that AE offers higher stability and up to 34 dB higher SNR for the detection of SAM under varying operational conditions. The results shown in this investigation enable AE technique to be further investigated to detect rotor-dynamic faults.

Future work

WP-ACF method has been shown to perform effectively in spherical and tapered roller bearings and bevel gears. However, the effectiveness of the proposed method has not been validated in other types of common bearings and gears such as ball and needle roller bearings and helical and spurs gears. In addition, the WP-ACF method has been validated for steel bearings. Thus the application of this novel method in other type of bearings which are currently being used in the industry such as ceramic and plastic bearings should be further investigated.

Similarly, in the present research, the validation of the WP-ACF method for bearings has been carried out in the outer race. As concluded by other researchers [85][12], inner race defects are

more difficult to detect due to the higher attenuation of the AE signals generated in the defect that have to travel to the outer race and bearing housing. For this reason, more investigations should be conducted to investigate the performance of the WP-ACF for inner race defects.

An exhaustive investigation regarding the optimal frequencies for signal de-noising using wavelet packets has been presented in several scenarios. In addition, the impact of distance from the defect to the sensor on the optimal WP node has been investigated. The author believes that the impact of the joints that the AE signals cross to reach the sensor must have high impact on the selection of the optimal WP node for AE signal de-noising. Therefore, this should be further investigated.

Although the detection of SAM has been investigated in this thesis, any other type of rotor-dynamic faults such as unbalance, looseness, etc. may be detected combining AE and envelope analysis as they also cause a periodic displacement of the shaft leading to periodic variations of rotor-stator rubbing. Thus, the application of the proposed method on other types of rotor-dynamic faults would be an interesting subject for further investigations. In addition, the misalignment severity investigated was not varied due to test rig limitations. Further experiments can be carried out to investigate the impact on the AE envelope spectrum for varying misalignment severity.

The ultimate aim of CM is not only to detect the fault. The diagnosis and prognosis are also important aspects of CM. This investigation has focused on fault detection. Further work must be carried out for diagnosis and prognosis using the WP-ACF methods which are vital aspects for predictive maintenance [149].

References

[1] S. Soua, P. V. Lieshout, A. Perera, T. Gan and B. Bridge, "Determination of the combined vibrational and acoustic emission signature of a wind turbine gearbox and generator shaft in service as pre-requisite for effective condition monitoring," *Renewable Energy,* vol. 51, pp. 175-181, 2013.

[2] C.J. Li and J. Ma, "Wavelet decomposition of vibration for detection of bearing-localized defects," *NDT,* vol. 30, p. 143–149, 1997.

[3] M. Khonsari and E. Booser, "An engineering guide for bearing selection," Tribology and Lubrication Technology, 2004.

[4] M.R Wilkinson, F. Spinato and P. J. Tavner, "Condition monitoring of generators and other subassemblies in wind turbine drive trains," in *IEEE International Symposium on Diagnostics for Electric Machines, Power Electronics and Drive*, 388-392, 2007.

[5] Air accident investigation branch, "AAIB Ref: EW/C2009/04/01," AAIB, http://www.aaib.gov.uk/cms_resources.cfm?file=/G-REDL%20-%20Initial%20AAIB%20Report.pdf, 2009.

[6] A. S. Sekhar and B. S. Prabhu, "Effects of coupling misalingment on vibrations of rotating machinery," *Journal of Sound and Vibration,* vol. 185, no. 4, pp. 544-560, 1995.

[7] S.R. Bognatz, "Alignment of critical and non-critical machines," *Orbit,* pp. 23-25, 1995.

[8] D. Mba, "Applicability of acoustic emission to monitoring the mechanical integrity of bolted structures in low speed rotating machinery: case study," *NDT and E International,* vol. 35, no. 5, p. 293–300, 2002.

[9] Kittiwake Holroyd Ltd©, "http://www.kittiwakeholroyd.com/acoustic-emission-products.htm," [Online].

[10] SKF limited, "CMON 2504 acoustic emission (AE) interface card for the SKF Multilog On-line System IMx," [Online]. Available: http://www.skf.com/group/products/condition-monitoring/surveillance-systems/on-

line-systems/monitoring-systems/cmon-2504-ae-interface-card/index.html.

[11] Ch. Zhou and Y. Zhang, "Particle filter based noise removal method for acoustic emission signals," *Mechanical systems and signal processing,* vol. 28, pp. 63-77, 2012.

[12] D. Mba and Raj B.K.N. Rao, "Development of Acoustic Emission Technology for Condition Monitoring and Diagnosis of Rotating Machines; Bearings, Pumps, Gearboxes, Engines and Rotating Structures," *The shock and vibration digest,* vol. 38, pp. 3-16, 2006.

[13] C. Zuluaga-Giraldo, D. Mba and M. Smart, "Acoustic emission during run-up and run-down of a power generation turbine," *Tribology International,* vol. 37, p. 415–422, 2004.

[14] M. Purat and P. Noll, "A new orthonormal wavelet packet decomposition for audio coding using frequency-varying modulated lapped transform," in *IEEE workshop on applications of Signal Processing to Audio and Acoustics*, New York, 1995.

[15] I. Redmond and K. Al-Hussain, "Misalignment as a source of vibration in rotating shaft systems," in *IMAC XIX - 19th International Modal Analysis Conference - Future Directions in Structural Dynamics*, 2002.

[16] Y-H Pao, R.R Gajewski,A.N. Ceranoglu, "Acoustic emission and transient waves in an elastic plate," *J. Acoust. Soc. Am.,* vol. 65, no. 1, p. 10, 1979.

[17] NDT resource center, [Online]. Available: http://www.ndt-ed.org/EducationResources/CommunityCollege/Other%20Methods/AE/AE_Theory-Sources.htm. [Accessed 2014 June 17].

[18] B. Eftekharnejad, Condition monitoring of gearboxes using Acoustic Emission, Cranfield university: PhD thesis, 2009-2010.

[19] R. Li and D. He, "Rotational Machine Health Monitoring and Fault Detection Using EMD-Based Acoustic Emission Feature Quantification," *IEE transactions on instrumentation and measurement,* vol. 61, no. 4, 2012.

[20] C. P. Hsiao, R. A. Kline and K. A. Grasse, "A theoretical and experimental study on the propagation of acoustic emission signals in polymeric media," Ultrasonic symposium,

1986.

[21] C. Hellier, Handbook of Non-destructive Evaluation, McGraw-Hill, 2001.

[22] P. Laugier and G. Haitat, Bone Quantitative Ultrasound, Springer, 2011.

[23] N. N. Hsu and F.R. Breckenridge, "Characterization and Calibration of Acoustic Emission Sensors," *Materials Evaluation,* vol. 39, pp. 60-68, 1981.

[24] G. C. McLaskey and S. D. Glase, "Acoustic Emission Sensor Calibration for Absolute Source Measurements," *J Nondestruct Eval,* vol. 31, no. 2, pp. 157-168, 2012.

[25] K. Ono, H. Cho and T. Matsuo, "Transfer functions of acoustic emission sensors," *J. Acoustic Emission,* vol. 26, 2008.

[26] D. Lekou, "Fused Acoustic Emission and Vibration Techniques for Health Monitoring of Wind Turbine Gearboxes and Bearings," in *European Wind Energy Associacion Conference (EWEA)*, Marseille, 2009.

[27] C. U. Grosse and M. Ohtsu, Acoustic Emission Testing, Springer-Verlag Berlin Heidelberg, 2008.

[28] M. A. Elforjani, Condition Monitoring of Slow Speed Rotating Machinery Using Acoustic Emission Technology, PhD thesis, Cranfield University, 2010.

[29] "Mistras Group," [Online]. Available: http://www.mistrasgroup.com/services/advancedndt/acousticemission/. [Accessed 3 June 2014].

[30] V. Baranov, E. Kudryavtsev, G. Sarychev and V. Schavelin, Acoustic Emission in Friction, Moscow: Tribology and Interface engineering series, 2007.

[31] D. Van Hemelrijck, Emerging Technologies in NDT: Proceedings of the 2nd International Conference, Taylor & Francis, 2004.

[32] B. Lu, "A review of recent advances in wind turbine condition monitoring and fault diagnosis," *Power Electronics and Machines in Wind Applications,* pp. 1-7, 2009.

[33] N. Tandom. and A.Choudhury, "Review of vibration and acoustic measurement

methods for the detection of defects in rolling element bearings," *Tribology International,* vol. 32, no. 8, p. 469–480, 1999.

[34] J. Keprt, P. Benes, "Determination of uncertainty in calibration of acoustic emission," in *4th International Conference on NDT*, Crete, Greece, 2007.

[35] V. Hartmut, " AE Testing Fundamentals,Equipment, Applications.," *The e-Journal of Nondestructive ,* vol. 7, 2007.

[36] "Acoustic Emission Sensors specification," Vallen Gmbh, 2012.

[37] J. Z. Sikorska and D. Mba, "Challenges and obstacles in the application of acoustic emission to process machinery," *Proceedings of the Institution of Mechanical Engineers,* vol. 222, no. 1, p. 1, 2008.

[38] Vallen GMBH, "Acoustic emission sensors," 12 2012. [Online]. Available: http://www.vallen.de/sites/default/files/sov1212_0.pdf.

[39] A. S. E1106-86, Standard Method forPrimary Calibration of Acoustic Emission Sensors, Philadelphia: ASTM, 1986.

[40] N. 2109-91, Method for Absolute Calibration of Acoustic Emission Transducers by Reciprocity Technique, The Japanese Society for Non-Destructive Inspection, 1991.

[41] S. Dia ,T. Monnier, N. Godin and F. Zhang, "Primary Calibration of Acoustic Emission Sensors by the Method of Reciprocity, Theoretical and Experimental Considerations," in *30th European Conference on Acoustic Emission Testing & 7th International Conference on Acoustic Emission*, University of Granada, 12-15 September 2012.

[42] A. S. E1781-96, Standard Practice for Secondary Calibration of Acoustic Emission Sensors, Philadelphia: ASTM, 1996.

[43] P. Theobald,B. Zeqiri and J. Avinson, "Couplants and their influence on a AE sensor sensitivity," *Journal of Acoustic Emission,* vol. 26, pp. 91-97, 2008.

[44] ASTM E650 / E650M - 12, *Standard Guide for Mounting Piezoelectric Acoustic Emission Sensors.*

[45] GE Energy Co., " http://www.gepower.com.," [Online].

[46] A. Andhare, Condition Monitoring of Rolling Element Bearings, Saarbrucken, Germany: Lambert Academic Publishing, 2010.

[47] T. Ohira and Y. Pao , "Microcrack initiation and acoustic emission during fracture toughness tests of A533B steel," *Metallurgical Transactions ,* vol. 17, no. 5, pp. 843-852 , 1986.

[48] A. Palmgren, "NASA technical memorandum 107440, A basis for bearing life prediction," Cleveland, Ohio, 1997.

[49] Longo, "ROLLING BEARING FAILURES," [Online]. Available: http://www.elongo.com/pdfs/BearingFailures990519.pdf. [Accessed 25 July 2013].

[50] SKF, "Bearing failures and their causes," [Online]. Available: https://ec.kamandirect.com/content/resources/2010/downloads/skf_bearing_failureandcauses.pdf. [Accessed 25 July 2013].

[51] R. Poore, "WindPACT Drive Train Designs Study," NREL Report, National Renewable Energy Laboratory, Golden, Colorado, 2003.

[52] Yanhui Feng, Novel acoustic emission signal processing methods for bearing condition monitoring, University of Leicester, PhD thesis, 2008.

[53] A. M. Al-Ghamda and D. Mba, "A comparative experimental study on the use of acoustic emission and vibration analysis for bearing defect identification and estimation of defect size," *Mechanical Systems and Signal Processing ,* vol. 20, p. 1537–1571, 2006.

[54] N. Tandon and B. C. Nakra, "Defect Detection of Rolling Element Bearings by Acoustic Emission Method," *Journal of Acoustic Emission,* vol. 9, no. 1, pp. 25-28, 1990.

[55] M. Elforjani and D. Mba, "Accelerated natural fault diagnosis in slow speed bearings with Acoustic Emission," *Engineering Fracture Mechanics,* vol. 77, pp. 112-127, 2010.

[56] A. Choundhury and N. Tandon, "Application of acoustic emission technique for the detection of defects in rolling element bearings," *Tribology International,* vol. 33, pp. 39-45,

2000.

[57] A. Morhain and D. Mba, "Bearing defect diagnosis and acoustic emission," *Journal of Engineering Tribology,* vol. 217, no. 4, pp. 272-275.

[58] G. Ghodrati Amiri and A. Asadi , "Comparison of Different Methods of Wavelet and Wavelet Packet Transform in Processing Ground Motion Records," *International Journal of Civil Engineering,* vol. 7, no. 4, 2009.

[59] Z. K. Peng and F. L. Chu, "Application of Wavelet Transform in Machine Condition Monitoring and Fault Diagnostics: A Review with Bibliography," *Mechanical Systems and Signal Processing,* vol. 18, pp. 199-221, 2004.

[60] R. Yan, R. X. Gao and X. Chan, "Wavelets for fault diagnosis of rotary machinery: a review with applications," *Signal processing,* vol. 96, pp. 1-15, 2014.

[61] Y. Feng, S. Thanagasundram and F. S. Schlindwein, "Discrete wavelet-based thresholding study on acoustic emission signal to detect bearing defect on a rotating machine," *The thirteenth international congress on sound an vibration,* 2006.

[62] Ch. Changzheng, S. Changcheng, Z. Yu and W. Nan, "Fault Diagnosis for Large-scale Wind Turbine Rolling Bearing Using Stress Wave and Wavelet Analysis," in *Proceedings of the Eighth International Conference on Electrical Machines and Systems, ICEMS*., 2005.

[63] Yanhui Feng and Fernando S.Schlindwein, "Normalised wavelet packets quantifiers for condition monitoring," *Mechanical SystemsandSignalProcessing,* vol. 23, p. 712–723, 2009.

[64] K. Asamenea, M. Sundaresana, "Analysis of Experimentally Generated Friction Related Acoustic Emission Signals," *Wear,* vol. 296, no. 1–2, p. 607–618, 2012.

[65] X. Wang, C. M. Zhu, H. L. Mao and Z. F. Huang, "Wavelet packet analysis for the propagation of acoustic emission signals across turbine runners," *NDT & E International,* vol. 42, no. 1, pp. 42-46, 2009.

[66] Z. Bo and Z. Yu, "A New method on fault diagnosis of low-speed rolling bearing using stress waves," in *International Conference on Intelligent System Design and Engineering Application (ISDEA)*, 2010.

[67] D. L. Donoho, "De-noising by soft thresholding," *IEEE Transaction on Information Theory,* vol. 41, pp. 613-627., 1995.

[68] L. Law, J. H. Kim, W. Y. H. Liew and S. Lee, "An approach based on wavelet packet decomposition and Hilber-Huang transform (WPD-HHT) for spindle bearings condition monitoring," *Mechanical systems and signal processing,* vol. 33, pp. 197-211, 2012.

[69] T. Loutas, G. Sotiriades, I. Kalaitzoglou and V. Kostopoulos, "Condition monitoring of a single-stage gearbox with artificially induced gear cracks utilizing on-line vibration and acoustic emission measurements," *Applied Acoustics,* vol. 70, no. 9, p. 1148–1159, 2009.

[70] Z. Taha and K. Widiyati, "Artificial neural network for bearing defect detection based on acoustic emission," *Int J Adv Manuf Technol ,* vol. 50, p. 289–296, 2010.

[71] J. Wu, J.i Chan, "Faulted gear identification of a rotating machinery based on wavelet transform and artificial neural network," *Expert Systems with Applications,* vol. 36 , p. 8862–8875, 2009.

[72] K. F. Al-Raheem, A. Roy, K. P. Ramachandran, D. K. Harrison and S. Grainger, "Rolling element bearing fault diagnosis using Laplace/wavelet envelope power spectrum," *EURASIP Journal on advances in signal processing,* no. 1, pp. 1-14, 2007.

[73] B. Samanta, K.R. Al-Balushi and S.A. Al-Araimi, "Artificial neural networks and support vector machines with genetic algorithm for bearing fault detection," *Engineering Applications of Artificial Intelligence,* vol. 16, p. 657–665, 2003.

[74] A. Widodo, B. Yang, E. Kim, A. Tan and J. Mathew, "Fault diagnosis of low speed bearing based on acoustic emission signal and multi-class relevance vector machine," *Nondestructive Testing and Evaluation ,* vol. 24, no. 4, pp. 313-328, 2009.

[75] M. Feldman, "Hilbert transform in vibration analysis," *Mechanical Systems and Signal Processing,* vol. 25, no. 3, p. 735–802, 2011.

[76] B. S. Kim, D. S. Gu, Y. C. Kim,B. K. Choi , "Rolling element bearing fault detection using acoustic emission signal analyzed by envelope analysis with discrete wavelet transform," *Engineering Asset Lifecycle Management,* pp. 596-602, 2010.

[77] W. A. Gardnera, A. Napolitanob and L. Paura, "Cyclostationarity: Half a century of research," *Signal Processing,* vol. 86, no. 4, p. 639–697, 2006.

[78] R.B. Randall, J. Antoni, S. Chobsaard, "The relationship between spectral correlation and envelope analysis in the diagnosis of bearing faults and other cyclostationary machine signals," *Mechanical Systems and Signal Processing,* vol. 15, no. 5, p. 945–962, 2001.

[79] B. Kilundu, X. Chiementin, J. Duez and D. Mba, "Cyclostationarity of Acoustic Emissions (AE) for monitoring bearing defects," *Mechanical Systems and Signal Processing,* vol. 25, no. 6, p. 2061–2072, 2011.

[80] C. Molina Vicuña, "Effects of operating conditions on the Acoustic Emissions (AE) from planetary gearboxes," *Applied Acoustics,* vol. 77, p. 150–158, 2014.

[81] P.Borghesani , P.Pennacchi, R.Ricci and S.Chatterton, "Testing second order cyclostationarity in the squared envelope spectrum of non-white vibration signals," *Mechanical Systems and Signal Processing,* vol. 40, p. 38–55, 2013.

[82] L. Lin,W. Lu and F. Chu, "Application of AE techniques for the detection of wind turbine using Hilbert-Huang transform," in *Prognostics & System Health Management Conference*, Macau, 2010.

[83] T. Lin, E. Kim and A. Tan, "A practical signal processing approach for condition monitoring of low speed machinery using Peak-Hold-Down-Sample algorithm," *Mechanical systems and signal processing,* vol. 36, no. 2, pp. 256-270, 2013.

[84] Y. He, X. Zhang and M. I. Friswell, "Defect Diagnosis for Rolling Element Bearings Using Acoustic Emission," *Journal of Vibration and Acoustics,* vol. 131, 2009.

[85] J. Shiroisi, Y. Li, S. Liang, T. Kurfess and S. Danyluk, "Bearing condition diagnostic via vibration and acoustic emission measurements," *Mechanical Systems and Signal Processing,* vol. 11, no. 5, pp. 582-694, 1997.

[86] X. Li, J. Yang, M. Li, J. Xu, "A new de-noising method for acoustic emission signal of rolling bearings with low speed based on morphological filtering in frequency domain," *Journal of Vibration and Shock,* vol. 32, no. 1, pp. 65-68, 2013.

[87] S. Edwards, A.W. Lees and M.I. Friswell, "Fault diagnosis of rotating machinery," *Shock and Vibration Digest,* vol. 30, no. 1, pp. 4-13, 1998.

[88] A. S. Sekhar, "Identification of Unbalance and Crack Acting Simultaneously in a Rotor System: Modal Expansion versus Reduced Basis Dynamic Expansion," *Journal of Vibration and Control,* vol. 11, p. 1125, 2005.

[89] Z. Liu, X. Wang and W. Dou, "Using Acoustic Emission and Vibration Detection to Identify the Rotor-Stator Rubbing," in *Biennial Conference on Mechanical Vibration and Noise, Parts A, B, and C*, USA, 2007.

[90] L. D. Hall and D. Mba, "Acoustic Emissions diagnosis of rotor-stator rubs using the KS statistic," *Mechanical Systems and Signal Processing,* vol. 18, no. 4, pp. 849-868, 2004.

[91] L.D. Hall and D. Mba, "Diagnosis of continuous rotor–stator rubbing in large scale turbine units using acoustic emissions," *Ultrasonics,* vol. 41, no. 9, p. 765–773, 2004.

[92] A.W. Lees, "Misalignment in rigidly coupled rotors," *Journal of Sound and Vibration,* vol. 305, p. 261–271, 2007.

[93] P. Pennacchi, A. Vania and S. Chatterton, "Nonlinear effects caused by coupling misalignment in rotors," *Mechanical Systems and Signal Processing,* vol. 30, pp. 306-322, 2011.

[94] M. A. Hili, T. Fakhfakh, L. Hammami and M. Haddar, "Shaft misalignment effect on bearings dynamical behavior," *The International Journal of Advanced Manufacturing Technology,* vol. 26, no. 5-6, pp. 615-622, 2005.

[95] K.M. Al-Hussain, "Dynamic stability of two rigid rotors connected by a flexible coupling with angular misalignment," *Journal of Sound and Vibration,* vol. 266, no. 2, 2003.

[96] S. Ganeriwala, S. Patel and H. Hartung, "The Truth Behind Misalignment Vibration Spectra of Rotating Machinery," in *17th International Modal Analysis Conference* , 1999.

[97] M. toth and S. ganeriwala, "A comprehensive study of shaft/coupling misalignment signature using vibration analysis," in *The Eleventh International Conference on Condition Monitoring and Machinery Failure*, Manchester, 2014.

[98] D. Gu, J. kim, Y. An and B. Choi, "Detection of faults in gearboxes using acoustic emission signal," *Journal of Mechanical Science and Technology,* vol. 25, no. 5, pp. 1279-1286, 2011.

[99] T. Toutountzakis and D. Mba, "Observations of acoustic emission activity during gear defect diagnosis," *NDT&E International,* vol. 36, p. 471–477, 2003.

[100] L. Nohál, F. Hort, J. Dvořáček and P. Mazal, "An experimental investigation of rolling contact fatigue of steels using acoustic emission method," *Insight - Non-Destructive Testing and Condition Monitoring,* vol. 55, pp. 665-669, 2013.

[101] B. Eftekharnejadn, M.R. Carrasco, B. Charnley and D. Mba, "The application of spectral kurtosis on Acoustic Emission and vibrations from a defective bearing," *Mechanical Systems and Signal Processing,* vol. 25, p. 266–284, 2011.

[102] Y. Fan, F. Gu, and A.Ball, "Modelling acoustic emissions generated by sliding friction," *Wear,* vol. 268, pp. 811-815, 2010.

[103] L. E. Morando, "Measuring shock pulses is ideal for bearing condition monitoring," *Pulp and paper,* pp. 96-98, 1988.

[104] J. Miettinen and P. Andersson, "Acoustic emission of rolling bearings lubricated with contaminated grease," *Tribology International 33 (2000) ,* vol. 33, p. 777–787, 2000.

[105] C. K. Tan and D. Mba, "Identification of the acoustic emission source during a comparative study on diagnosis of a spur gearbox," *Tribology International,* vol. 38, p. 469–480, 2005.

[106] D. Mba, "Acoustic emission and monitoring bearing health," *Tribology Transactions,* vol. 46, no. 3, pp. 447-451, 2003.

[107] N. Tandon and B. C. Nakra, "Comparison of vibration and acoustic measurement techniques for the condition monitoring of rolling element bearings," *Tribology International,* vol. 25, no. 3, p. 205–212, 1992.

[108] S. Al-Dossary, R. Hamzah and D. Mba, "Observations of changes in acoustic emission waveform for varying seeded defect sizes in a rolling element bearing," *Applied Acoustics,*

vol. 70, no. 1, p. 58–81, 2009.

[109] N. Tandon, G.S. Yadava and K.M. Ramakrishna, "A comparison of some condition monitoring techniques for the detection of defect in induction motor ball bearings," *Mechanical Systems and Signal Processing,* vol. 21, p. 244–256, 2007.

[110] K. Al-Balushi, A. Addali, B. Charnley and D. Mba, "Energy index technique for detection of acoustic emission associated with incipient bearing failures," *Applied Acoustics,* vol. 71, no. 9, p. 812–821, 2010.

[111] N. Jamaludin and D. Mba, "Condition monitoring of slow-speed rolling element bearings using stress waves," *NDT & E International,* vol. 35, no. 6, p. 349–358, 2002.

[112] K. Miyachika, S. Oda, and T. Koide, "Acoustic Emission of bending fatigue process of spur gear teeth," *Transactions of the Japan Society of Mechanical Engineers,* vol. 72, pp. 2392-2398, 2005.

[113] B. Eftekharnejad and D. Mba, "Seeded fault detection on helical gears with acoustic emission," *Applied Acoustics,* vol. 70, no. 4, p. 547–555, 2008.

[114] T. Toutountzakis , C.K. Tan ,D. Mba, "Aplication of acoustic emission to seeded gear fault detection," *NDT E Int,* vol. 38, no. 1, pp. 27-36, 2005.

[115] C. K. Tan and D. Mba, "Limitation of acoustic emission for identifying seeded defects in gearboxes," *Journal of Nondestructive Evauation,* vol. 24, no. 1, pp. 11-28, 2005.

[116] R. Hamzah and D. Mba, "The influence of opereating condition on acoustic emission (AE) generation during meshing of helical and spur gear," *Tribology International,* vol. 42, no. 1, p. 3–14, 2009.

[117] B. Eftekharnejad, A. Addali, D. Mba, "Shaft crack diagnostics in a gearbox," *Applied Acoustics,* vol. 73, no. 9, p. 723–733, 2012.

[118] Y. Qu, E. Bechhoefer, D. He and J. Zhu, "A New Acoustic Emission Sensor Based Gear Fault Detection Aproach," *International Journal of Prognostics and Health Management,,* vol. 4, 2013.

[119] W. Reimche et al., "Basic of vibration monitoring for fault detection and process control," in *III Pan-American Conference for Nondestructive Testing*, Rio de Janeiro, 2003.

[120] S.l Raadnui and S. Kleesuwan, "Low-cost condition monitoring sensor for used oil analysis," *Wear,* vol. 259, no. 7-12, p. 1502–1506, 2005.

[121] K. Maier, "Magnetic methods of condition monitoring," in *Proceedings of Vibration and Wear in High Speed*, 1989.

[122] J. Ma and C. Li, "Detection of localised defects in rolling element bearing via composite hypothesis test," *Mechanical systems and signal processing,* vol. 9, pp. 63-75, 1995.

[123] Y. T. Sheen, "On the study of applying Morlet wavelet to the Hilbert transform for the envelope detection of bearing vibrations," *Mechanical Systems and Signal Processing,* vol. 23, no. 5, p. 1518–1527, 2009.

[124] D. Abhijeet Shinde, A Wavelet Packet Based Sifting Process and Its Application for Structural Health Monitoring, Faculty of Worcester Polytechnic Institute: Master Thesis , 2004.

[125] Matlab documentation, "Mathworks," 22 7 2014. [Online]. Available: http://www.mathworks.co.uk/help/wavelet/ref/scal2frq.html.

[126] "Understanding bearing vibration frequencies," Electrical Aparatus Service Association, 2003.

[127] S. Shi, R. Randall and J. Antoni, "Rolling element bearing fault detection using improved envelope analysis," in *8th international conference on vibrations in rotating machinery*, Cardiff, UK, 2011.

[128] W. Musial and S. Butterfield, "Improving wind turbine gearbox reliabiliy," in *European Wind Energy Conference*, Milan, Italy, 2007.

[129] L. J. Graham and G. A. Alers, "Acoustic emission the frequency domain," in *Monitoring Structural Integrity by Acoustic Emission*, American society for testing and materials, 1975, pp. 11-39.

[130] A. Singh, D. R. Houser and S. Vijayakar, " Detecting gear tooth breakage using acoustic emission: a feasibility and sensor placement study," *J Mech Des.,* vol. 121, p. 587–593, 1999.

[131] Spectraquest inc., "http://spectraquest.com/," [Online].

[132] Sectraquest Inc., User operating manual for machinery fault simulator.

[133] D. Zappalà, P. J. Tavner and C. J. Crabtree, "Gear Fault Detection Automation Using WindCon Frequency Tracking," in *Europe's premier wind energy event*, Copenhagen, 2012.

[134] D. Zappalà, P. Tavner and C. Crabtree, "Sideband algorithm for automatic wind turbine gearbox fault detection and diagnosis," National Renewable Energy Laboratory, Austria, 2013.

[135] J. Hanna, C. Hatch, M. Kalb, A. Weiss and H. Luo , "Detection of Wind Turbine Gear Tooth Defects Using Sideband Energy Ratio™ - Wind energy resource assessment and forecasting," GE Energy, Nevada USA 89423.

[136] R. B. Randall, "A new method of modelling gear faults," *Journal of Mechanical Design,* vol. 104, pp. 259-267, 1982.

[137] A. Bilošová and J. Biloš, Vibration diagnostics, 2012.

[138] J. Sun and G. Changlin, "Hydrodynamic lubrication analysis of journal bearing considering misalignment caused by shaft deformation," *Tribology International,* vol. 2004, no. 10, pp. 841-848, 2004.

[139] P. G. Nikolakopoulos and C. A. Papadopoulos, "A study of friction in worn misaligned journal bearings under severe hydrodynamic lubrication," *Tribology International,* vol. 41, no. 6, p. 461–472, 2008.

[140] D. Mba and L.D. Hall, "The transmission of acoustic emission across large-scale turbine rotors," *NDT&E International ,* vol. 35 , p. 529–539, 2002.

[141] H. Kakishima, T. Nagatomo, H. Ikeda, T. Yoshioka and A. Korenaga, "Measurement of Acoustic Emisión and vibration of rolling bearings with an artificial defect," *QR of RTRI,*

vol. 41, no. 3, pp. 127-130, 2000.

[142] Vibration analysis Category I - Accredited Training Manual ISO 18436-2, Reliability Maintenance Solutions ltd., 2010.

[143] Ralph T. Buscarello, Practical Solutions to Machinery and Maintenance Vibration Problems, Online Book, 2002.

[144] John Piotrowski, Shaft alignment handbook - Third edition, CRC Press, 2007.

[145] Brüel & Kjær Vibro A/S, *Detecting Faulty Rolling Element Bearings,* Application note.

[146] S. Bagnoli, R. Capitani and P. Citti, "Comparison of accelerometer and acoustic emission signals as diagnostic tools in assesing bearings," in *2nd International Conference on Condition Monitoring*, London, Uk, 1988.

[147] D. Dowson, "Elastohydrodynamic and micro-elastohydrodynamic lubrication," *Wear,* p. 125–138, 1995.

[148] Y. Hayashi, M. Zenbutsuand H. Suzuki, H, "Analysis of Fluctuations in Bearing Preload and Optimal Design of Tapered Roller Bearings for Pinion Shaft Support in Differential Gearboxes," *SAE Technical Paper ,* 2001.

[149] A. Heng , S. Zhang, A. C. Tan and J. Mathew, "Rotating machinery prognostics: State of the art, challenges and opportunities," *Mechanical systems and signal processing,* vol. 23, no. 3, p. 724–739, 2009.